Linear sloshing in vertical circular cylindrical containers with different configurations under the influence of surface tension

A Thesis submitted

in partial fulfillment of the requirements

for the degree of

DOCTOR OF PHILOSOPHY

by

Neelam Choudhary

Roll Number: 10612307

DEPARTMENT OF MATHEMATICS

INDIAN INSTITUTE OF TECHNOLOGY GUWAHATI

GUWAHATI-781039, INDIA

November, 2015

CERTIFICATE

It is certified that the work contained in the thesis titled **"Linear sloshing in vertical circular cylindrical containers with different configurations under the influence of surface tension"** by **Neelam Choudhary**, a student in the Department of Mathematics, Indian Institute of Technology Guwahati for the award of the degree of Doctor of Philosophy has been carried out under my supervision and this work has not been submitted elsewhere for a degree.

November, 2015

Dr. Swaroop Nandan Bora
Professor
Department of Mathematics
Indian Institute of Technology Guwahati, India

Dedicated

To

My Family ..

Acknowledgements

Though this thesis has my name on its cover page, it would not have been possible without contributions of several individuals who in different ways gave me the energy to carry out this study.

I am grateful to God for giving me all the good health, wisdom and perseverance to make this thesis possible.

First and foremost, I would like to grab this opportunity to express my deepest gratitude to Prof. Swaroop Nandan Bora who not only guided me impeccably but also showered me with his affection. In reality, it will not be fair to acknowledge him with only a few words. However, I cannot resist thanking him for his inspiring guidance, friendly advice and continuous support for my Ph.D study. He has been a tremendous mentor for me. I must say I have never seen such a disciplined, energetic and helpful person in my life. I will be forever indebted to him for his encouragement in every aspect of my life. Thank you very much, Sir!

With great appreciation, I would like to thank the members of my Doctoral Committee, Prof. D. C. Dalal, Prof. Rajen K. Sinha and Prof. Natesan Srinivasan, for annually reviewing my work, their great ideas and encouragement that enabled me to complete this thesis. I would like to thank Dr. P. A. S. Sree Krishna and Dr. Arnab Kumar De for helping me in learning the basics during my course-work which immensely benefitted me in carrying out my research. I must convey my sincere thanks to Dr. Sriparna Bandopadhyay and Dr. Anjan K. Chakrabarty with whom non-academic light conversations filled me with energy.

I would like to acknowledge Indian Institute of Technology Guwahati for providing my academic and financial support during my stay at IIT Guwahati. I would also like to extend my thanks to technical and non-technical staff of Department of Mathematics for providing all the necessary support during my study at IIT Guwahati.

I have always had a great time at IIT Guwahati with my friends. Apart from fun, some of them have also been great sources of learning and have gifted me memories that I will cherish forever. A special thank to Punit for all his help and patience in enhancing my programming skills. I would like to thank Saloni for her cheerful company. I would like to thank Nasim, Swarup, Jayanta Borah, Ankita, Swathi, Dishari, Madhu, Sunanda and Mridusmita, who made my stay comfortable at one of the most beautiful places, that is, IIT Guwahati. I must say thank to my seniors Namita Behra, Jhuma Sengupta and Santu Das, for all their help in the initial phase of my research. I cannot thank enough Mrs. Swapnali Bora, for all her love and emotional support making my life more beautiful and meaningful.

Many other people have touched my life in a wonderful manner. I extend my sincere thank and gratitude to one and all. I am indebted of my school mathematics teacher, Late Shri Hari Singh who taught me the lesson to dream high.

Last but definitely not the least, I owe special thanks to my family who supported my every decision and provided me enough opportunities throughout my life to be where I am today. I don't have words to express my gratitude for my mother's prayers for me and my father's confidence in me. I recognize your unconditional love, patience and understanding towards me. You are the best thing that has ever happened to me!

November, 2015 **Neelam Choudhary**

Abstract

The presence of free surface of a liquid in a partially filled container forces the liquid to perform motion with oscillating free surface subject to some external disturbances. This phenomenon is known as sloshing. In this thesis, free surface flows are investigated under various considerations. We investigate sloshing problems for different configurations and try to solve them such that the unfavourable effect of sloshing on stability of the system reduces. We evaluate sloshing frequency of the liquid subject to different conditions: (i) changing the geometry of the container (ii) introducing slosh suppression device such as a rigid baffle. A semi-analytical approach based on linear water wave theory is employed to model some specific sloshing problems in terms of potentials. Sloshing problem is an eigenvalue problem. We investigate the effects of various parameters on sloshing frequency of liquid subject to various conditions:

- Liquid has a complete free surface
- A free surface covered in part by an annular rigid baffle
- Rigid baffle placed inside the fluid domain

The work carried out in this thesis focuses mainly on determining sloshing modes and sloshing frequencies in circular cylindrical containers with different configurations. In some of the problems, the effect of the surface tension at the free surface is considered for discussing sloshing. Sloshing frequencies are computed for both single-layer and two-layer fluid systems. In all the two-layer fluid problems, the effect of the surface tension at free surface and surface of separation is neglected and fluids are considered to be immiscible. Furthermore, the solutions are obtained under the assumption of linear and time harmonic motion of the liquid. The thickness of rigid baffle is considered negligible compared to its radius. We observe the effect of surface tension on sloshing frequencies when a rigid baffle is placed on the free surface in a vertical coaxial annular circular cylinder or a vertical circular cylinder. We also study the effect of an uneven bottom of a cylindrical container on sloshing frequencies. We restrict ourselves to studying the free oscillations of the free surface.

Analytical solutions for velocity potentials are obtained by means of separation of variables by using the prescribed rigid boundary conditions on the boundary of the container under consideration and then an infinite system of linear homogenous equations is obtained by using free surface condition. This infinite linear homogenous system is solved to evaluate sloshing frequencies. After obtaining solutions in terms of potentials by using separation of variables method for the single-layer fluid problem with and without a baffle at the free surface, the free surface condition is utilized by means of point allocation method by choosing equidistant points on the free surface. The free surface

condition is used to find the eigenfrequency equation for determining the sloshing frequency. The effects of fluid height, container radius, baffle width and surface tension are studied on sloshing frequency. It is shown that the introduction of a baffle at the free surface dampens the sloshing.

When a baffle is placed inside the fluid domain for single-layer and two-layer fluid problems, the complex fluid domain is divided into sub-domains to get the solutions. The boundary value problem is set up for each sub-domain and the corresponding potentials are found by using separation of variable method. Matching conditions are used at the free surface and interfaces of two consecutive sub-domains to maintain the continuity of pressure and velocity. The eigenfrequency equation is obtained with the help of matching conditions by using Fourier and Bessel series expansions. The sloshing frequencies are obtained by solving the homogenous linear system presented by matching conditions. The effects of fluid height, inner-outer container radii and baffle-container radius ratio are investigated on sloshing.

In the sloshing problem concerned with two inviscid and immiscible fluids, frequencies are computed with the help of a linear homogenous system set up by using matching conditions at the free surface and the surface of separation. The sloshing frequencies in the presence of a complete free surface and partially covered free surface are determined. The effects of lower and upper fluid heights, density ratio and baffle are investigated on sloshing frequencies. It is shown that increasing density ratio lowers the sloshing.

Most part of the thesis is devoted to the investigations of the effect of a rigid annular baffle on sloshing frequencies placed on the free surface and inside the liquid domain for different configurations. The benefit of a partly covered free surface is that it increases the natural frequencies and decreases the sloshing mass participating in the dynamic motion of the system. It is shown that the baffle is effective on controlling sloshing frequencies when it is placed near and on the free surface. It is observed that when the baffle is nearer the free surface, it is more effective in controlling the sloshing as compared to the case corresponding to the increase of liquid level in the container. The influence of the baffle placed inside liquid domain is less.

In the present study, it is observed that sloshing behaviour of partially filled liquid containers depends on the geometry and size of the container and also on those of the cover. We discuss sloshing in some special types of containers like a cylinder with a semi cover (baffle), a coaxial cylindrical wall, and a cylinder with a spherical bottom. We examine the effect of the various parameters such as radius, bottom, liquid depth, baffle width etc. on sloshing. Further, we consider sloshing in a two-layer fluid and also examine the effect of the baffle on sloshing frequencies. Surface tension, instead of gravity, plays a significant role in sloshing phenomenon.

Contents

List of Figures

List of Tables

Chapter 1

Introduction

In modern science, the term 'matter' is used in different ways in different fields. There is no single definition of matter which is accepted universally in a scientific way. The most common way of defining matter is in terms of mass. Mass is the scientifically accepted term. Anything that has mass and volume is termed as matter. Based on physical and chemical properties, matter is made up of atoms. In modern science and engineering, matter is further classified according to its physical properties. The most common observed states of matter are solid, liquid, gas and plasma. In solid state, matter has a fixed shape and volume. In liquid state, matter has a fixed volume but a variable shape adapting to fit a container. In gaseous state, matter varies both in shape and volume. In plasma state also both shape and volume are variable. In the universe, visible matters are commonly found in plasma state.

Fluid dynamics is the study of movement of liquids and gases. A matter which is capable of flowing is a fluid. For a fluid, particle can move freely past one another. Liquid and gas are fluids. All fluids flow freely and take the shape of the container in which they are filled. When a fluid flows, it changes its shape under an applied shear stress, i.e., fluids cannot be at rest under applied forces. When a fluid is at rest and a shear stress is applied to a fluid, it will not be in equilibrium state anymore, no matter how small the shear stress is. Further, fluids are basically classified into two categories: Newtonian fluids and non-Newtonian fluids. Newtonian fluids (water, air, oil, ethyl alcohol, etc.) obey the Newton's law of viscosity, i.e., viscous stresses at every point in the fluid are linearly proportional to the rate of strain. For Newtonian fluids, viscosity depends on pressure and temperature of the fluid. Non-Newtonian fluids do not follow the Newton's law of viscosity. They are complex fluids such as paint, blood, shampoo, paste, etc.

Further, fluid flows are classified into different categories based upon different properties. Fluid flows characterized on the basis of density are compressible flow and incom-

pressible flow. If the fluid density changes with change in pressure or temperature, then the flow is termed as compressible flow. And if the fluid density remains constant with change in pressure and temperature, then the flow is considered incompressible flow. Compressible and incompressible flows are characterized by Mach number. Fluid flows classified on the basis of viscosity are termed as viscous flow and inviscid flow. The flow is inviscid if the fluid does not have the property to resist deformation; otherwise the flow is viscous flow. If fluid properties are invariant in the system with respect to time, the flow is termed as steady flow. If fluid properties change with time, then the flow is an unsteady flow. Fluid flow is uniform if the magnitude and direction of the fluid velocity do not change within the fluid; otherwise the flow becomes non-uniform flow. Fluid flows described by the velocity and viscosity of the fluid are laminar flow and turbulent flow. In laminar flow, the fluid flows in orderly layers without any disruption. If the fluid velocity and pressure fluctuate in time in a random manner, the flow is described as turbulent flow. In fluid dynamics, potential flows are very common flows describing fluid properties and applications in engineering. In potential flow, fluid velocity can be written as the gradient of a scaler function, called velocity potential. Potential flows are applicable only to frictionless and ideal fluids. For these flows, the equation of continuity simply becomes the Laplace's equation which is satisfied by the velocity potential.

Fluid flows having a free surface are known as free surface fluid flows. The free surface is formed by the surface of a fluid. Free surface is the property of liquids since gases are unable to form a free surface on their own. Free surface is free to move in absence of external forces. When the free surface of liquid is disturbed due to some external force, waves are generated. The surface waves are gravity waves since gravitational force acting on the free surface tries to stabilize the disturbed free surface. Such flows are visible in water waves. Free surface flows problem generally occurs in rivers, oceans, flood overflow, tsunamis and flow in structures. The velocity of free surface flows depends on the wavelength of the wave. The gravity waves generated at the free surface moves faster for greater wavelength. Free surface flows due to some external forces have been studied because of wide applications in water waves or due to moving structures such as ships.

When a liquid surface performs motion in a partially filled container and interacts with some container wall, the pressure due to this interaction may affect the stability of the container as well as the supporting structure. The presence of a free surface in a partially filled liquid container allows for a liquid motion relative to the container. This phenomenon is referred to as 'liquid sloshing' which can occur under various circumstances and may have a significant influence on the response of the container. There are infinitely many natural frequencies at which liquid surface moves inside the container,

but only a few lower modes are usually excited by the motion of the supporting structure. The lowest natural frequencies corresponding to these lower modes are defined as fundamental frequencies. The liquid motion at these fundamental frequencies is called sloshing and the fundamental frequencies are referred as 'sloshing frequencies'. Splashing of coffee from a coffee cup while moving is an example of sloshing. If we carry a bucket of water, liquid motion arising in the bucket is also another example of sloshing in daily life.

The concept of sloshing came into existence due to the failure of several launch vehicles. Sloshing was first encountered in the control of guided missiles in the aerospace industry. In this application it was found that sloshing in the fuel tanks could represent instabilities. Similar problems have been encountered in the control of aeroplanes. As an example, a Jupiter flight had gone out of control because the fundamental sloshing frequency was not taken care of. Another missile named Blue Streak failed in flight as slosh induced instabilities to the system which resulted in structural failure. It is necessary to perform the movement in such a way that the liquid does not splash out of the container. If liquid is allowed to perform its motion freely, it may produce various forces which can be dangerous to the stability of the container and can lead to the failure of the operation of the structure. When the motion of any vehicle or structure containing liquid free surface is considered, then sloshing is the result of the resonant excitation of the tank liquid. Excitation with frequencies in the vicinity of the lowest natural frequency is of primary practical interest. Resonant free surface flows in tanks in aircrafts, missiles and rockets have been the focus of extensive research.

Liquid sloshing also poses a severe problem while transporting liquid in containers both on sea and on land. Sloshing has significant effects on the stability of the vehicle carrying liquid containers. Sloshing generates severe hydrodynamic loads that can be dangerous for structural integrity and stability of rockets, satellites, ships, trucks and even stationary petroleum containers. The problem of sloshing remains a great concern to aerospace, civil, mechanical, nuclear engineers; physicists, road and ship tankers, and applied mathematicians. In aerospace engineering, the effect of sloshing on the stability of the vehicles has been a great concern to a wide range of researchers as well as engineers since early 1960s. In launch vehicles, a large amount of initial weight is fuel. If fuel sloshing frequencies and structural frequencies are close to each other, it is very likely that instability can occur. Surface tension, instead of gravity, plays a significant role in sloshing. In a low or almost zero gravity field, if sloshing frequencies are low and forces applied on the vehicle are not significantly strong, instability can take place in such a manner that the liquid motion can have large amplitude oscillations resulting in structure operational failure. To control these amplitudes arising due to liquid sloshing,

damping devices have been used to maintain structural stability. In offshore industry also, sloshing is a key factor for the motion of a ship carrying liquid tanks. This is because oscillations generated by the motion of a wave-induced ship may have a great effect on its motion and stability. Sloshing may have a significant effect if excitation frequencies of the ship are close to its natural frequencies. Sloshing affects the efficiency of oil and gas production platforms also. While constructing the platforms to extract oil in Bohai Sea in China, ice effect was not taken into account. Due to the presence of ice, vibrations induced by it resulted in the collapse of several platforms. In civil engineering, sloshing has a great significant importance from vehicle design to building industry. A wide range of researchers have been studying the effect of sloshing on oil tanks, water towers, LPG (liquefied petroleum gas) tankers, and dams. LPG tankers and other inflammable liquid tankers are of primary interest to the researchers as any instability caused by sloshing may be quite harmful. A large number of researchers in structural engineering has been working on damping devices such as TLD (tuned liquid damper) to reduce oscillations of a structure. A TLD is a device used in structures to control the amplitude of oscillations with the help of liquid motion in a rigid tank. In seismology, effect of water tanks on the roof of tall buildings have been investigated and it has been found that the tanks reduce the vibrations of buildings during earthquakes. In coastal engineering also, sloshing has a great impact. Vibrations in harbours are of primary concern in coastal engineering. The vertical motion of the water surface may by very high for some points in the basin at harbour vibrations. Tsunami waves caused by earthquake may excite the harbour vibrations.

1.1 Modeling of slosh

This section describes the theory and equations that constitute very important parts of sloshing problems. Linear water wave theory is the theory which describes the modeling of ocean surface waves (surface of fluids) in the study of ocean engineering, coastal engineering and naval architecture with many engineering applications. This theory can also be appropriately applied to problems in closed domains, such as containers filled with liquid. In general, surface waves are nonlinear. Amplitude of the surface wave is assumed sufficiently small which makes the surface almost linear. In linear wave theory, amplitude of the surface wave is small and the law of conservation of mass holds within the fluid domain. Incompressible, inviscid and irrotational flow are some important assumptions in modelling linear waves. Linear water wave theory is generally employed to model some specific sloshing problems. Here we emphasize only on free oscillations of the free surface. So the modeling will be applicable to only free oscillation sloshing

problems. Fluid motion within the fluid domain is defined by Euler equations. The equations of motion are given in vector form. If the fluid is incompressible and inviscid, equations for the conservation of mass and momentum are, respectively, given by

$$\nabla.\mathbf{v} = 0, \tag{1.1}$$

$$\frac{\partial \mathbf{v}}{\partial t} + (\mathbf{v}.\nabla)\mathbf{v} = -\frac{1}{\rho}\nabla p + \mathbf{g}, \tag{1.2}$$

where $\mathbf{v}$ is the velocity vector, ρ is the constant fluid density, $\mathbf{g}$ is the acceleration due to gravity and p is the pressure in the fluid relative to the atmospheric pressure. Inserting the vector identity

$$(\mathbf{v}.\nabla)\mathbf{v} = \frac{\mathbf{1}}{\mathbf{2}}\nabla|\mathbf{v}|^{\mathbf{2}} + (\nabla \times \mathbf{v}) \times \mathbf{v}$$

into Eq. (1.2), it gets converted to

$$\frac{\partial \mathbf{v}}{\partial t} + \frac{1}{2}\nabla|\mathbf{v}|^2 + (\nabla \times \mathbf{v}) \times \mathbf{v} = -\frac{1}{\rho}\nabla p + \mathbf{g}. \tag{1.3}$$

Assuming that gravity acts in the negative direction of the z-axis, we can write

$$\mathbf{g} = \nabla(-gz). \tag{1.4}$$

Therefore the momentum equation gets converted to

$$\frac{\partial \mathbf{v}}{\partial t} + \frac{1}{2}\nabla|\mathbf{v}|^2 + (\nabla \times \mathbf{v}) \times \mathbf{v} = -\frac{1}{\rho}\nabla p - \nabla(gz). \tag{1.5}$$

Flow is assumed irrotational which can now be termed as a potential flow. For potential flows, there exists a potential Φ whose gradient gives the fluid velocity:

$$\mathbf{v} = \nabla\mathbf{\Phi}. \tag{1.6}$$

Inserting Eq. (1.6) into Eq. (1.1), we get

$$\nabla.\nabla\Phi = \nabla^2\Phi = 0, \tag{1.7}$$

which is the well-known Laplace's equation which serves as the governing equation for sloshing problems. Since the flow is irrotational, it leads to

$$\nabla \times \mathbf{v} = \mathbf{0}. \tag{1.8}$$

Insertion of Eqs. (1.6) and (1.8) into Eq. (1.5) gives us

$$\nabla\left\{\frac{\partial \Phi}{\partial t} + \frac{1}{2}\nabla\Phi.\nabla\Phi + \frac{p}{\rho} + gz\right\} = 0, \tag{1.9}$$

which can be written as

$$\frac{\partial \Phi}{\partial t} + \frac{1}{2}\nabla\Phi.\nabla\Phi + \frac{p}{\rho} + gz = C(t), \tag{1.10}$$

where $C(t)$ is an arbitrary function of time and Eq. (1.10) is known as Bernoulli's equation. The container walls and bottom of the container are the fluid boundaries. No flow condition is to be satisfied at the wetted bottom and boundary walls of the container which gives

$$\mathbf{n}.\mathbf{v} = 0 \tag{1.11}$$

$$\Rightarrow \mathbf{n}.\nabla\mathbf{\Phi} = 0, \tag{1.12}$$

where $\mathbf{n}$ is the outward normal to the fluid boundaries.

On the free surface $z = \eta(x,t)$ of the fluid, there are two boundary conditions: kinematic boundary condition and dynamic boundary condition.

Kinematic condition:

$$\frac{\partial \Phi}{\partial z} = \frac{\partial \eta}{\partial t} + \frac{\partial \eta}{\partial x}\frac{\partial \Phi}{\partial x}, \tag{1.13}$$

which states that the vertical velocity component of fluid particles on free surface should be the same as the vertical velocity component of free surface, i.e., fluid particle on free surface will always remain on the free surface. The dynamic boundary condition for a potential flow can be written as Bernoulli's equation.

Dynamic condition:

$$\frac{\partial \Phi}{\partial t} + \frac{1}{2}\nabla\Phi.\nabla\Phi + \frac{p}{\rho} + g\eta = \mathbf{0}. \tag{1.14}$$

The constant $C(t)$ is chosen as zero for simplification.

Only the free surface conditions have nonlinearity in sloshing problems. The nonlinear conditions at free surface can be linearized by the fact that amplitude of the fluid motion is sufficiently small compared to the wavelength. Since linear water wave theory is employed, so the free surface conditions can be linearized as

$$\frac{\partial \Phi}{\partial z} = \frac{\partial \eta}{\partial t}, \qquad z = 0, \tag{1.15}$$

$$\frac{\partial \Phi}{\partial t} + g\eta = 0, \qquad z = 0, \tag{1.16}$$

assuming atmospheric pressure at the free surface to be zero. The complete modeling for the boundary value problem of sloshing in terms of velocity potential can be written as

$$\nabla^2\Phi = 0, \quad \text{within the fluid domain}, \tag{1.17}$$

with rigid boundary conditions

$$\frac{\partial \Phi}{\partial \mathbf{n}} = 0 \quad \text{on fluid boundaries}. \tag{1.18}$$

Free surface conditions given by Eqs. (1.15) and (1.16) can be combined to get a free surface condition at $z = 0$ as follows:

$$\frac{\partial \Phi}{\partial z} + \frac{1}{g}\frac{\partial^2 \Phi}{\partial t^2} = 0. \tag{1.19}$$

The above defined boundary value problem will be solved analytically to get the velocity potential in a closed form and consequently the free surface equation will give the natural frequencies of the free surface.

1.2 Literature survey

Liquid sloshing inside different kinds of containers has been a great concern and importance to a wide range of researchers. The sloshing problems in containers of different sizes and shapes have been investigated by a reasonable number of researchers. The sloshing problem with a free surface can be considered in liquid tanks, immiscible multi-fluids, fluid-structure interaction and blood flows, and there are many other real world examples of sloshing. A large class of liquid tanks exists in many configurations but cylindrical and rectangular containers are the most preferred containers for transporting liquid from one place to another. While designing a liquid tank, an estimate of natural frequencies is a mandatory step for the stability of the container. In the sloshing problem with a free surface, the free surface can have different kinds of motion such as, planner or non-planner, rotational and chaotic.

Liquid sloshing in rectangular and cylindrical tanks has been studied theoretically, experimentally and numerically by many researchers over a wide range of disciplines. Jacobsen [22] discussed sloshing in a rigid cylindrical container and found a closed-form solution for the Laplace's equation. (The problem considered by Jacobsen was first studied by Professor L. M. Hoskins of Stanford University. But he did not properly utilize the properties of modified Bessel functions which led to a lot of computational work.) Ockendon et al. [30] described an asymptotic approach to obtain multiple periodic solutions for resonant sloshing in shallow water. They assumed that the wave number appearing in dispersion relation was small, and mainly discussed dissipative effect. Evans [12] used wide-spacing approximation to discuss the scattering of waves from an arbitrary number of identical bodies and calculated the resonant frequencies. He determined the resonant frequencies just for a single obstacle and then generalized it to n symmetric obstacles by a compact expression for the n-th power of a 2×2 matrix. Expressions for transmission and reflection coefficients were also obtained. Rocca et al. [32] derived a fully nonlinear mathematical model by applying a variational method for sloshing in a rectangular tank rotating around a horizontal axis. They investigated $2D$ and $3D$

surface waves. Both theoretical and experimental studies were found to be in very good agreement. Buldakov [8] investigated sloshing in a 2-D rectangular tank filled with an incompressible fluid. The horizontal and vertical excitation of tank were also considered. A Lagrangian approach was used to model the problem.

Faltinsen et al. [13] carried out an investigation in which they studied nonlinear sloshing in a partially filled rectangular tank. They used Bateman-Luke variational principle and derived infinite-dimensional modal system of ordinary differential equations in terms of generalized time dependent coordinates of free surface elevation and velocity potential. Faltinsen and Timokha [14] studied two-dimensional nonlinear sloshing in a rectangular tank and also described surge and pitch excitations. No overturning waves and infinite tank roof height were assumed. By assuming fluid amplitude to be small compared to fluid depth and tank width, asymptotic modal analysis was done. But this approach becomes invalid when the excitation amplitude is not very small and fluid depth is shallow. When $h/l > 0.24$ (where l is the tank breadth and h is mean fluid depth) and depth is shallow, their theory does not match the experimental results. Faltinsen and Timokha [15] repeated the work carried out in [14] with a revised modal system for a fluid in a rectangular tank. The nonlinear violent resonant waves were discussed in detail with intermediate depth ($0.1 \leq h/l \leq 0.24$) forced by surge and pitch excitations. The derived model for the modal system was considered as a conservative mechanical system and found to be useful for simulation of transient sloshing. Faltinsen et al. [16] modified their multimodal approach to handle three-dimensional sloshing in a rectangular-based basin. Faltinsen et al. [17] extended the work done in [16] and showed the validity of their results by comparing with experimental data. Thiagarajan et al. [43] studied sloshing in a rectangular tank and discussed the wave motion and pressure at different filled levels of tanks. They used finite volume approximation to model the fluid domain and air-water interface was tackled with the help of volume-of-fluid technique. Shankar and Kidambi [36] developed a modal method to investigate two-dimensional nonlinear sloshing of incompressible and inviscid liquid in a rectangular container. The capillary effects were also considered in the formulation of the nonlinear problem. The boundary value problem was reduced to a set of nonlinear ordinary differential equations with the help of modal analysis. Sirwah [40] investigated sloshing in a horizontally oscillating rectangular tank filled with heated viscoelastic fluid. The mathematical formulation was done based on linearized form of Navier-Stokes equations. The boundary value problem was solved by using Laplace transform. The effects of Reynolds number and relaxation time parameter were shown on the free surface elevation numerically.

Zhou et al. [50] investigated the three-dimensional oscillatory behaviour of a flexible rectangular container filled with liquid. Oscillations of the liquid free surface were also

studied to evaluate sloshing modes. An analytical method was presented to discuss coupled vibrations of the system by using superposition principle and separation of variables method. According to the matching conditions at liquid-tank interfaces, the coefficients in the solutions were obtained in the form of integrals. The eigenfrequency equation to evaluate frequency was derived with the help of Rayleigh-Ritz and Galerkin methods.

Cylindrical containers are usually preferred as containers by fuel tank and oil tank designers. A reasonable number of researchers have been investigating sloshing in cylindrical containers. McIver and McIver [25] studied the longitudinal modes of gravity waves in a horizontal cylinder with uniform cross section. They investigated the low and high frequency behaviour for a symmetric container of arbitrary geometry. They found that the high-frequency limit of the modes depended on the angle of intersection of the container with the free surface. They also discussed the approach to find an upper bound and a lower bound for the frequencies of symmetric and antisymmetric modes. Miles [26] studied nonlinear gravity surface waves in a closed basin. The continuum mechanical problem in cylindrical basin was converted into classical mechanics problem by setting up Lagrangian and Hamiltonian for liquid inside cylindrical basin in terms of generalized co-ordinates. The problem was solved by using variational principle to investigate free and forced oscillations of liquid. Miles [27] described nonlinear free oscillations in a circular cylinder. The natural frequencies of liquid with finite amplitude of free surface were calculated as a function of fluid depth and cylindrical radius. Shankar [38] developed a technique to investigate the sloshing frequencies of liquid of highly curved free surface with pinned contact line under the gravity-capillary effect. Results obtained by Shankar were found to be accurate as per comparison with available experimental data and previous analytical solutions. Sakata et al. [33] investigated nonlinear behaviour of liquid surface inside a cylinder subjected to lateral excitation of the cylindrical tank. They used a variational approach to formulate the problem for an incompressible and inviscid liquid. With the help of numerical results it was shown that linear theory was not always sufficient to evaluate the mean response of the liquid displacement. Takahara and Kimura [42] studied the oscillations of liquid surface in presence of nonlinearity. Planar and rotary motions of liquid inside an annular cylindrical container subjected to pitching excitations were investigated. A good agreement was confirmed between analytical and experimental data obtained by them. It was observed from the results that nonlinear properties of liquid motion inside an annular cylindrical containers was much more complicated as compared to a circular cylindrical container. Yin et al. [48] presented an analytical study describing the nonlinear sloshing inside a circular cylindrical tank filled with liquid subjected to pitching excitation. The analytical approach

they used was based on variational principle and Lagrangian. They were the first ones who studied the nonlinear sloshing analytically under forced excitation. Ockendon and Ockendon [29] discussed small amplitude forced oscillations of a rectangular container filled with liquid having a free surface and showed the effects on liquid motions. They considered the forced horizontal as well as vertical oscillations of the tank. Explicit asymptotic solutions for the motion of liquid were obtained.

Bian et al. [6] considered a liquid slug in a circular tube and determined the the natural frequencies. Gravitational and viscous effects were neglected and contact lines were assumed to be pinned or governed by small slip coefficient. Bauer and Eidel [5] found that insertion of a baffle at the free surface of the container increased the frequencies. They numerically evaluated the response to the translational excitation which showed the shifting of the resonance to higher values. They found that the increment in the baffle width reduced the sloshing mass. Wang et al. [46] developed a semi-analytical method in obtaining the natural frequencies and modes of the sloshing liquid in a rigid cylindrical container with a rigid annular baffle inside the fluid domain. They introduced a number of artificial interfaces to subdivide the fluid domain into sub-domains and obtained the exact velocity potentials in the sub-domains. They derived the frequency equation by means of Fourier-Bessel expansion on the introduced artificial interfaces and the free surface. Wang et al. [47] extended their previous work in [46] by considering multiple baffles inside the fluid domain by the same approach employed in [46]. They discussed the effects of baffle positions and inner radius on natural frequencies. Biswal et al. [7] studied sloshing in a rigid cylindrical tank filled with liquid. They calculated the natural frequencies of liquid with and without baffle. The natural frequencies were determined for the case of rigid and flexible baffle. Papaspyrou et al. [31] investigated sloshing in a horizontal cylinder and developed a mathematical model in which the general solution of sloshing potential was written as a series expansion of the time function, and they obtained a semi-analytical solution resulting in a system of linear ordinary differential equations. Sloshing frequencies of half-full horizontal cylinder and hydrodynamic forces were computed. Gavrilyuk et al. [19] examined sloshing in a vertical circular cylinder filled with deep fluid having a rigid baffle by using asymptotic modal system and found that sloshing was affected by the size and location of the baffle. They discussed the effects of the position and radius of the baffle on frequency domains of resonant waves occurring due to lateral excitations. Yuanjun et al. [49] discussed nonlinear sloshing in a circular cylindrical tank under pitching excitation by using variational principle. The nonlinear equations with kinematic and dynamic free surface boundary conditions through variation were derived and solved by multiple-scale method. Planar motion and rotary motion of liquid were studied under the pitch excitation of the tank. It was shown

that both stable and unstable motions depended on the radius and height of the tank. Sinai [39] discussed sloshing frequencies of a stratified two-layer fluid in a closed tank. He considered a two-layer fluid in a fully filled vertical circular cylinder and annular cylinder and obtained a semi-analytical solution for the sloshing frequencies. Sciortino et al. [35] described sloshing of a layered fluid system in a cylindrical tank with an arbitrary shape by introducing Hamiltonian mathematical model and showed its validity by laboratory experiments. The mathematical model composed of partial differential equations of first order in four canonical unknowns. The numerical integration of the derived mathematical model was accomplished by a suitable Galerkin projection of the equations. A good agreement was observed between numerical laboratory experiments even in the case of strong nonlinearity.

While looking at different types of sloshing problems, it has come to our notice that some important works have been carried out for sloshing related to structures other than rectangular and cylindrical tanks. Albright and Concus [1] determined the small amplitude periodic sloshing modes of a liquid in a vertical right circular cylinder in the presence of surface and gravitational forces. They considered the cylinder with a concave spheroidal bottom where the whole free surface was not above the bottom. The container for which they obtained the numerical results, were used for the storage of liquid fuel in space vehicles. Gavrilyuk et al. [18] considered sloshing problem in a circular conical tank and derived a nonlinear finite dimensional asymptotic modal system. They discussed the secondary resonance and shallow fluid problem in detail. Cox et al. [10] investigated the behaviour of steady profiles for periodically forced KdVB and extended KdVB equations. The existence of profiles, closed to two basic profiles, was shown. They used the theory of topological degree to discuss chaotic behaviour. The results presented by Cox et al. [10] are also applicable to forced nonlinear oscillations in presence of viscous damping.

Jaiswal et al. [21] performed an experimental and numerical study to calculate sloshing frequencies in different shaped tanks (like canonical, truncated pyramid, etc.) with internal obstruction. Results found in their study showed a good agreement for first sloshing frequency in circular, square and rectangular tank with analytical solutions. It was shown that sloshing frequency decreased with increasing size of internal obstruction. Shankar [37] considered spherical and cylindrical geometries to calculate sloshing frequencies of liquid in a low-gravity field. He expanded interface displacement and velocity potential in two independent set of spatial functions which were used to obtain a standard eigenvalue problem to compute frequency. For a flat meniscus, where Bond number is considered as infinity, results matched well with the previous available results. The method presented by Shankar works well for large volume tanks accurately.

Several important works have been accomplished with regard to sloshing in multi-layer fluids in rectangular and cylindrical containers. Ambrosi [2] presented a Hamiltonian approach to describe the layered-fluid sloshing applied to an unbounded domain. To formulate the Hamiltonian sum of kinetic energy and potential energy, for a free oscillating system, free surface elevation, interface elevation and the jump in momentum potential density at interface were used as canonical variables. With the help of a theoretical approach, Sciortino et al. [34] investigated the modeling of immiscible two-layer fluid problem with free surface within a prismatic tank. Bauer [4] discussed sloshing frequencies in a rectangular container filled with two immiscible liquids with different densities. He also discussed the pressure distribution and the moments for the interface system. Some numerical experiments were also introduced for an infinitely long rectangular container. Molin et al. [28] carried out an experimental study on sloshing in a rectangular tank filled with immiscible three-layer fluids of different densities taken as dichloromethane, fresh water and cyclohexane. They considered the sway and roll motions of the tank and energy dissipation effects at the interfaces. They compared their findings with analytical model using linearized potential flow theory in the tank which showed a good agreement. Vaziri et al. [44] studied internal waves in a rectangular tank filled with two-layer stratified liquid. A pseudospectral σ-transformation was used to map the fluid domain having free surface and surface of separation of two-layers onto a pair of rectangular domains. The effects of surge and heave excitations were also discussed on sloshing. Ansari et al. [3] discussed two-layer fluid sloshing in a rectangular tank. They used modal analysis to describe two-phase nonlinear sloshing. Chen et al. [9] investigated the pressure on the walls of a rectangular tank subjected to the roll motion considered for the sloshing problem. The numerical study was performed by using smoothed particle hydrodynamics (SPH) method. Kuttler and Sigillito [23] presented a method to find a good estimate of sloshing frequencies with strong error bounds. The sloshing problem in a cylindrical tank with circular cross section partially filled with an ideal fluid was formulated as an integral equation by using conformal mapping. They used the method of posteriori analysis to solve the problem. Mackey and Cox [24] considered a two-layer fluid problem in a rectangular tank and discussed the fluid oscillation in a horizontal direction. They used asymptotic expansion method and derived a periodically forced second order ordinary differential equation which was a reduced form of the extended forced Korteweg de Vries (efKdV) equation. By using Melnikov theory, they showed the existence of a class of periodic solutions. They analyzed these solutions analytically and numerically.

1.3 Mathematical tools

In order to solve the boundary value problems considered in the thesis, the mathematical tools utilized are as following:

1. **Separation of variables method:** In order to solve a linear homogenous partial differential equation with homogenous boundary conditions applied to bounded domain, method of separation of variables is a powerful tool. Separation of variables method works with the assumption that the solution is the product of functions of the independent variables.

2. **Point allocation method:** Method of point allocation is a simple and widely used approach. Although there is no theoretical foundation for point allocation, but due to the simplicity of the method, it is commonly used. The points are allocated based on requirements. In Chapters 2 and 4, in order to use free surface condition, we use point allocation choosing equidistant points on the free surface.

3. **Finite Hankel Transform:** If $f(r)$ is defined in $0 \leq r \leq a$, then Finite Hankel Transform of $f(r)$ of order m is defined by [11]

$$\mathcal{H}_m\{f(r)\} = \bar{f}_n(k_i) = \int_0^a r f(r) J_m(rk_i) dr,$$

where k_i is the transformed variable.

The inversion of finite Hankel transform is then defined by

$$\mathcal{H}_m^{-1}\{\bar{f}_n(k_i)\} = f(r) = \sum_{i=1}^{\infty} \bar{f}_n(k_i) \frac{J_m(rk_i)}{\bar{f}_{n+1}^2(ak_i)},$$

where summation is taken over all positive roots of $J_m(ak) = 0$. A basic operation property of finite Hankel transform is the derivative property which is very useful in finding solutions of differential equations in cylindrical polar coordinates. It is as follows:

$$\mathcal{H}_m\{f'(r)\} = \frac{k_i}{2m}[(m-1)\mathcal{H}_{m+1}\{f(r)\} - (m+1)\mathcal{H}_{m-1}\{f(r)\}], \qquad m \geq 1,$$

where $f(r)$ is finite at $r = 0$.

An important result involving Bessel differential operator is

$$\mathcal{H}_m\left\{\left(\nabla^2 - \frac{m^2}{r^2}\right) f(r)\right\} = -k_i^2 \bar{f}_n(k_i),$$

where ∇^2 is the Laplacian.

For $m = 1$, the finite Hankel transform of order 1 of a derivative is

$$\mathcal{H}_1\{f'(r)\} = -k_i \mathcal{H}_0\{f(r)\} = -k_i \bar{f}_0(k_i),$$

and

$$\mathcal{H}_1\Big\{f''(r) + \frac{1}{r}f'(r) - \frac{1}{r^2}f(r)\Big\} = -k_i^2 \bar{f}_1(k_i) - ak_i f(a) J_1'(ak_i).$$

The definition and the properties can be extended to functions of several variables.

4. **Eigenfunction expansion method:** Eigenfunction method is one of the most powerful methods to solve eigenvalue problems of mathematical physics. The eigenfunction expansion method is used to find particular solution for an eigenvalue problem which is quite similar to separation of variables method. The solution is written as an infinite series of eigenfunctions. In Chapters 3, 5 and 6, we use Fourier-Bessel series expansion across the interfaces.

5. **Perturbation method:** Perturbation methods are mathematical methods which are used to find an approximation of a solution to the problem. Perturbation methods works with the exact solution of a related problem. In perturbation method, solution is written in the form of a power series in a small parameter. The leading term of the power series in terms of small parameter is the exact solution of the related solvable problem and remaining terms are the perturbed solutions of the problem. Perturbation methods are used when a problem cannot be solved exactly in its present form. With the help of approximation of the solution, the problem gets converted into solvable problem.

   If Φ is the solution of any problem, then the series in a chosen small parameter ϵ is

   $$\Phi = \Phi_0 + \epsilon\Phi_1 + \epsilon^2\Phi_2 + \ldots,$$

   where Φ_0 is the solution of related solvable problem.

1.3.1 Some definitions

1. **Surface tension:** Surface tension is the property of liquids which enables liquid surface to acquire minimum surface area. Surface tension is a very important property of liquids. Surface tension can allow things to float on water which are denser than water. Surface tension is measured as force per unit length.

2. **Bond number:** Bond number is a dimensionless quantity which measures the importance of surface tension compared to body forces. Bond number is represented by the symbol *Bo*.

1.4 Outline of the thesis

This thesis is concerned with determining sloshing modes and sloshing frequencies of liquid inside circular cylindrical containers with different configurations. It is organized into seven chapters. Present chapter deals with the definition and cause of sloshing, applications in industry and limited literature review. The analytical approach to model the sloshing problem with basic linear water wave theory is also described in the present chapter.

In Chapter 2, we calculate the sloshing frequencies of liquid in a vertical annular cylindrical container with and without a rigid annular baffle placed at the free surface of the liquid. The effect of surface tension is also considered. The boundary value problem is solved by means of separation of variables method in fluid domain. To utilize the free surface condition and rigid baffle condition, point allocation method is used. We choose equidistant points some of which satisfy the baffle condition and rest all satisfy the free surface condition. Substitution of velocity potential for these two conditions at chosen points leads to a linear homogenous system in terms of an infinite series. A linear homogenous system is set up after truncating the infinite series upto a finite number of terms. The condition of non-trivial solution of linear homogeneous system gives us the frequency. We study the effects of baffle-width, fluid depth and surface tension on sloshing frequencies. It is observed that surface tension plays a significant role in the control of sloshing.

Chapter 3 is an extension of the work described in Chapter 2. In this chapter an annular rigid baffle is placed inside the fluid domain to investigate sloshing in a vertical annular cylindrical container. In order to solve the boundary value problem, the fluid domain is sub-divided into four sub-domains. To solve the boundary value problem in each sub-domain, artificial boundary conditions are imposed at the interfaces of the liquid sub-domains. Velocity potential in each sub-domain is obtained with the help of separation of variables method and superposition principle. Continuity of velocity and pressure is used at interfaces in terms of matching conditions which are used for a truncating series of solutions upto a finite number of terms. Fourier-Bessel series expansion method is used to eliminate the variables which leads to a linear homogenous system of equations in which the elements are coefficients of a Fourier-Bessel series. The condition of vanishing determinant of the matrix gives the value of non-dimensional frequency. We calculate the non-dimensional frequency for various values of fluid depth, baffle position, baffle-width and inner-outer radius ratio of the container.

In Chapter 4, in order to discuss sloshing in the presence of surface tension, we consider a vertical circular cylinder with a curved bottom. A rigid annular baffle is intro-

duced at the free surface. To describe sloshing in the cylinder, two cases are considered with a complete free surface and a partially covered free surface. The problem formulated here cannot be solved directly due to the uneven bottom of the container. The boundary value problem in the fluid domain is split into two boundary value problems by employing a perturbation technique. The velocity potentials for the two problems are found with the help of separation of variables method and finite Hankel transform. Non-dimensional frequency is evaluated by using point allocation method for the free surface condition with the same approach described in Chapter 2. Non-dimensional frequency is plotted against fluid-depth to container radius ratio, baffle-width for different values of Bond number.

Chapter 5 is concerned with describing the interfacial waves in a two-fluid system. A vertical circular cylindrical container filled with two inviscid and immiscible fluids with different densities is considered to describe sloshing. The velocity potentials for both fluids are obtained with the approach used in Chapter 3. Matching conditions for continuity and pressure are used at the interface of the two fluids. Matching conditions along with free surface condition satisfied by upper fluid forms a linear homogenous system of equations which is used to calculate non-dimensional frequency. The effect of upper fluid height, lower fluid depth and density ratio have been investigated on sloshing. A comparison study is also done by considering a single-layer fluid problem and reducing the two-layer fluid into a single-layer fluid taking upper fluid height as zero.

Chapter 6 is an extension of the work described in Chapter 5. Here we consider the same geometry considered above with the introduction of a rigid annular baffle at the free surface which reduces the extent of the free surface. The free surface condition due to the presence of the baffle is now converted into equations as a baffle condition and a reduced free surface condition. The fluid domain is divided into sub-domains to get the potentials in the sub-domains. The sloshing frequencies are computed with the same approach used above. After obtaining the potentials in each sub-domain, matching conditions are used to maintain continuity of pressure and velocity across the surface of separation of the two fluids and successive interfaces. Matching conditions, along with the free surface condition, lead to a homogenous system. The effect of upper fluid height, lower fluid depth, density ratio and baffle on sloshing are investigated.

At the end, Chapter 7 highlights a brief summary of the work presented in this thesis and puts forward some future scopes of investigation of sloshing problems under various conditions.

Chapter 2

Linear sloshing frequencies in the annular region of a circular cylindrical container in presence of a baffle

2.1 Introduction

A partly covered free surface shifts the natural frequency above and away from the control frequency of the vehicle, in which the liquid-filled container is placed, which results in the reduction of sloshing mass participating in the dynamic motion of the system. The fundamental natural frequency of an inviscid and incompressible liquid is determined for increasing width of the baffle which is attached to the outer tank wall at the free surface. It is observed that by increasing the width of the baffle, natural frequencies can be significantly increased. Investigations are also carried out for different values of Bond number which depicts the different states of surface tension and for varying values of the part of the radius in the fluid region. It is also observed that by increasing the fluid height inside the container, the natural frequencies can be increased which results in reduction of sloshing.

2.2 Statement and formulation of the problem

An incompressible and inviscid fluid is assumed to perform irrotational motion in the annular region between two coaxial vertical circular cylinders with a common base. The radius of the inner cylinder is taken as R_1 and that of the outer cylinder as R_2. The annular region of the cylinder is filled with a liquid upto a constant height h. We introduce a rigid annular baffle at the free surface mounted on the cylindrical wall $r = R_2$ such that the width of the free surface becomes αR_2, $0 \leq \alpha \leq 1 - (R_1/R_2)$. Cylindrical coordinate system (r, θ, z) is considered in which z is measured vertically upwards from

the undisturbed water level $z = 0$ with the origin on it (Fig. 2.1). It is to be noted that any such arrangement of partial covering of the free surface exhibits an increase of the natural frequencies as well as a reduction of the participating sloshing mass. The geometry considered in the problem is shown in Fig. 2.1 below.

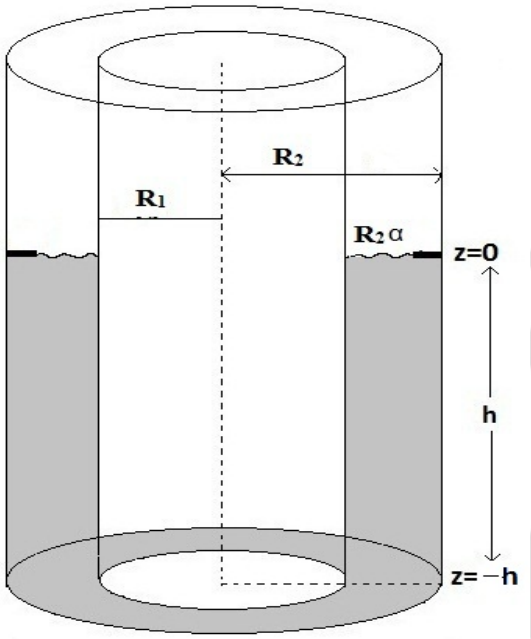

Figure 2.1: Schematic diagram for the problem

The boundary value problem (BVP) for the sloshing problem in the cylindrical container is given by Laplace's equation

$$\nabla^2\Phi(r,\theta,z,t) = 0, \quad R_1 < r < R_2, \quad 0 \le \theta \le 2\pi, \quad -h < z < 0, \tag{2.1}$$

i.e.,

$$\frac{\partial^2\Phi}{\partial r^2} + \frac{1}{r}\frac{\partial\Phi}{\partial r} + \frac{1}{r^2}\frac{\partial^2\Phi}{\partial\theta^2} + \frac{\partial^2\Phi}{\partial z^2} = 0, \quad R_1 < r < R_2, \quad 0 \le \theta \le 2\pi, \quad -h < z < 0, \tag{2.2}$$

with the boundary wall conditions

$$\frac{\partial\Phi}{\partial r} = 0, \quad r = R_1 \quad \text{and} \quad r = R_2, \tag{2.3}$$

and bottom boundary condition

$$\frac{\partial\Phi}{\partial z} = 0, \quad z = -h. \tag{2.4}$$

In addition, there are impermeable conditions to be satisfied due to the presence of the baffle at the free surface:

(i)

$$\frac{\partial \Phi}{\partial z} = 0, \quad z = 0, \quad R_1 + R_2\alpha \leq r \leq R_2. \tag{2.5}$$

The condition at $z = 0$ in the range $R_1 < r < R_1 + R_2\alpha$ is obtained from the kinematic condition

$$\frac{\partial \Phi}{\partial z} = \frac{\partial \eta}{\partial t}, \tag{2.6}$$

and the dynamic boundary condition with surface tension:

$$\frac{\partial \Phi}{\partial t} + g\eta - \frac{\sigma}{\rho}\left[\frac{\partial^2 \eta}{\partial r^2} + \frac{1}{r}\frac{\partial \eta}{\partial r} + \frac{1}{r^2}\frac{\partial^2 \eta}{\partial \theta^2}\right] = \text{constant}, \tag{2.7}$$

where $\eta(r, \theta, t)$ is the free surface elevation, σ the surface tension, ρ the constant mass density and g the gravitational constant. Equations (2.6) and (2.7) can be combined to get the free surface condition as

(ii)

$$\frac{\partial^2 \Phi}{\partial t^2} + g\frac{\partial \Phi}{\partial z} + \frac{\sigma}{\rho}\frac{\partial^3 \Phi}{\partial z^3} = 0 \quad \text{at} \quad z = 0, \quad R_1 < r < R_1 + R_2\alpha. \tag{2.8}$$

Due to the presence of the annular baffle at the wall, the upper surface condition is split as Eqs. (2.5) and (2.8), respectively, at the baffle and at the reduced free surface.

2.3 Method of solution

In order to solve the BVP, we apply the separation of variables method to governing equation (2.1) by assuming a solution of the form

$$\Phi(r, \theta, z, t) = R(r)Z(z)\exp\{\iota(m\theta + \omega t)\}. \tag{2.9}$$

We know that the governing equation gets converted to two ordinary differential equations - one each in r and z, the solutions of which can be found as

$$R(r) = AJ_m(kr) + BY_m(kr),$$

and

$$Z(z) = C\cosh kz + D\sinh kz,$$

where $J_m(kr)$ and $Y_m(kr)$ are Bessel functions of the first and second kind, respectively, of order m.

Using boundary conditions (2.3) and (2.4), the velocity potential is obtained as

$$\Phi(r, \theta, z, t) = \sum_{m=0}^{\infty}\sum_{n=1}^{\infty} A_{mn}\frac{\cosh\left\{\frac{k_{mn}}{R_2}(z+h)\right\}}{\cosh\left(\frac{k_{mn}}{R_2}h\right)}\left\{\frac{J_m(\frac{k_{mn}}{R_2}r)Y_m'(k_{mn}) - J_m'(k_{mn})Y_m(\frac{k_{mn}}{R_2}r)}{Y_m'(k_{mn})}\right\} \times \exp\{\iota(m\theta + \omega t)\}, \tag{2.10}$$

where k_{mn} are the zeros of

$$J'_m\left(k_{mn}\frac{R_1}{R_2}\right)Y'_m(k_{mn}) - J'_m(k_{mn})Y'_m\left(k_{mn}\frac{R_1}{R_2}\right) = 0, \tag{2.11}$$

with $'$ denoting differentiation with respect to r. These zeros are evaluated based on a method devised by Sorolla et al. [41]. The same procedure is followed in the subsequent chapters while dealing with roots of such equations. The coefficients A_{mn} and the angular frequency ω appearing in Eq. (2.10) are still not known. After introducing an annular baffle at the free surface mounted on the wall of the outer cylinder, for a fixed angular mode m, we choose N_1+1 points including the end points in $R_1 + R_2\alpha \leq r \leq R_2$ at the free surface so as to get the impermeability condition split from the free surface condition as

$$\sum_{n=1}^{N_1+N_2}\frac{A_{mn}}{Y_m(k_{mn})}\frac{k_{mn}}{R_2}\tanh\left(k_{mn}\frac{h}{R_2}\right)\times\left[J_m\left\{k_{mn}\left(\alpha+\frac{R_1}{R_2}+\frac{(1-\alpha-\frac{R_1}{R_2})n_1}{N_1}\right)\right\}\right.$$
$$\left.Y'_m(k_{mn}) - Y_m\left\{k_{mn}\left(\alpha+\frac{R_1}{R_2}+\frac{(1-\alpha-\frac{R_1}{R_2})n_1}{N_1}\right)\right\}J'_m(k_{mn})\right] = 0 \tag{2.12}$$

for $n_1 = 0, 1, 2, ...N_1$,
and choose $N_2 - 1$ points satisfying the reduced free surface condition

$$\sum_{n=1}^{N_1+N_2}\frac{A_{mn}}{Y'_m(k_{mn})}\left[J_m\left\{k_{mn}\left(\frac{R_1}{R_2}+\frac{\alpha n_2}{N_2}\right)\right\}Y'_m(k_{mn}) - Y_m\left\{k_{mn}\left(\frac{R_1}{R_2}+\frac{\alpha n_2}{N_2}\right)\right\}\right.$$
$$\left.\times J'_m(k_{mn})\right]\times\left[\omega^2 - \left\{g\frac{k_{mn}}{R_2}+\frac{\sigma}{\rho}\left(\frac{k_{mn}}{R_2}\right)^3\right\}\tanh\left(k_{mn}\frac{h}{R_2}\right)\right] = 0 \tag{2.13}$$

for $n_2 = 1, 2, ...N_2 - 1$.
Equations (2.12) and (2.13) represent N_1+N_2 homogenous algebraic equations in the coefficients $A_{m1}, A_{m2}, \ldots, A_{m\ N_1+N_2}$. The condition of nonzero solution for a homogeneous system, due to truncation up to a finite number of points, gives rise to the frequency equation for the determination of sloshing frequencies of the liquid in the container.

2.4 Numerical results and discussion

Our main aim is to find the relevant frequency equation for different values of R_1 and R_2. After obtaining the semi-analytical solution, we proceed to evaluate numerically the fundamental sloshing frequencies. For an annular baffle of width $w = R_2(1-\alpha) - R_1$, $0 < \alpha \leq 1-(R_1/R_2)$, covering the free surface, we consider different cases and determine

the sloshing frequencies for the lowest mode m. We examine the effect of baffle-width, liquid height as well as surface tension on sloshing frequencies. For $\alpha = 1 - (R_1/R_2)$, there is no baffle inserted at the free surface. We evaluate the fundamental frequency ω^*_{mn} by non-dimensionalising the frequency equation as

$$\omega^{*2}_{mn} = \frac{\omega^2_{mn}}{g/R_2} = k_{mn}\left(1 + \frac{k^2_{mn}}{Bo}\right)\tanh\left(k_{mn}\frac{h}{R_2}\right), \tag{2.14}$$

where the Bond number $Bo = (\rho g R_2^2)/\sigma$ is taken as 100 for various α values. We evaluate frequencies for the angular mode $m = 1$ and $n = 1$, i.e., for ω^*_{11} which is determined from the values k_{11} from Eq. (2.11). The lower modes are the modes which exhibit the larger sloshing mass participating in the slosh phenomenon.

2.4.1 Case I: $R_2/R_1 = 2$, relevant upper surface conditions and numerical results:

Here we consider the radius of the inner cylinder as half of that of the outer cylinder, i.e., in this case $\alpha \in (0, \frac{1}{2}]$. Consequently Eqs. (2.12) and (2.13) reduce to

$$\sum_{n=1}^{N_1+N_2} \frac{A_{mn}}{Y_m(k_{mn})}\frac{k_{mn}}{R_2}\tanh\left(k_{mn}\frac{h}{R_2}\right) \times \left[J_m\left\{k_{mn}\left(\alpha + \frac{1}{2} + \frac{(\frac{1}{2}-\alpha)n_1}{N_1}\right)\right\}Y'_m(k_{mn}) - Y_m\left\{k_{mn}\left(\alpha + \frac{1}{2} + \frac{(\frac{1}{2}-\alpha)n_1}{N_1}\right)\right\}J'_m(k_{mn})\right] = 0 \tag{2.15}$$

for $n_1 = 0, 1, 2, ...N_1$,
and

$$\sum_{n=1}^{N_1+N_2} \frac{A_{mn}}{Y'_m(k_{mn})}\left[J_m\left\{k_{mn}\left(\frac{1}{2} + \frac{\alpha n_2}{N_2}\right)\right\}Y'_m(k_{mn}) - Y_m\left\{k_{mn}\left(\frac{1}{2} + \frac{\alpha n_2}{N_2}\right)\right\}J'_m(k_{mn})\right] \times \left[\omega^2 - \left\{g\frac{k_{mn}}{R_2} + \frac{\sigma}{\rho}\left(\frac{k_{mn}}{R_2}\right)^3\right\}\tanh\left(k_{mn}\frac{h}{R_2}\right)\right] = 0 \tag{2.16}$$

for $n_2 = 1, 2, ...N_2 - 1$.
Here we determine the dimensionless fundamental sloshing frequency as a function of liquid height ratio h/R_2 for a fixed Bond number and for various α values as shown in Fig. 2.2. Curves shown in Fig. 2.2 are plotted for the lowest sloshing mode $\omega^*_{11}(m = 1, n = 1)$, which exhibits the largest sloshing mass participating in the motion. The curve for $w/R_2 = 0$ corresponds to the free surface in its entirety, i.e., there is no baffle on the free surface. Curves are drawn for various α values in increasing order of baffle-width w/R_2.

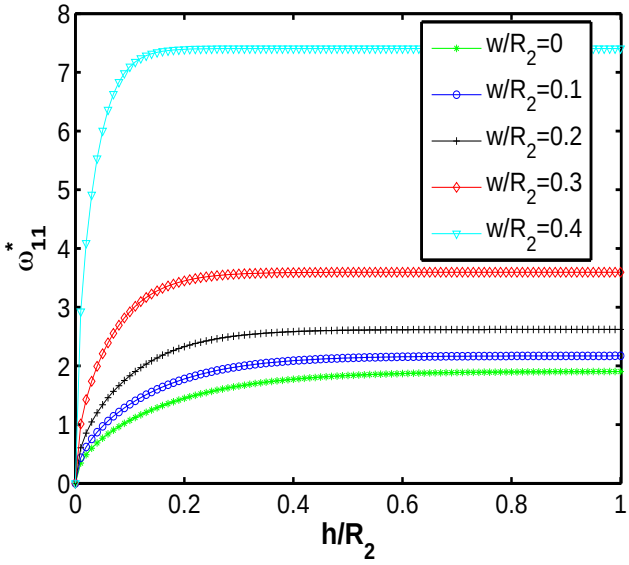

Figure 2.2: Sloshing frequency $\omega_{11}^*(m=1,n=1)$ for different annular baffles of width $(w=(\frac{1}{2}-\alpha)R_2)$ vs height ratio h/R_2 for $Bo=100$;

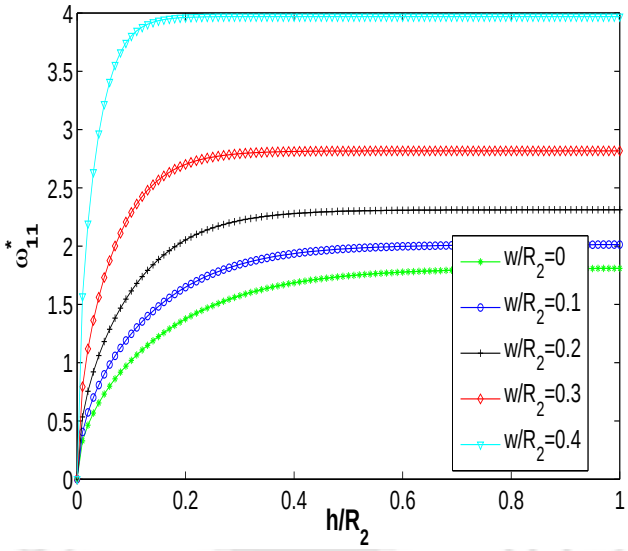

Figure 2.3: Sloshing frequency for $\omega_{11}^*(m=1,n=1)$ different annular baffles of width $(w=(\frac{1}{2}-\alpha)R_2)$ vs height ratio h/R_2 without surface tension σ

We choose the intermediate value of Bond number $Bo=(\rho g R_2^2)/\sigma=100$ which includes the effect of surface tension. A baffle with width of about $w=0.3a$ doubles the fundamental natural frequency. For very small values of h/R_2, dimensionless frequency ω_{11}^* increases rapidly and then for higher values, it becomes stable. For the baffle-width $w=0.4R_2$, ω_{11}^* becomes twice as much as for the baffle-width $w=0.3R_2$. The value of ω_{11}^* for the baffle-width $w=0.4R_2$ is much higher as compared to when there is no baffle at the free surface. We observe that the natural frequency ω_{11}^* increases with increasing

baffle-width as well as for increasing height ratio h/R_2.

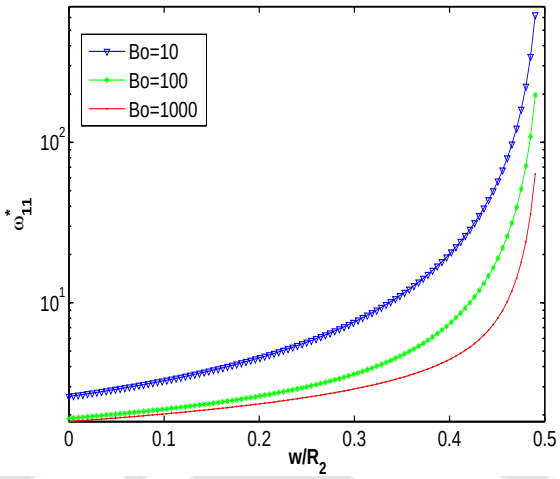

Figure 2.4: Effect of baffle-width $w/R_2 = (\frac{1}{2} - \alpha)$ on $\omega^*_{11}(m = 1, n = 1)$ at height ratio $h/R_2 = 1$ for different Bond numbers

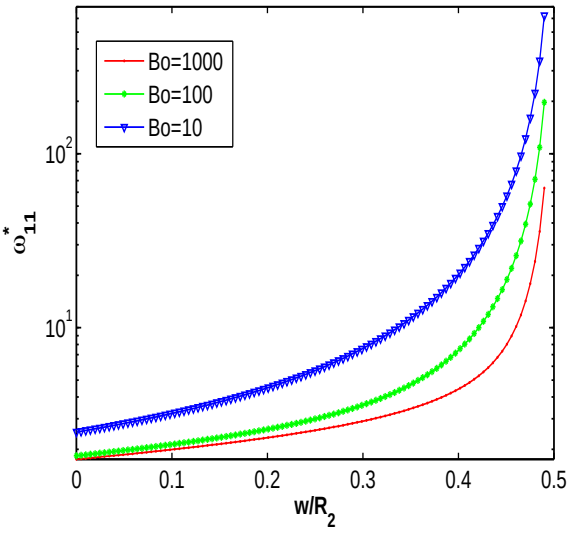

Figure 2.5: Effect of baffle-width $w/R_2 = (\frac{1}{2} - \alpha)$ on $\omega^*_{11}(m = 1, n = 1)$ at height ratio $h/R_2 = \frac{1}{2}$ for different Bond numbers

Figure 2.3 shows the curves drawn for ω^*_{11} as a function of liquid height ratio h/R_2 for various α values in which surface tension σ is assumed to be absent. It is observed that for various α values, the effect of baffle-width remains the same resulting in reduced sloshing frequency. In the absence of surface tension, sloshing is observed to be more. For the annular baffle-width $w = 0.4R_2$, ω^*_{11} is reduces to nearly half as compared to ω^*_{11} with surface tension σ. It is observed that the natural frequency reduces in this case,

i.e., without surface tension the natural frequency is less in comparison to what we get with the one in which Bond number $Bo = 100$ was considered.

In Figs. 2.4 and 2.5, we show the dimensionless fundamental sloshing frequency as a function of the magnitude of the annular baffle-width $w/R_2 = 1/2 - \alpha$ for fixed liquid height ratio $h/R_2 = 1, 1/2$, respectively, for different Bond numbers $Bo = 10, 100, 1000$. Here it is observed that frequency increases when the value of Bond number decreases, i.e., when surface tension increases.

Figures $2.2 - 2.5$ establish that natural frequency increases with increasing baffle-width, increasing height ratio and with decreasing Bond number.

2.4.2 Case II: $R_2/R_1 = 3$, relevant upper surface conditions and numerical results:

Here we consider the radius of the inner cylinder as one third of that of the outer cylinder, i.e., in this case $\alpha \in (0, \frac{2}{3}]$. Consequently Eqs. (2.12) and (2.13) reduce to

$$\sum_{n=1}^{N_1+N_2} \frac{A_{mn}}{Y_m(k_{mn})} \frac{k_{mn}}{R_2} \tanh\left(k_{mn}\frac{h}{R_2}\right) \left[J_m\left\{k_{mn}\left(\alpha + \frac{1}{3} + \frac{(\frac{2}{3}-\alpha)n_1}{N_1}\right)\right\} Y'_m(k_{mn}) - Y_m\left\{k_{mn}\left(\alpha + \frac{1}{3} + \frac{(\frac{2}{3}-\alpha)n_1}{N_1}\right)\right\} J'_m(k_{mn})\right] = 0 \tag{2.17}$$

for $n_1 = 0, 1, 2, ...N_1$,
and

$$\sum_{n=1}^{N_1+N_2} \frac{A_{mn}}{Y'_m(k_{mn})} \left[J_m\left\{k_{mn}\left(\frac{1}{3} + \frac{\alpha n_2}{N_2}\right)\right\} Y'_m(k_{mn}) - Y_m\left\{k_{mn}\left(\frac{1}{3} + \frac{\alpha n_2}{N_2}\right)\right\} J'_m(k_{mn})\right] \times \left[\omega^2 - \left\{g\frac{k_{mn}}{R_2} + \frac{\sigma}{\rho}\left(\frac{k_{mn}}{R_2}\right)^3\right\} \tanh\left(k_{mn}\frac{h}{R_2}\right)\right] = 0 \tag{2.18}$$

for $n_2 = 1, 2, ...N_2 - 1$.

Here also we determine the dimensionless fundamental sloshing frequency as a function of liquid height ratio h/R_2 for a fixed Bond number and for various α values as shown in Fig. 2.6. Curves shown in Fig. 2.6 are plotted for the lowest sloshing mode $\omega^*_{11}(m = 1, n = 1)$. Dimensionless fundamental sloshing frequency ω^*_{11} increases smoothly with increasing height ratio h/R_2 for various α values and fixed Bond number $Bo = 100$.

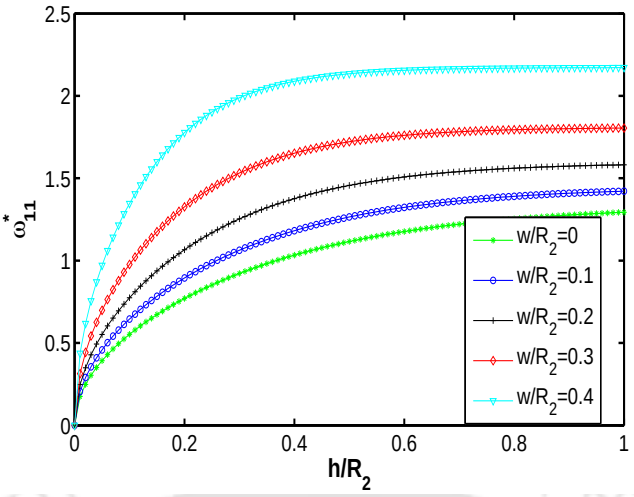

Figure 2.6: Sloshing frequency $\omega^*_{11}(m = 1, n = 1)$ for different annular baffles of width $(w = (\frac{2}{3} - \alpha)R_2)$ vs height ratio h/R_2 for $Bo = 100$

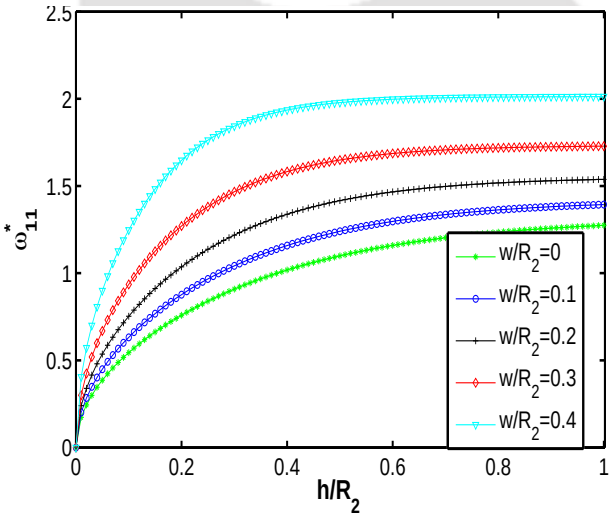

Figure 2.7: Sloshing frequency $\omega^*_{11}(m = 1, n = 1)$ for different annular baffles of width $(w = (\frac{2}{3} - \alpha)R_2)$ vs height ratio h/R_2 without surface tension σ

A baffle with width of about $w = 0.4R_2$ doubles the fundamental natural frequency. Frequency attains higher values corresponding to higher values of height ratio h/R_2. By comparison with Fig. 2.2, where $R_2/R_1 = 2$, here the values of natural frequency are smaller which implies that the sloshing mass will be higher. In the earlier case the frequencies doubled even for an increase of baffle-width 0.1 whereas in this case this doubling occurs when an increase of $w/R_2 = 0.4$ takes place.

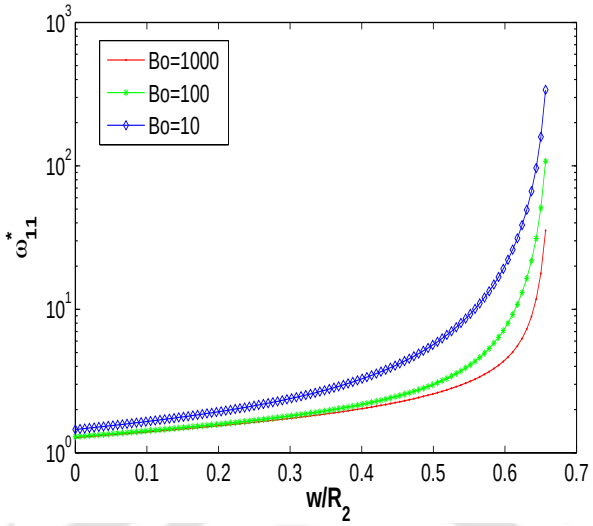

Figure 2.8: Effect of baffle-width $w/R_2 = (\frac{2}{3} - \alpha)$ on $\omega^*_{11}(m = 1, n = 1)$ at height ratio $h/R_2 = 1$ for different Bond numbers

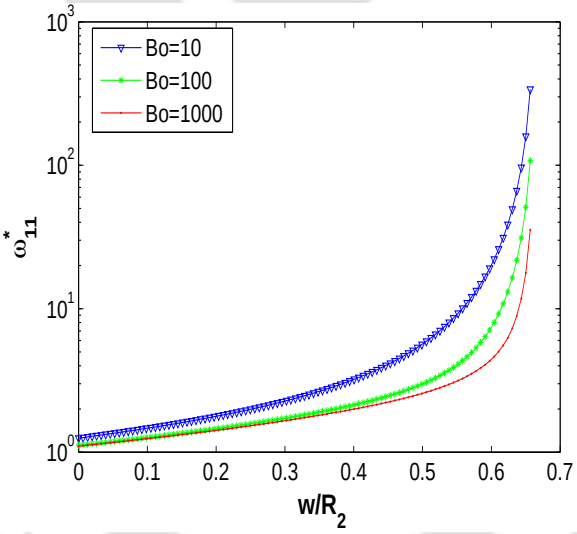

Figure 2.9: Effect of baffle-width $w/R_2 = (\frac{2}{3} - \alpha)$ on $\omega^*_{11}(m = 1, n = 1)$ at height ratio $h/R_2 = \frac{1}{2}$ for different Bond numbers

Figure 2.7 shows the curves drawn for ω^*_{11} as a function of liquid height ratio h/R_2 for various α values in which surface tension σ is assumed to be absent. It is observed that for various α values, the effect of baffle-width remains the same resulting in reduced sloshing frequency. In the absence of surface tension, sloshing is observed to be more. It is observed that frequency reduces in this case, i.e., without surface tension the natural frequency reduces in comparison with the case when $Bo = 100$.

In Figs. 2.8 and 2.9, we show the dimensionless fundamental sloshing frequency as a function of the magnitude of the annular baffle-width $w/R_2 = 2/3 - \alpha$ for fixed liquid

height ratio $h/R_2 = 1, 1/2$, respectively, for different Bond numbers $Bo = 10, 100, 1000$. Here it is observed that frequency increases when the value of Bond number decreases, i.e., when surface tension increases. Figures $2.6 - 2.9$ establish that frequency increases with increasing baffle-width, increasing height ratio and with decreasing Bond number.

2.4.3 Case III: $R_2/R_1 = 4$, relevant upper surface conditions and numerical results:

Here we consider the radius of the inner cylinder as one fourth of that of the outer cylinder, i.e., in this case $\alpha \in (0, \frac{3}{4}]$. Consequently Eqs. (2.12) and (2.13) reduce to

$$\sum_{n=1}^{N_1+N_2} \frac{A_{mn}}{Y_m(k_{mn})} \frac{k_{mn}}{R_2} \tanh\left(k_{mn}\frac{h}{R_2}\right) \times \left[J_m\left\{k_{mn}\left(\alpha + \frac{1}{4} + \frac{(\frac{3}{4}-\alpha)n_1}{N_1}\right)\right\} Y'_m(k_{mn}) - Y_m\left\{k_{mn}\left(\alpha + \frac{1}{4} + \frac{(\frac{3}{4}-\alpha)n_1}{N_1}\right)\right\} J'_m(k_{mn})\right] = 0 \tag{2.19}$$

for $n_1 = 0, 1, 2, ...N_1$,
and

$$\sum_{n=1}^{N_1+N_2} \frac{A_{mn}}{Y'_m(k_{mn})} \left[J_m\left\{k_{mn}\left(\frac{1}{4} + \frac{\alpha n_2}{N_2}\right)\right\} Y'_m(k_{mn}) - Y_m\left\{k_{mn}\left(\frac{1}{4} + \frac{\alpha n_2}{N_2}\right)\right\} J'_m(k_{mn})\right] \times \left[\omega^2 - \left\{g\frac{k_{mn}}{R_2} + \frac{\sigma}{\rho}\left(\frac{k_{mn}}{R_2}\right)^3\right\} \tanh\left(k_{mn}\frac{h}{R_2}\right)\right] = 0 \tag{2.20}$$

for $n_2 = 1, 2, ...N_2 - 1$.

Here we again determine the dimensionless fundamental sloshing frequency as a function of liquid height ratio h/R_2 for a fixed Bond number and for various α values as shown in Fig. 2.10. Curves shown in Fig. 2.10 are plotted for the lowest sloshing mode $\omega^*_{11}(m = 1, n = 1)$, which exhibits the largest sloshing mass participating in the motion. Dimensionless fundamental sloshing frequency ω^*_{11} increases rapidly with increasing height ratio h/R_2 for various α values and fixed Bond number $Bo = 100$.

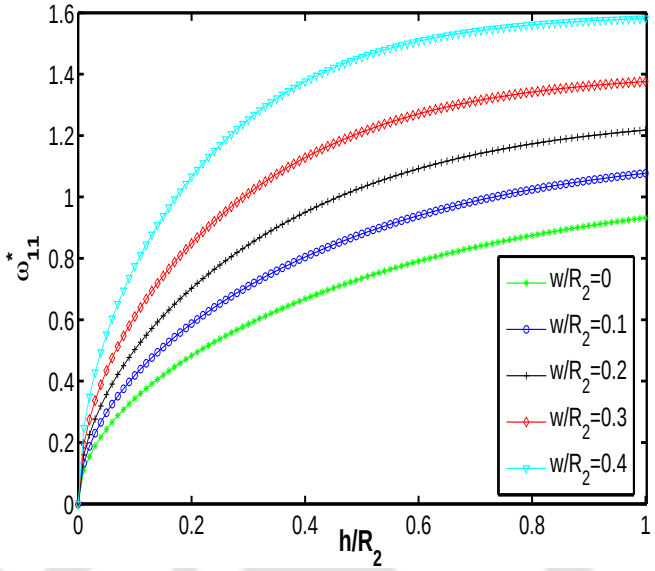

Figure 2.10: Sloshing frequency $\omega_{11}^*(m=1,n=1)$ for different annular baffles of width $(w=(\frac{3}{4}-\alpha)R_2)$ vs height ratio h/R_2 for $Bo=100$

A baffle with width of about $w=0.4R_2$ doubles the fundamental natural frequency, i.e., for the case when $w/R_2=0$. Frequency changes to higher values corresponding to the higher values of height ratio h/R_2. Frequency also increases continuously with increasing values of baffle-width.

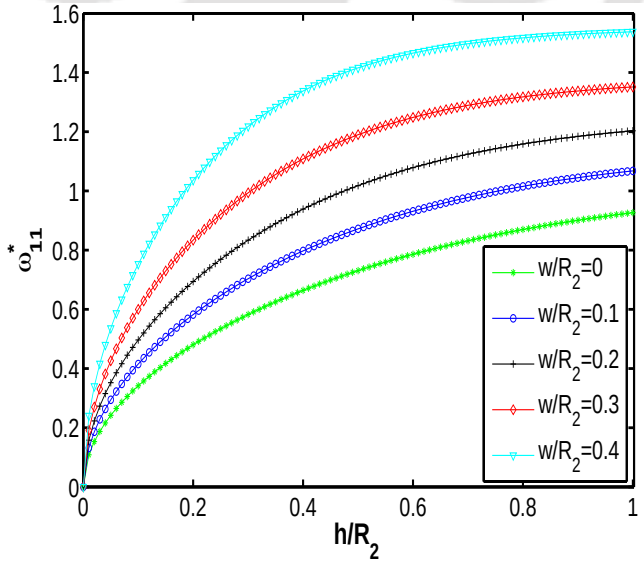

Figure 2.11: Sloshing frequency $\omega_{11}^*(m=1,n=1)$ for different annular baffles of width $(w=(\frac{3}{4}-\alpha)R_2)$ vs height ratio h/R_2 without surface tension σ

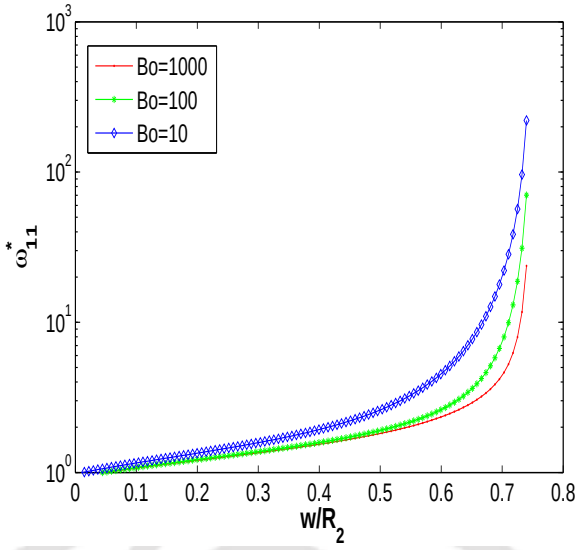

Figure 2.12: Effect of baffle-width $w/R_2 = (\frac{3}{4} - \alpha)$ on $\omega^*_{11}(m = 1, n = 1)$ at height ratio $h/R_2 = 1$ for different Bond numbers

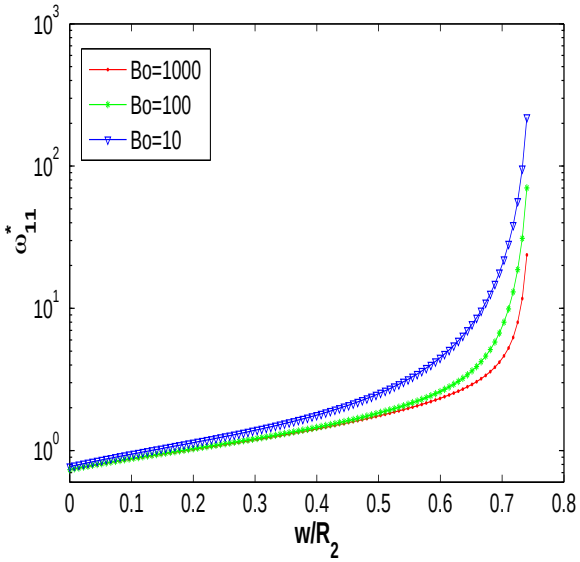

Figure 2.13: Effect of baffle-width $w/R_2 = (\frac{3}{4} - \alpha)$ on $\omega^*_{11}(m = 1, n = 1)$ at height ratio $h/R_2 = \frac{1}{2}$ for different Bond numbers

Figure 2.11 shows the curves drawn for ω^*_{11} as a function of liquid height ratio h/R_2 for various α values in which surface tension σ is assumed to be absent. It is observed that for various α values, the effect of baffle-width remains the same resulting in reduced sloshing frequency. In the absence of surface tension, sloshing is observed to be more. For the baffle-width $w = 0.4R_2$, ω^*_{11} is twice as compared to the value when there is no baffle on the free surface. It is observed that frequency reduces without surface tension.

In Figs. 2.12 and 2.13, we show the dimensionless fundamental sloshing frequency as

a function of the magnitude of the annular baffle-width $w/R_2 = 3/4 - \alpha$ for fixed liquid height ratio $h/R_2 = 1, 1/2$, respectively, for different Bond numbers $Bo = 10, 100, 1000$. Here it is observed that frequency increases when the value of Bond number decreases, i.e., when surface tension increases. Figures 2.10−2.13 establish that frequency increases with increasing baffle-width, increasing height ratio and with decreasing Bond number.

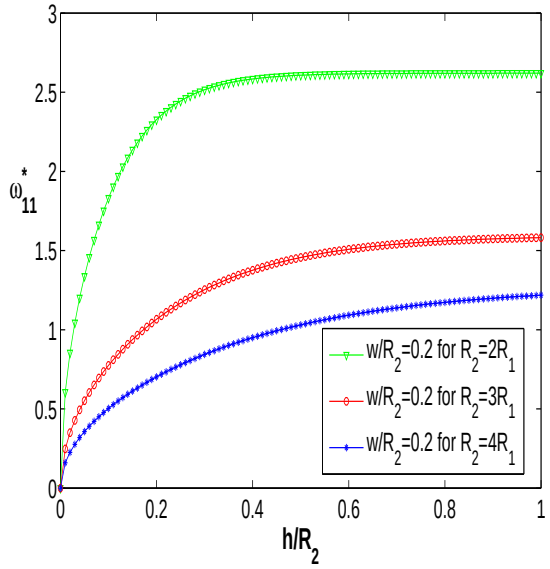

Figure 2.14: Sloshing frequency $\omega_{11}^*(m = 1, n = 1)$ for different cases with an annular baffle of width $(w = 0.2R_2)$ vs height ratio h/R_2 for $Bo = 100$

2.4.4 Comparison of all cases:

We want to sum up the effect of the sloshing frequency due to the changing fluid domain for different R_2/R_1 ratios.

In Fig. 2.14, curves are drawn for the fixed baffle-width $w/R_2 = 0.2$ for various cases of R_2/R_1. For the case $R_2 = 2R_1$, frequency is more than twice as compared to the frequency for $R_2 = 4R_1$. ω_{11}^* is nearly twice for $R_2 = 2R_1$ as compared to ω_{11}^* for $R_2 = 3R_1$. It is observed that for $R_2 = 2R_1$, frequency becomes stable as liquid height ratio h/R_2 increases which is not significant in the other two cases. After comparing all three cases, sloshing is observed to be more when free surface is wider for a fixed baffle-width. That is, sloshing is more when R_2 is much greater than R_1. In this case, the best option is to increase the baffle-width so as to reduce the free surface and also to have the container filled with more volume of liquid at the same time.

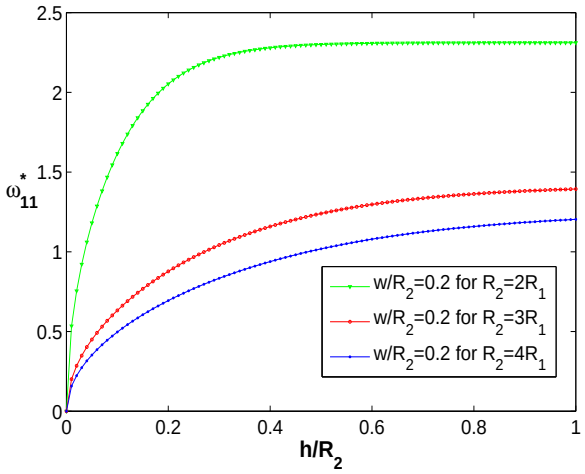

Figure 2.15: Sloshing frequency $\omega^*_{11}(m = 1, n = 1)$ for different cases with an annular baffle of width $(w = 0.2R_2)$ vs height ratio h/R_2 without surface tension σ

Figure 2.15 shows the curves drawn for ω^*_{11} as a function of liquid height ratio h/R_2 for fixed baffle-width $w/R_2 = 0.2$ for various cases which are considered in which surface tension σ is assumed to be absent. It is observed that the effect of baffle-width remains the same resulting in reduced sloshing frequency. In the absence of surface tension, sloshing is observed to be more.

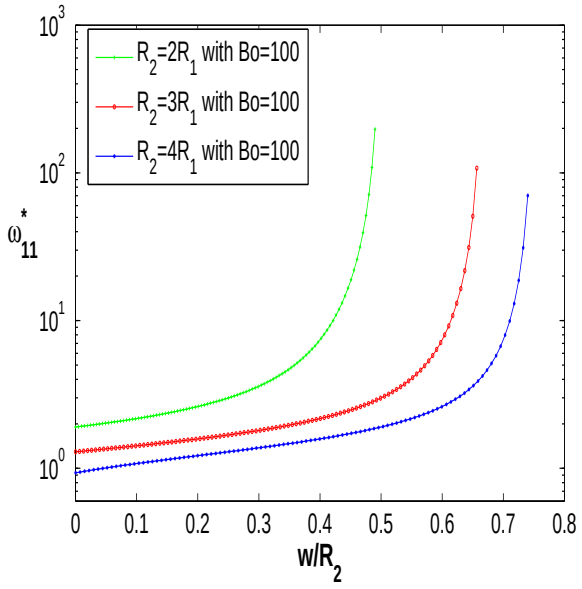

Figure 2.16: Effect of baffle-width $w/R_2 = (1 - \alpha) - \frac{R_1}{R_2}$ on $\omega^*_{11}(m = 1, n = 1)$ at height ratio $h/R_2 = 1$ for Bond number $Bo = 100$

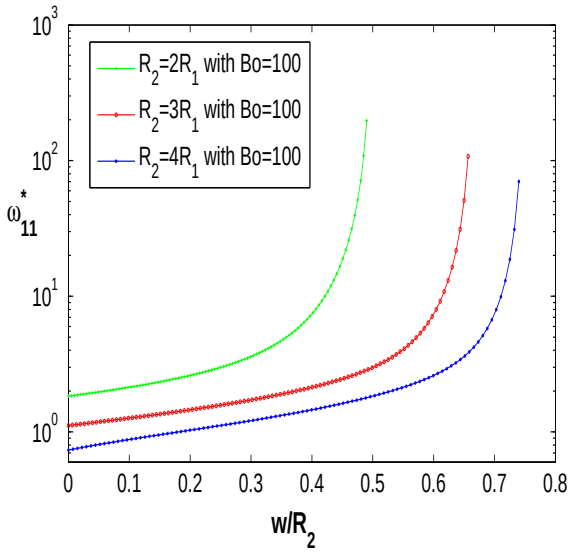

Figure 2.17: Effect of baffle-width $w/R_2 = (1-\alpha) - \frac{R_1}{R_2}$ on $\omega^*_{11}(m=1, n=1)$ at height ratio $h/R_2 = \frac{1}{2}$ for Bond number $Bo = 100$

In Figs. 2.16 and 2.17, curves are drawn for all cases, for fixed height ratio $h/R_2 = 1, 1/2$, respectively, corresponding to a fixed Bond number $Bo = 100$. For the case $R_2 = 2R_1$, frequency is very high as compared to the other cases. For the case $R_2 = 3R_1$, ω^*_{11} is higher than that for the case $R_2 = 4R_1$. Curves show that for fixed height ratio h/R_2, frequency increases as baffle-width increases. For $R_2 = 2R_1$, frequency increases at a very high rate as compared to the other cases. For wider free surface, sloshing is observed to be more. Figures $2.14 - 2.17$ show that frequency increases with increasing baffle-width as well as with increasing height ratio, i.e., frequency increases with decreasing free surface. These results suggest us to use such a cylindrical container so that sloshing is less but at the same time more fluid can be filled.

It is to be noted that the free surface and its baffle conditions were usually satisfied at $N_1 + N_2 = 10$ equidistantly distributed points. Further, if this whole investigation is carried out by placing the baffle on the outside wall of the inner cylinder, it is still possible to obtain similar results.

2.5 Conclusions

In this work, we consider a circular cylindrical container of specific size in which fluid is filled in the annular region of the container. We introduce an annular baffle mounted on the wall of the outer cylinder at the free surface. We investigate the sloshing frequencies for different baffle-width, fluid height and radial values of the annular region. Result shows the dependence of sloshing frequencies on baffle-width as well as on liquid height

ratio. It is shown that fundamental sloshing frequency increases when baffle-width increases. It is clear that when an annular baffle is introduced at the container wall in the free liquid surface plane, it yields increased natural frequencies. Partial coverage of the free surface has a beneficial effect on the system. It is also shown that in presence of surface tension, frequency increases. Three different cases are solved numerically for increasing ring baffle with fixed Bond number $Bo = 100$. We also investigate the sloshing frequencies against baffle-width for different Bond numbers. Fundamental sloshing frequency increases gradually as baffle-width as well as liquid height ratio increase. It is shown that the liquid sloshing frequency inside the container decreases with the increasing baffle-width for a constant height ratio $h/R_2 = 1$. As the natural frequency increases, the sloshing mass decreases thereby bringing stability to the overall structure including the vehicle in which the liquid container is being transported. In other words, the annular baffle plays a very important role on the sloshing frequency of liquid. It is found that even for larger radius values for the fluid domain, sloshing can be controlled by inserting wider annular baffles accordingly. The method presented here is expected to be easily applicable to any structural system in the free surface plane.

Chapter 3

Sloshing frequencies in an annular region of a rigid circular container with a baffle placed inside liquid

3.1 Introduction

For a specially designed circular cylindrical container filled with an inviscid, incompressible and homogenous liquid, if an annular baffle is attached to the outer cylinder wall in the annular region of the cylinder at some depth, the natural frequencies and the response of the liquid in the container undergo a drastic change. Such an introduction of a baffle divides the liquid region into four. Boundary value problems are set up for the potential in each of these regions, and with the help of the matching conditions across the virtual interfaces, we set up a system of linear equations by solving which we determine the natural frequencies. A partly covered interface shifts the natural frequency above and away from the control frequency of the vehicle, in which the liquid-filled container is placed, which results in the reduction of sloshing mass participating in the dynamic motion of the system. The fundamental natural frequency of the liquid is determined for different width and positions of the baffle in addition to different configurations. It is observed that the effect of baffle position on frequency is non-monotonic. It is also observed that when a baffle is placed nearer to the free surface, it has a greater significance on frequency. It is observed that frequency decreases with increasing baffle depth. The effect of the inner radius of the baffle on frequency is almost monotonic while with increasing inner radius of container, frequency increases monotonically. All our observations are supported by relevant graphs.

3.2 Statement and formulation of the problem

An incompressible and inviscid fluid is assumed to perform irrotational motion in the annular region between two coaxial vertical circular cylinders with a common base. The radius of the inner cylinder is taken as R_1 and that of the outer cylinder as R_2. The annular region of the cylinder is filled with a fluid of uniform density ρ up to a constant height h_2. A thin rigid annular baffle is placed in the fluid and is mounted on the cylindrical wall with radius R_2 at height h_1 from the bottom of the cylinder. The baffle is considered very thin compared to its raidus and hence thickness can be neglected. We introduce cylindrical coordinate system (r, θ, z) in which z is measured vertically upwards from the bottom of cylinder which is $z = 0$ with the origin O chosen on it. Linear water wave theory is employed to describe the liquid motion inside the annular region of the container. Figure 3.1 depicts the physical problem.

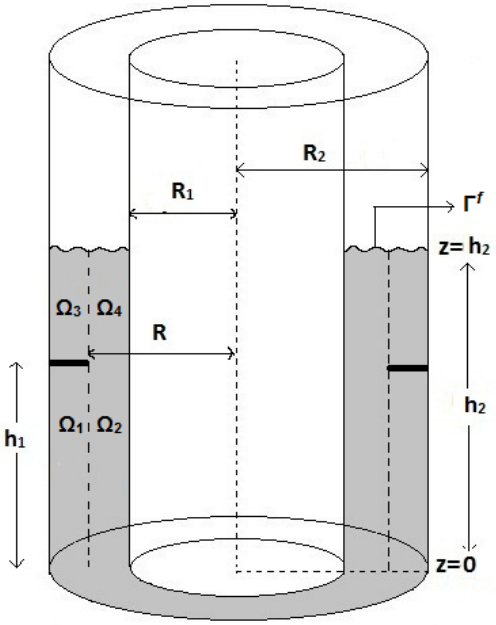

Figure 3.1: Schematic diagram of the problem

With the above assumptions, the liquid flow can now be defined in terms of a velocity potential Φ which satisfies Laplace's equation

$$\frac{\partial^2 \Phi}{\partial r^2} + \frac{1}{r}\frac{\partial \Phi}{\partial r} + \frac{1}{r^2}\frac{\partial^2 \Phi}{\partial \theta^2} + \frac{\partial^2 \Phi}{\partial z^2} = 0 \qquad \text{in} \quad \Omega, \tag{3.1}$$

where Ω is the liquid domain of the container,

with rigid boundary conditions

$$\frac{\partial \Phi}{\partial \mathbf{n}} = 0 \qquad \text{on} \quad \Gamma, \tag{3.2}$$

where Γ is the wetted solid interface and $\mathbf{n}$ is the outward normal to Γ,
and free surface condition

$$\frac{\partial \Phi}{\partial \mathbf{n}} + \frac{1}{g}\frac{\partial^2 \Phi}{\partial t^2} = 0 \qquad \text{on} \quad \Gamma^f, \tag{3.3}$$

where Γ^f is the free surface.

3.2.1 Boundary value problems in sub-domains

Due to the presence of the rigid baffle inside the fluid domain, solution to the boundary-value problem (3.1) – (3.3) cannot be obtained directly. In order to find an analytical solution for the BVP, a semi-analytical approach is used for which the liquid domain is divided into four sub-domains. For each sub-domain, velocity potential $\Phi(r, \theta, z, t)$ can be written as $\Phi_i(r, \theta, z, t)$, $(r, \theta, z) \in \Omega_i$, $i = 1, 2, 3, 4$. According to Eq. (3.1), each velocity potential satisfies Laplace's equation

$$\frac{\partial^2 \Phi_i}{\partial r^2} + \frac{1}{r}\frac{\partial \Phi_i}{\partial r} + \frac{1}{r^2}\frac{\partial^2 \Phi_i}{\partial \theta^2} + \frac{\partial^2 \Phi_i}{\partial z^2} = 0 \qquad \text{in} \quad \Omega_i. \tag{3.4}$$

The corresponding impermeability conditions at rigid boundaries are given by

$$\left(\frac{\partial \Phi_1}{\partial r}\right)_{r=R_2} = 0, \quad \left(\frac{\partial \Phi_1}{\partial z}\right)_{z=0} = 0, \quad \left(\frac{\partial \Phi_1}{\partial z}\right)_{z=h_1} = 0, \tag{3.5a}$$

$$\left(\frac{\partial \Phi_2}{\partial r}\right)_{r=R_1} = 0, \quad \left(\frac{\partial \Phi_2}{\partial z}\right)_{z=0} = 0, \tag{3.5b}$$

$$\left(\frac{\partial \Phi_3}{\partial r}\right)_{r=R_2} = 0, \quad \left(\frac{\partial \Phi_3}{\partial z}\right)_{z=h_1} = 0, \tag{3.5c}$$

$$\left(\frac{\partial \Phi_4}{\partial r}\right)_{r=R_1} = 0. \tag{3.5d}$$

Free surface condition is satisfied by the velocity potentials Φ_3 and Φ_4 since both domains Ω_3 and Ω_4 contain free surface. Now the corresponding free surface conditions are as follows:

$$\frac{\partial \Phi_3}{\partial z} + \frac{1}{g}\frac{\partial^2 \Phi_3}{\partial t^2} = 0 \qquad \text{at} \quad z = h_2, \tag{3.6}$$

$$\frac{\partial \Phi_4}{\partial z} + \frac{1}{g}\frac{\partial^2 \Phi_4}{\partial t^2} = 0 \qquad \text{at} \quad z = h_2. \tag{3.7}$$

3.2.2 Solutions of BVPs in various sub-domains

We write the velocity potential as time harmonic in the following form

$$\Phi(r,\theta,z,t) = \phi(r,\theta,z)e^{\iota\omega t}, \tag{3.8}$$

which defines natural wave frequency ω and Φ is 2π-periodic. Corresponding potentials in different domains take the form as follows:

$$\Phi_i(r,\theta,z,t) = \phi_i(r,\theta,z)e^{\iota\omega t}. \tag{3.9}$$

Inserting Eq. (3.9) into Eqs. $(3.5a)-(3.5d)$, the corresponding conditions get converted to

$$\left(\frac{\partial\phi_1}{\partial r}\right)_{r=R_2} = 0, \quad \left(\frac{\partial\phi_1}{\partial z}\right)_{z=0} = 0, \quad \left(\frac{\partial\phi_1}{\partial z}\right)_{z=h_1} = 0, \tag{3.10a}$$

$$\left(\frac{\partial\phi_2}{\partial r}\right)_{r=R_1} = 0, \quad \left(\frac{\partial\phi_2}{\partial z}\right)_{z=0} = 0, \tag{3.10b}$$

$$\left(\frac{\partial\phi_3}{\partial r}\right)_{r=R_2} = 0, \quad \left(\frac{\partial\phi_3}{\partial z}\right)_{z=h_1} = 0, \tag{3.10c}$$

$$\left(\frac{\partial\phi_4}{\partial r}\right)_{r=R_1} = 0. \tag{3.10d}$$

On the basis of assumption of linear water wave theory, the boundary value problem (3.1) – (3.3) is a linear eigenvalue problem. We employ superposition principle to find the mode shape of the liquid domain. In every sub-domain, there are rigid boundaries as well as non-rigid boundaries. Non-rigid boundaries are the liquid interfaces between two successive sub-domains. In order to set up and solve BVPs in each sub-domain independently, we are required to impose extra (otherwise non-existent) boundary conditions at the interface due to lack of sufficient boundary conditions - one or two at a time for one component, depending on the number of interfaces available in each sub-domain. It is to be noted that these extra conditions are later suitably absorbed while using the overall matching conditions across the interfaces. By superposition principle, ϕ_i in Ω_i can be written as

$$\phi_i = \sum_{j=1}^{k_i} \phi_i^j, \tag{3.11}$$

where ϕ_i^j is the j-th component of ϕ_i and k_i denotes the number of liquid interfaces in Ω_i. With the help of (3.11), each ϕ_i in corresponding Ω_i takes the following form:

$$\phi_1 = \phi_1^2, \tag{3.12}$$

$$\phi_2 = \phi_2^2 + \phi_2^3, \tag{3.13}$$

$$\phi_3 = \phi_3^1 + \phi_3^2, \tag{3.14}$$

$$\phi_4 = \phi_4^1 + \phi_4^2 + \phi_4^3, \tag{3.15}$$

where ϕ_i^1 corresponds to the component of the velocity potential in the respective region due to the non-rigid condition at the free surface $z = h_2$ only; ϕ_i^2 to that component of the velocity potential due to the non-rigid condition at the vertical interface $r = R$ only and ϕ_i^3 to that component of the velocity potential due to the non-rigid condition at the horizontal interface $z = h_1$ only. In order to maintain the periodicity of Φ, ϕ_i^j is written in the form

$$\phi_i^j = \sum_{m=0}^{\infty} \phi_{im}^j \cos m\theta. \tag{3.16}$$

The boundary conditions for ϕ_i^j in the sub-domains can be found out with the help of Eqs. $(3.10a) - (3.10d)$. Rigid boundary conditions in different sub-domains are obtained as follows:

For Ω_1:

$$\left(\frac{\partial \phi_1^2}{\partial r}\right)_{r=R_2} = 0, \qquad \left(\frac{\partial \phi_1^2}{\partial z}\right)_{z=0} = 0, \qquad \left(\frac{\partial \phi_1^2}{\partial z}\right)_{z=h_1} = 0. \tag{3.17}$$

For Ω_2:

$$\left(\frac{\partial \phi_2^2}{\partial r}\right)_{r=R_1} = 0, \qquad \left(\frac{\partial \phi_2^2}{\partial z}\right)_{z=0} = 0, \qquad \left(\frac{\partial \phi_2^2}{\partial z}\right)_{z=h_1} = 0, \tag{3.18}$$

$$\left(\frac{\partial \phi_2^3}{\partial r}\right)_{r=R_1} = 0, \qquad \left(\frac{\partial \phi_2^3}{\partial r}\right)_{r=R} = 0, \qquad \left(\frac{\partial \phi_2^3}{\partial z}\right)_{z=0} = 0. \tag{3.19}$$

For Ω_3:

$$\left(\frac{\partial \phi_3^2}{\partial r}\right)_{r=R_2} = 0, \qquad \left(\frac{\partial \phi_3^2}{\partial z}\right)_{z=h_1} = 0, \qquad \left(\phi_3^2\right)_{z=h_2} = 0, \tag{3.20}$$

$$\left(\frac{\partial \phi_3^1}{\partial r}\right)_{r=R_2} = 0, \qquad \left(\frac{\partial \phi_3^1}{\partial r}\right)_{r=R} = 0, \qquad \left(\frac{\partial \phi_3^1}{\partial z}\right)_{z=h_1} = 0. \tag{3.21}$$

For Ω_4:

$$\left(\frac{\partial \phi_4^1}{\partial r}\right)_{r=R_1} = 0, \qquad \left(\frac{\partial \phi_4^1}{\partial r}\right)_{r=R} = 0, \qquad \left(\frac{\partial \phi_4^1}{\partial z}\right)_{z=h_1} = 0, \tag{3.22}$$

$$\left(\frac{\partial \phi_4^2}{\partial r}\right)_{r=R_1} = 0, \qquad \left(\frac{\partial \phi_4^2}{\partial z}\right)_{z=h_1} = 0, \qquad \left(\phi_4^2\right)_{z=h_2} = 0, \tag{3.23}$$

$$\left(\frac{\partial \phi_4^3}{\partial r}\right)_{r=R_1} = 0, \qquad \left(\frac{\partial \phi_4^3}{\partial r}\right)_{r=R} = 0, \qquad \left(\phi_4^3\right)_{z=h_2} = 0. \tag{3.24}$$

Now we introduce the following dimensionless quantities in order to non-dimensionalize the parameters:

$$\xi = \frac{r}{R_2}, \quad \eta = \frac{z}{R_2}, \quad \alpha = \frac{R_1}{R_2}, \quad \gamma = \frac{R}{R_2},$$
$$\beta_1 = \frac{h_1}{R_2}, \quad \beta_2 = \frac{h_2}{R_2}, \quad \omega^* = \omega\sqrt{\frac{R_2}{g}}. \tag{3.25}$$

The boundary value problems in different sub-domains allow separation of variables in (r, θ, z)-coordinate system for ϕ_i^j and permit the exact solutions which can be obtained in terms of eigenfunctions. The corresponding solutions for different sub-domains can be written as follows:

For sub-domain Ω_1:

$$\phi_1^2 = \sum_{n=1}^{\infty} A_{1mn}^2 \cos\left(\frac{n\pi}{\beta_1}\eta\right) \frac{\left[I_m\left(\frac{n\pi}{\beta_1}\xi\right) K_m'\left(\frac{n\pi}{\beta_1}\right) - I_m'\left(\frac{n\pi}{\beta_1}\right) K_m\left(\frac{n\pi}{\beta_1}\xi\right)\right]}{K_m'\left(\frac{n\pi}{\beta_1}\right)} + A_{1m0}^2\left(\xi^m + \xi^{-m}\right)\delta_m^2 + A_{100}^2\delta_m^1, \tag{3.26}$$

where δ_m^1 and δ_m^2 are defined as

$$\delta_m^1 = \begin{cases} 1, & \text{if } m = 0, \\ 0, & \text{otherwise,} \end{cases}$$

$$\delta_m^2 = \begin{cases} 0, & \text{if } m = 0, \\ 1, & \text{otherwise.} \end{cases}$$

For sub-domain Ω_2:

$$\begin{aligned} \phi_2^2 &= \sum_{n=1}^{\infty} A_{2mn}^2 \frac{\left[I_m\left(\frac{n\pi}{\beta_1}\xi\right) K_m'\left(\frac{n\pi}{\beta_1}\alpha\right) - I_m'\left(\frac{n\pi}{\beta_1}\alpha\right) K_m\left(\frac{n\pi}{\beta_1}\xi\right)\right]}{K_m'\left(\frac{n\pi}{\beta_1}\alpha\right)} \\ &\quad \times \cos\left(\frac{n\pi}{\beta_1}\eta\right) + A_{2m0}^2\left(\xi^m + \alpha^{2m}\xi^{-m}\right)\delta_m^2 + A_{200}^2\delta_m^1, \end{aligned} \tag{3.27}$$

$$\begin{aligned} \phi_2^3 &= \sum_{n=1}^{\infty} A_{2mn}^3 \left[e^{k_{mn}\eta} + e^{-k_{mn}\eta}\right] \left[J_m\left(k_{mn}\xi\right) Y_m'\left(k_{mn}\alpha\right) - \right. \\ &\quad \left. J_m'\left(k_{mn}\alpha\right) Y_m\left(k_{mn}\xi\right)\right] + A_{200}^3\delta_m^1, \end{aligned} \tag{3.28}$$

where k_{mn} are the zeros of

$$J_m'(k_{mn}\alpha)Y_m'(k_{mn}\gamma) - J_m'(k_{mn}\gamma)Y_m'(k_{mn}\alpha) = 0. \tag{3.29}$$

For sub-domain Ω_3:

$$\begin{aligned} \phi_3^1 &= \sum_{n=1}^{\infty} A_{3mn}^1 \left[e^{\lambda_{mn}\eta} + e^{\lambda_{mn}(2\beta_1-\eta)}\right] \left[J_m\left(\lambda_{mn}\xi\right) Y_m'\left(\lambda_{mn}\right) - \right. \\ &\quad \left. J_m'\left(\lambda_{mn}\right) Y_m\left(\lambda_{mn}\xi\right)\right] + A_{300}^1\delta_m^1, \end{aligned} \tag{3.30}$$

$$\begin{aligned} \phi_3^2 &= \sum_{n=1}^{\infty} A_{3mn}^2 \cos\left(\frac{(2n-1)\pi}{2(\beta_2-\beta_1)}(\eta-\beta_1)\right) \times \\ &\quad \frac{\left[I_m\left(\frac{(2n-1)\pi}{2(\beta_2-\beta_1)}\xi\right) K_m'\left(\frac{(2n-1)\pi}{2(\beta_2-\beta_1)}\right) - I_m'\left(\frac{(2n-1)\pi}{2(\beta_2-\beta_1)}\right) K_m\left(\frac{(2n-1)\pi}{2(\beta_2-\beta_1)}\xi\right)\right]}{K_m'\left(\frac{(2n-1)\pi}{2(\beta_2-\beta_1)}\right)}, \end{aligned} \tag{3.31}$$

where λ_{mn} are the zeros of

$$J'_m(\lambda_{mn})Y'_m(\lambda_{mn}\gamma) - J'_m(\lambda_{mn}\gamma)Y'_m(\lambda_{mn}) = 0. \tag{3.32}$$

For sub-domain Ω_4:

$$\begin{aligned}
\phi_4^1 &= \sum_{n=1}^{\infty} A_{4mn}^1 \left[e^{k_{mn}\eta} + e^{k_{mn}(2\beta_1-\eta)}\right] \left[J_m\left(k_{mn}\xi\right) Y'_m\left(k_{mn}\alpha\right) - \right. \\
&\left. J'_m\left(k_{mn}\alpha\right) Y_m\left(k_{mn}\xi\right)\right] + A_{400}^1\delta_m^1, \qquad (3.33) \\
\phi_4^2 &= \sum_{n=1}^{\infty} A_{4mn}^2 \cos\left(\frac{(2n-1)\pi}{2(\beta_2-\beta_1)}(\eta-\beta_1)\right) \times \\
&\frac{\left[I_m\left(\frac{(2n-1)\pi}{2(\beta_2-\beta_1)}\xi\right) K'_m\left(\frac{(2n-1)\pi}{2(\beta_2-\beta_1)}\alpha\right) - I'_m\left(\frac{(2n-1)\pi}{2(\beta_2-\beta_1)}\alpha\right) K_m\left(\frac{(2n-1)\pi}{2(\beta_2-\beta_1)}\xi\right)\right]}{K'_m\left(\frac{(2n-1)\pi}{2(\beta_2-\beta_1)}\alpha\right)}, \qquad (3.34) \\
\phi_4^3 &= \sum_{n=1}^{\infty} A_{4mn}^3 \left[e^{k_{mn}\eta} - e^{k_{mn}(2\beta_2-\eta)}\right] \left[J_m\left(k_{mn}\xi\right) Y'_m\left(k_{mn}\alpha\right) - \right. \\
&\left. J'_m\left(k_{mn}\alpha\right) Y_m\left(k_{mn}\xi\right)\right] + A_{400}^3\delta_m^1(\eta-\beta_2). \qquad (3.35)
\end{aligned}$$

The coefficients A_{imn}^j are still unknown. To find A_{imn}^j and the non-dimensional frequency ω^*, we apply the matching conditions at the interfaces and use Eqs. (3.6) and (3.7) for ϕ_i^j where $i = 3, 4$ and $j = 1, 2, 3$.

3.2.3 Matching conditions

In order to use the matching conditions on the interfaces, we truncate the series of solutions after N terms. These conditions imply the continuity of pressure and velocity across the interfaces. The following are the matching conditions used across different interfaces:

(A) $\phi_1 = \phi_2$ at $\xi = \gamma$:

$$\begin{aligned}
&\sum_{n=1}^{N} A_{1mn}^2 \cos\left(\frac{n\pi}{\beta_1}\eta\right) \frac{\left[I_m\left(\frac{n\pi}{\beta_1}\gamma\right) K'_m\left(\frac{n\pi}{\beta_1}\right) - I'_m\left(\frac{n\pi}{\beta_1}\right) K_m\left(\frac{n\pi}{\beta_1}\gamma\right)\right]}{K'_m\left(\frac{n\pi}{\beta_1}\right)} \\
&+A_{1m0}^2\left(\gamma^m + \gamma^{-m}\right)\delta_m^2 + A_{100}^2\delta_m^1 = \sum_{n=1}^{N} A_{2mn}^2 \cos\left(\frac{n\pi}{\beta_1}\eta\right) \times \\
&\frac{\left[I_m\left(\frac{n\pi}{\beta_1}\gamma\right) K'_m\left(\frac{n\pi}{\beta_1}\alpha\right) - I'_m\left(\frac{n\pi}{\beta_1}\alpha\right) K_m\left(\frac{n\pi}{\beta_1}\gamma\right)\right]}{K'_m\left(\frac{n\pi}{\beta_1}\alpha\right)} + \\
&A_{2m0}^2\left(\gamma^m + \alpha^{2m}\gamma^{-m}\right)\delta_m^2 + A_{200}^2\delta_m^1 + \sum_{n=1}^{N} A_{2mn}^3\left[e^{k_{mn}\eta} + e^{-k_{mn}\eta}\right] \\
&\times\left[J_m\left(k_{mn}\gamma\right) Y'_m\left(k_{mn}\alpha\right) - J'_m\left(k_{mn}\alpha\right) Y_m\left(k_{mn}\gamma\right)\right] + A_{200}^3\delta_m^1. \qquad (3.36)
\end{aligned}$$

(B) $\frac{\partial\phi_1}{\partial\xi} = \frac{\partial\phi_2}{\partial\xi}$ at $\xi = \gamma$:

$$\sum_{n=1}^{N} A_{1mn}^2 \left(\frac{n\pi}{\beta_1}\right) \cos\left(\frac{n\pi}{\beta_1}\eta\right) \frac{\left[I_m'\left(\frac{n\pi}{\beta_1}\gamma\right) K_m'\left(\frac{n\pi}{\beta_1}\right) - I_m'\left(\frac{n\pi}{\beta_1}\right) K_m'\left(\frac{n\pi}{\beta_1}\gamma\right)\right]}{K_m'\left(\frac{n\pi}{\beta_1}\right)}$$
$$+A_{1m0}^2 m\left(\gamma^{m-1} - \gamma^{-m-1}\right)\delta_m^2$$
$$= \sum_{n=1}^{N} A_{2mn}^2 \left(\frac{n\pi}{\beta_1}\right) \cos\left(\frac{n\pi}{\beta_1}\eta\right) \frac{\left[I_m'\left(\frac{n\pi}{\beta_1}\gamma\right) K_m'\left(\frac{n\pi}{\beta_1}\alpha\right) - I_m'\left(\frac{n\pi}{\beta_1}\alpha\right) K_m'\left(\frac{n\pi}{\beta_1}\gamma\right)\right]}{K_m'\left(\frac{n\pi}{\beta_1}\alpha\right)}$$
$$+A_{2m0}^2 m\left(\gamma^{m-1} - \alpha^{2m}\gamma^{-m-1}\right)\delta_m^2. \tag{3.37}$$

(C) $\phi_2 = \phi_4$ at $\eta = \beta_1$:

$$\sum_{n=1}^{N} A_{2mn}^2 (-1)^n \frac{\left[I_m\left(\frac{n\pi}{\beta_1}\xi\right) K_m'\left(\frac{n\pi}{\beta_1}\alpha\right) - I_m'\left(\frac{n\pi}{\beta_1}\alpha\right) K_m\left(\frac{n\pi}{\beta_1}\xi\right)\right]}{K_m'\left(\frac{n\pi}{\beta_1}\alpha\right)}$$
$$+A_{2m0}^2\left(\xi^m + \alpha^{2m}\xi^{-m}\right)\delta_m^2 + A_{200}^2\delta_m^1 + \sum_{n=1}^{N} A_{2mn}^3\left[e^{k_{mn}\beta_1} + e^{-k_{mn}\beta_1}\right]$$
$$\times\left[J_m\left(k_{mn}\xi\right) Y_m'\left(k_{mn}\alpha\right) - J_m'\left(k_{mn}\alpha\right) Y_m\left(k_{mn}\xi\right)\right] + A_{200}^3\delta_m^1 = \sum_{n=1}^{N} A_{4mn}^1$$
$$\times\left[2e^{k_{mn}\beta_1}\right]\left[J_m\left(k_{mn}\xi\right) Y_m'\left(k_{mn}\alpha\right) - J_m'\left(k_{mn}\alpha\right) Y_m\left(k_{mn}\xi\right)\right] + A_{400}^1\delta_m^1 +$$
$$\sum_{n=1}^{N} A_{4mn}^2 \frac{\left[I_m\left(\frac{(2n-1)\pi}{2(\beta_2-\beta_1)}\xi\right) K_m'\left(\frac{(2n-1)\pi}{2(\beta_2-\beta_1)}\alpha\right) - I_m'\left(\frac{(2n-1)\pi}{2(\beta_2-\beta_1)}\alpha\right) K_m\left(\frac{(2n-1)\pi}{2(\beta_2-\beta_1)}\xi\right)\right]}{K_m'\left[\frac{(2n-1)\pi}{2(\beta_2-\beta_1)}\alpha\right]}$$
$$+\sum_{n=1}^{N} A_{4mn}^3\left[e^{k_{mn}\beta_1} - e^{k_{mn}(2\beta_2-\beta_1)}\right]\left[J_m\left(k_{mn}\xi\right) Y_m'\left(k_{mn}\alpha\right)\right.$$
$$\left.-J_m'\left(k_{mn}\alpha\right) Y_m\left(k_{mn}\xi\right)\right] + A_{400}^3\delta_m^1(\beta_1 - \beta_2). \tag{3.38}$$

(D) $\frac{\partial\phi_2}{\partial\eta} = \frac{\partial\phi_4}{\partial\eta}$ at $\eta = \beta_1$:

$$\sum_{n=1}^{N} A_{2mn}^3 k_{mn}\left[e^{k_{mn}\beta_1} - e^{-k_{mn}\beta_1}\right]\left[J_m\left(k_{mn}\xi\right) Y_m'\left(k_{mn}\alpha\right) -\right.$$
$$\left. J_m'\left(k_{mn}\alpha\right) Y_m\left(k_{mn}\xi\right)\right] = \sum_{n=1}^{N} A_{4mn}^3 k_{mn}\left[e^{k_{mn}\beta_1} + e^{k_{mn}(2\beta_2-\beta_1)}\right] \times$$
$$\left[J_m\left(k_{mn}\xi\right) Y_m'\left(k_{mn}\alpha\right) - J_m'\left(k_{mn}\alpha\right) Y_m\left(k_{mn}\xi\right)\right] + A_{400}^3\delta_m^1. \tag{3.39}$$

(E) $\phi_3 = \phi_4$ at $\xi = \gamma$:

$$\sum_{n=1}^{N} A^1_{3mn}\left[e^{\lambda_{mn}\eta}+e^{\lambda_{mn}(2\beta_1-\eta)}\right]\left[J_m\left(\lambda_{mn}\gamma\right)Y'_m\left(\lambda_{mn}\right)-J'_m\left(\lambda_{mn}\right)Y_m\left(\lambda_{mn}\gamma\right)\right]$$
$$+A^1_{300}\delta^1_m+\sum_{n=1}^{N} A^2_{3mn}\cos\left(\frac{(2n-1)\pi}{2(\beta_2-\beta_1)}(\eta-\beta_1)\right)\times$$
$$\frac{\left[I_m\left(\frac{(2n-1)\pi}{2(\beta_2-\beta_1)}\gamma\right)K'_m\left(\frac{(2n-1)\pi}{2(\beta_2-\beta_1)}\right)-I'_m\left(\frac{(2n-1)\pi}{2(\beta_2-\beta_1)}\right)K_m\left(\frac{(2n-1)\pi}{2(\beta_2-\beta_1)}\gamma\right)\right]}{K'_m\left(\frac{(2n-1)\pi}{2(\beta_2-\beta_1)}\right)}$$
$$=\sum_{n=1}^{N} A^1_{4mn}\left[e^{k_{mn}\eta}+e^{k_{mn}(2\beta_1-\eta)}\right]\left[J_m\left(k_{mn}\gamma\right)Y'_m\left(k_{mn}\alpha\right)-\right.$$
$$\left.J'_m\left(k_{mn}\alpha\right)Y_m\left(k_{mn}\gamma\right)\right]+A^1_{400}\delta^1_m+\sum_{n=1}^{N} A^2_{4mn}\cos\left(\frac{(2n-1)\pi}{2(\beta_2-\beta_1)}(\eta-\beta_1)\right)\times$$
$$\frac{\left[I_m\left(\frac{(2n-1)\pi}{2(\beta_2-\beta_1)}\gamma\right)K'_m\left(\frac{(2n-1)\pi}{2(\beta_2-\beta_1)}\alpha\right)-I'_m\left(\frac{(2n-1)\pi}{2(\beta_2-\beta_1)}\alpha\right)K_m\left(\frac{(2n-1)\pi}{2(\beta_2-\beta_1)}\gamma\right)\right]}{K'_m\left(\frac{(2n-1)\pi}{2(\beta_2-\beta_1)}\alpha\right)}$$
$$+\sum_{n=1}^{N} A^3_{4mn}\left[e^{k_{mn}\eta}-e^{k_{mn}(2\beta_2-\eta)}\right]\times$$
$$\left[J_m\left(k_{mn}\gamma\right)Y'_m\left(k_{mn}\alpha\right)-J'_m\left(k_{mn}\alpha\right)Y_m\left(k_{mn}\gamma\right)\right]+A^3_{400}\delta^1_m(\eta-\beta_2). \tag{3.40}$$

(F) $\frac{\partial\phi_3}{\partial\xi}=\frac{\partial\phi_4}{\partial\xi}$ at $\xi=\gamma$:

$$\sum_{n=1}^{N} A^2_{3mn}\left(\frac{(2n-1)\pi}{2(\beta_2-\beta_1)}\right)\cos\left(\frac{(2n-1)\pi}{2(\beta_2-\beta_1)}(\eta-\beta_1)\right)\times$$
$$\frac{\left[I'_m\left(\frac{(2n-1)\pi}{2(\beta_2-\beta_1)}\gamma\right)K'_m\left(\frac{(2n-1)\pi}{2(\beta_2-\beta_1)}\right)-I'_m\left(\frac{(2n-1)\pi}{2(\beta_2-\beta_1)}\right)K'_m\left(\frac{(2n-1)\pi}{2(\beta_2-\beta_1)}\gamma\right)\right]}{K'_m\left(\frac{(2n-1)\pi}{2(\beta_2-\beta_1)}\right)}$$
$$=\sum_{n=1}^{N} A^2_{4mn}\left(\frac{(2n-1)\pi}{2(\beta_2-\beta_1)}\right)\cos\left(\frac{(2n-1)\pi}{2(\beta_2-\beta_1)}(\eta-\beta_1)\right)\times$$
$$\frac{\left[I'_m\left(\frac{(2n-1)\pi}{2(\beta_2-\beta_1)}\gamma\right)K'_m\left(\frac{(2n-1)\pi}{2(\beta_2-\beta_1)}\alpha\right)-I'_m\left(\frac{(2n-1)\pi}{2(\beta_2-\beta_1)}\alpha\right)K'_m\left(\frac{(2n-1)\pi}{2(\beta_2-\beta_1)}\gamma\right)\right]}{K'_m\left(\frac{(2n-1)\pi}{2(\beta_2-\beta_1)}\alpha\right)}. \tag{3.41}$$

The potentials ϕ_3 and ϕ_4 satisfy the following free surface conditions, respectively:

$$\frac{\partial\phi_3}{\partial\eta}-\omega^{*2}\phi_3=0 \qquad \text{at} \quad \eta=\beta_2, \tag{3.42}$$
$$\frac{\partial\phi_4}{\partial\eta}-\omega^{*2}\phi_4=0 \qquad \text{at} \quad \eta=\beta_2. \tag{3.43}$$

Substituting ϕ_3 and ϕ_4 in Eqs. (3.42) and (3.43), respectively, we get

$$\sum_{n=1}^{N} A^1_{3mn}\lambda_{mn}\left[e^{\lambda_{mn}\beta_2}-e^{\lambda_{mn}(2\beta_1-\beta_2)}\right]\left[J_m\left(\lambda_{mn}\xi\right)Y'_m\left(\lambda_{mn}\right)-\right.$$
$$\left.J'_m\left(\lambda_{mn}\right)Y_m\left(\lambda_{mn}\xi\right)\right]+\sum_{n=1}^{n=N} A^2_{3mn}\frac{(2n-1)\pi}{2(\beta_2-\beta_1)}(-1)^n\times$$
$$\frac{\left[I_m\left(\frac{(2n-1)\pi}{2(\beta_2-\beta_1)}\xi\right)K'_m\left(\frac{(2n-1)\pi}{2(\beta_2-\beta_1)}\right)-I'_m\left(\frac{(2n-1)\pi}{2(\beta_2-\beta_1)}\right)K_m\left(\frac{(2n-1)\pi}{2(\beta_2-\beta_1)}\xi\right)\right]}{K'_m\left(\frac{(2n-1)\pi}{2(\beta_2-\beta_1)}\right)}$$
$$-\omega^{*2}\left[\sum_{n=1}^{N} A^1_{3mn}\left[e^{\lambda_{mn}\beta_2}+e^{\lambda_{mn}(2\beta_1-\beta_2)}\right]\times\right.$$
$$\left.\left[J_m\left(\lambda_{mn}\xi\right)Y'_m\left(\lambda_{mn}\right)-J'_m\left(\lambda_{mn}\right)Y_m\left(\lambda_{mn}\xi\right)\right]+A^1_{300}\delta^1_m\right]=0, \tag{3.44}$$

and

$$\sum_{n=1}^{N} A^1_{4mn}k_{mn}\left[e^{k_{mn}\beta_2}-e^{k_{mn}(2\beta_1-\beta_2)}\right]\left[J_m\left(k_{mn}\xi\right)Y'_m\left(k_{mn}\alpha\right)-\right.$$
$$\left.J'_m\left(k_{mn}\alpha\right)Y_m\left(k_{mn}\xi\right)\right]+\sum_{n=1}^{N} A^2_{4mn}\frac{(2n-1)\pi}{2(\beta_2-\beta_1)}(-1)^n\times$$
$$\frac{\left[I_m\left(\frac{(2n-1)\pi}{2(\beta_2-\beta_1)}\xi\right)K'_m\left(\frac{(2n-1)\pi}{2(\beta_2-\beta_1)}\alpha\right)-I'_m\left(\frac{(2n-1)\pi}{2(\beta_2-\beta_1)}\alpha\right)K_m\left(\frac{(2n-1)\pi}{2(\beta_2-\beta_1)}\xi\right)\right]}{K'_m\left(\frac{(2n-1)\pi}{2(\beta_2-\beta_1)}\alpha\right)}$$
$$+\sum_{n=1}^{N} A^3_{4mn}k_{mn}\left[e^{k_{mn}\beta_2}+e^{k_{mn}(\beta_2)}\right]\left[J_m\left(k_{mn}\xi\right)Y'_m\left(k_{mn}\alpha\right)-\right.$$
$$\left.J'_m\left(k_{mn}\alpha\right)Y_m\left(k_{mn}\xi\right)\right]+A^3_{400}\delta^1_m-\omega^{*2}\left[\sum_{n=1}^{N} A^1_{4mn}\left[e^{k_{mn}\beta_2}+e^{k_{mn}(2\beta_1-\beta_2)}\right]\right.$$
$$\left.\left[J_m\left(k_{mn}\xi\right)Y'_m\left(k_{mn}\alpha\right)-J'_m\left(k_{mn}\alpha\right)Y_m\left(k_{mn}\xi\right)\right]+A^1_{400}\delta^1_m\right]=0. \tag{3.45}$$

Equations (3.36) − (3.41) and (3.44) − (3.45) give rise to a homogenous linear system in $8N$ unknowns. Now to determine the unknowns and non-dimensional frequency, we truncate the system at a fixed number N, use Fourier-Bessel series expansion and then form a square matrix whose elements are coefficients of a Fourier-Bessel series. Here we get a square matrix of order $8N$ in A^j_{imn} unknowns which has the form

$$MX=0, \tag{3.46}$$

where

$$X=[A^2_{1mn},A^2_{2mn},A^3_{2mn},A^1_{3mn},A^2_{3mn},A^1_{4mn},A^2_{4mn},A^3_{4mn}]^T, \tag{3.47}$$

and

$$M = \begin{bmatrix} [a^{11}_{mn\bar{n}}] & [a^{12}_{mn\bar{n}}] & [0] & [0] & [0] & [0] & [0] & [0] \\ [a^{21}_{mn\bar{n}}] & [a^{22}_{mn\bar{n}}] & [a^{23}_{mn\bar{n}}] & [0] & [0] & [0] & [0] & [0] \\ [0] & [0] & [a^{33}_{mn\bar{n}}] & [0] & [0] & [0] & [0] & [a^{38}_{mn\bar{n}}] \\ [0] & [a^{42}_{mn\bar{n}}] & [a^{43}_{mn\bar{n}}] & [0] & [0] & [a^{46}_{mn\bar{n}}] & [a^{47}_{mn\bar{n}}] & [a^{48}_{mn\bar{n}}] \\ [0] & [0] & [0] & [0] & [a^{55}_{mn\bar{n}}] & [0] & [a^{57}_{mn\bar{n}}] & [0] \\ [0] & [0] & [0] & [a^{64}_{mn\bar{n}}] & [a^{65}_{mn\bar{n}}] & [a^{66}_{mn\bar{n}}] & [a^{67}_{mn\bar{n}}] & [a^{68}_{mn\bar{n}}] \\ [0] & [0] & [0] & [0] & [0] & [a^{76}_{mn\bar{n}}] & [a^{77}_{mn\bar{n}}] & [a^{78}_{mn\bar{n}}] \\ [0] & [0] & [0] & [a^{84}_{mn\bar{n}}] & [a^{85}_{mn\bar{n}}] & [0] & [0] & [0] \end{bmatrix}. \quad (3.48)$$

The expressions of the non-zero elements $a^{ij}_{mn\bar{n}}$ of the matrix are given by the coefficients of a Fourier-Bessel series. The system given by (3.46) must have a non-trivial solution for the vanishing determinant condition. The condition of the non-trivial solution of (3.46) gives us values of ω^*. The detailed expressions for the non-zero coefficients of the matrix M are provided in Appendix A.

3.3 Numerical results and discussion: Natural frequencies versus different parameter ratios

We carry out a number of numerical experiments to strengthen the analytical results obtained here. All numerical calculations are carried out by using MATHEMATICA. 'NIntegrate' command is used to calculate the integrals numerically to compute the frequencies. The system is truncated to a 24×24 one to calculate the frequencies. The zeros of the determinant of the truncated system are plotted versus different parameters. The curves are drawn for non-dimensional frequency versus different values of γ, α and for different baffle positions in the liquid domain for $m = 0, 1, 2$. Dimensionless sloshing frequency $\omega^{*2}_{mn}(m = 0, 1, 2; n = 1)$ is plotted as a function of the ratio of baffle positions to radius for various γ values in Figs. $3.2 - 3.4$. The effect of the baffle position is investigated for $\gamma = 0.7, 0.8, 0.9$ while $\alpha = 0.2$ is kept fixed.

In Fig. 3.2, it is observed that frequency decreases gradually as the baffle moves towards the free surface and the rate of decrease of frequency reduces with increasing values of γ, i.e., when a wider baffle is placed, frequency decreases rapidly. The curve corresponding to $\gamma = 0.7$ decreases rapidly as the baffle is shifted towards the free surface. The curve corresponding to $\gamma = 0.8$ decreases monotonically but a rapid fall is observed when the baffle is placed at $\beta_1 \simeq 0.86$. The effect of the baffle position on non-dimensional frequency corresponding to the curve for $\gamma = 0.9$ is less significant compared to the other two values of γ. This result suggests that corresponding to the frequency ω^{*2}_{01}, the proper baffle position should be at any depth above $\beta_1 = 0.4$ and preferably for a baffle with less width.

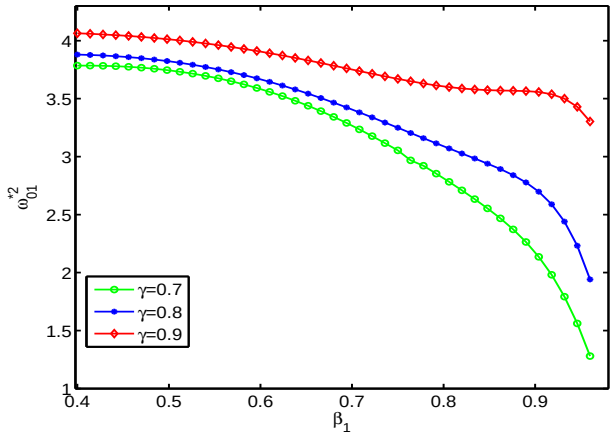

Figure 3.2: Non-dimensional sloshing frequency $\omega_{01}^{*2}(m=0,n=1)$ versus β_1 for different values of γ for $\beta_2=1$, $\alpha=0.2$

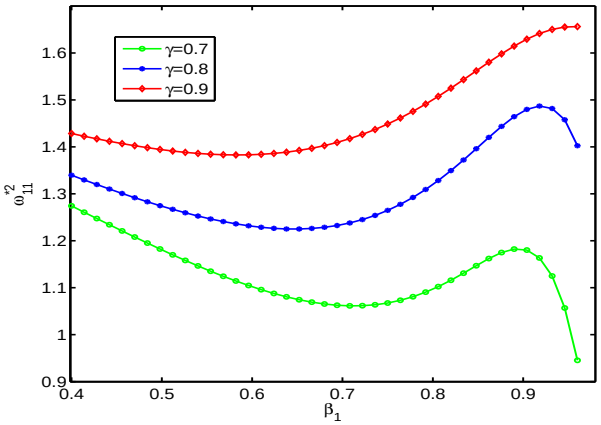

Figure 3.3: Non-dimensional sloshing frequency $\omega_{11}^{*2}(m=1,n=1)$ versus β_1 for different values of γ for $\beta_2=1$, $\alpha=0.2$

In Fig. 3.3, it is shown that initially non-dimensional frequency decreases as β_1 increases, and as β_1 takes higher value up to $\beta_1 \leq 0.9$, non-dimensional frequency increases gradually. And after that frequency shows a rapid reduction in its values for the curves corresponding to $\gamma = 0.7, 0.8$. Non-dimensional frequency increases gradually for the curve corresponding to $\gamma = 0.9$. This figure implies that the frequency ω_{11}^{*2} takes higher values for a baffle with less width and when the baffle is placed nearer to the free surface. In Fig. 3.4, It is observed that for $\gamma = 0.7$, frequency decreases as baffle moves towards the free surface. But for $\gamma = 0.8, 0.9$, initially non-dimensional frequency decreases as β_1 increases up to $\beta_1 \leq 0.78$ and as β_1 takes higher values up to $\beta_1 \leq 0.9$, non-dimensional frequency increases and at $\beta_1 = 0.9$, it changes its behaviour and decreases rapidly. This figure implies that the frequency ω_{11}^{*2} takes higher values for

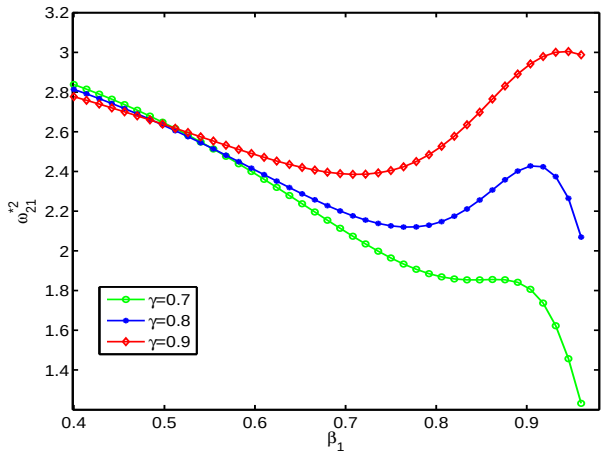

Figure 3.4: Non-dimensional sloshing frequency $\omega_{21}^{*2}(m = 2, n = 1)$ versus β_1 for different values of γ for $\beta_2 = 1$, $\alpha = 0.2$

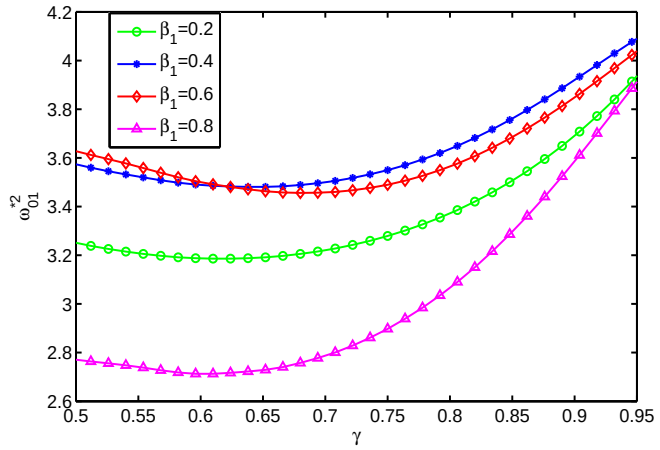

Figure 3.5: Non-dimensional sloshing frequency $\omega_{01}^{*2}(m = 0, n = 1)$ versus γ for different baffle position for $\beta_2 = 1$, $\alpha = 0.2$

a baffle with less width and when the baffle is placed nearer to the free surface. Same conclusion can be made about ω_{21}^{*2} as was made for ω_{01}^{*2} and ω_{11}^{*2}.

Figures $3.5 - 3.7$ show the dimensionless fundamental sloshing frequency versus γ for different baffle positions. To investigate the effect of the baffle radius on non-dimensional frequency, we consider different positions of the baffle as $\beta_1 = 0.2, 0.4, 0.6, 0.8$.

For small values of γ, most of the fluid below the baffle level is covered by the baffle, and the fluid above the baffle participates in the sloshing process. It shows that frequency increases for increasing inner radius of the baffle. In Fig. 3.5, non-dimensional frequency decreases upto $\gamma \simeq 0.62$ and for higher values of β_1, non-dimensional frequency increases. The curve corresponding to $\beta_1 = 0.8$ shows that non-dimensional frequency

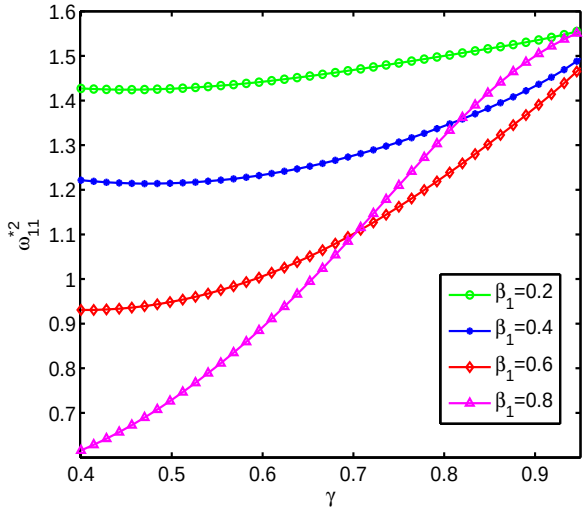

Figure 3.6: Non-dimensional sloshing frequency $\omega_{11}^{*2}(m = 1, n = 1)$ versus γ for different baffle position for $\beta_2 = 1$, $\alpha = 0.2$

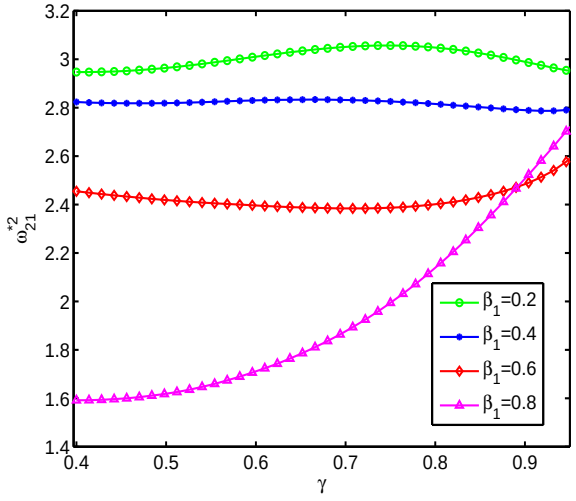

Figure 3.7: Non-dimensional sloshing frequency $\omega_{21}^{*2}(m = 2, n = 1)$ versus γ for different baffle position for $\beta_2 = 1$, $\alpha = 0.2$

versus γ increases more rapidly when the baffle is placed nearer to the free surface. In Fig. 3.6, non-dimensional frequency increases monotonically with increasing values of γ. It is also shown that non-dimensional frequency increases more rapidly as the baffle is placed nearer to the free surface. Curve corresponding to $\beta_1 = 0.8$ shows a fast increment in non-dimensional frequency compared to other baffle positions. From Fig. 3.7, no significant change is observed in the value of non-dimensional frequency with

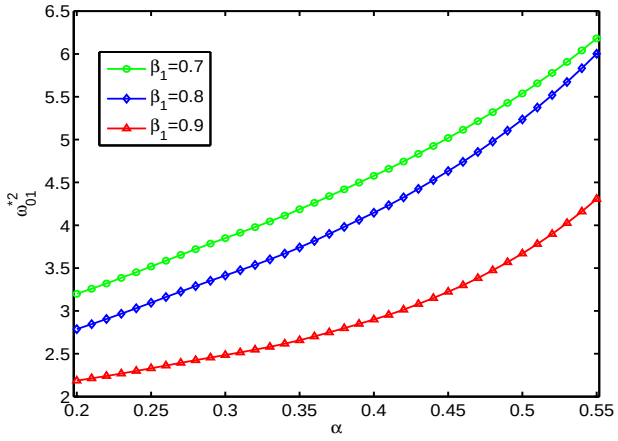

Figure 3.8: Non-dimensional sloshing frequency $\omega_{01}^{*2}(m=0,n=1)$ versus α for different values of β_1 for $\beta_2=1$, $\gamma=0.7$

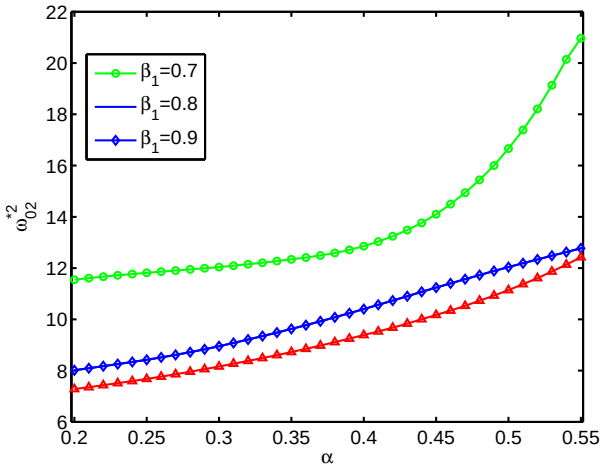

Figure 3.9: Non-dimensional sloshing frequency $\omega_{02}^{*2}(m=0,n=2)$ versus α for different values of β_1 for $\beta_2=1$, $\gamma=0.7$

respect to γ except for the curve corresponding to $\beta_1=0.8$ which shows that when a baffle is placed near the free surface, non-dimensional frequency increases monotonically. These figures also suggest higher values of frequency for lower baffle width.

Figures $3.8-3.13$ show the dimensionless fundamental sloshing frequency versus inner-outer radius ratio of the container for different baffle positions for a fixed inner radius ratio of the baffle. Curves are drawn for different baffle positions at $\beta_1=0.7,0.8,0.9$ and γ is kept fixed at $\gamma=0.7$. It is observed that frequency increases with increasing inner-outer radius ratio of the container. It is observed that a significant change in the value of $\omega_{mn}^{*2}(m=0,1,2;n=1,2)$ occurs only for higher values of β_1. As β_1 increases,

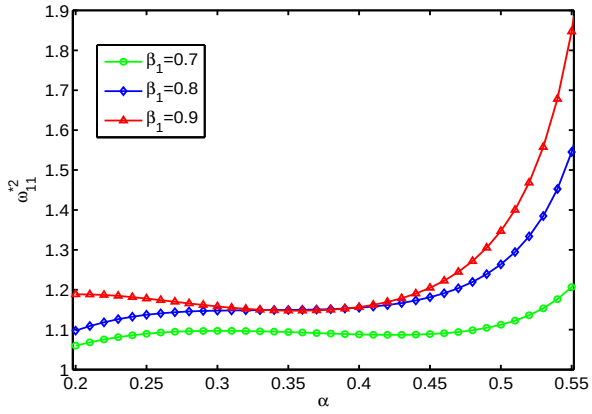

Figure 3.10: Non-dimensional sloshing frequency $\omega_{11}^{*2}(m=1,n=1)$ versus α for different values of β_1 for $\beta_2=1$, $\gamma=0.7$

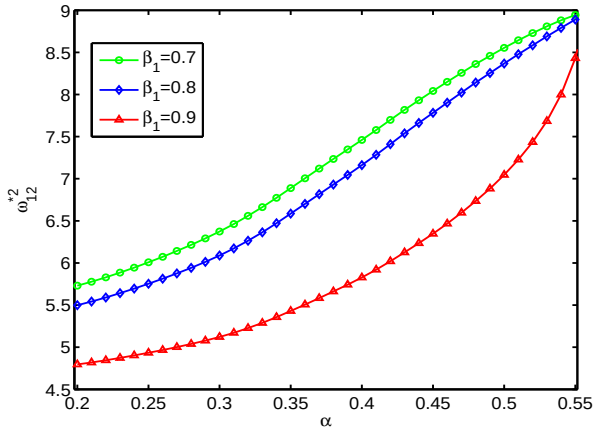

Figure 3.11: Non-dimensional sloshing frequency $\omega_{12}^{*2}(m=1,n=2)$ versus α for different values of β_1 for $\beta_2=1$, $\gamma=0.7$

the rate of increase of nondimensional frequency for increasing α. It is also observed that when the baffle is placed near the free surface, it shows a significant change in the value of frequency. Figures 3.8 and 3.9 show the first two non-dimensional frequency

curves versus α for different baffle positions. It is observed that non-dimensional frequency increases monotonically with increasing inner-outer radius ratio of the cylinder. Figures 3.10 and 3.11 illustrate the first two non-dimensional frequency curves versus α for various positions of the baffle. In Fig. 3.10, no significant increment is observed for $\alpha \leq 0.43$ and after that non-dimensional frequency increases rapidly. Figure 3.11 shows that non-dimensional frequency versus α increases monotonically for different

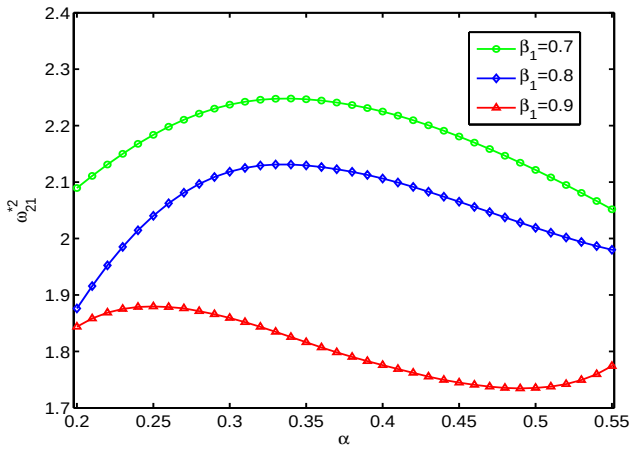

Figure 3.12: Non-dimensional sloshing frequency $\omega_{21}^{*2}(m = 2, n = 1)$ versus α for different values of β_1 for $\beta_2 = 1$, $\gamma = 0.7$

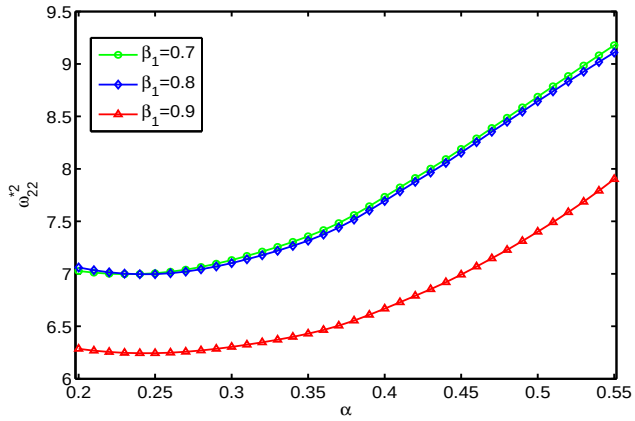

Figure 3.13: Non-dimensional sloshing frequency $\omega_{22}^{*2}(m = 2, n = 2)$ versus α for different values of β_1 for $\beta_2 = 1$, $\gamma = 0.7$

baffle positions.

Figures 3.12 and 3.13 show the first two non-dimensional frequency curves versus α for different baffle positions. Curves in Figs. 3.12 and 3.13 quantify a different behaviour for first two frequencies.

In Fig. 3.12, non-dimensional frequency increases for lower values of α and decreases slowly for higher values. In Fig. 3.13, non-dimensional frequency increases monotonically. Increasing non-dimensional frequency for increasing value of α is quite reasonable because increasing α reduces the free surface where sloshing takes place.

3.4 Conclusions

In the work presented here, a semi analytical approach is used to investigate the effect of a rigid annular baffle placed inside the fluid domain of a vertical circular cylindrical container with special configuration. Linear water wave theory is employed to investigate the sloshing frequencies in the configuration. We investigate sloshing frequencies for different baffle positions, different baffle-width and different configurations. It is observed that when the baffle is placed nearer the free surface, it has a greater significance on frequency and as it moves towards the bottom, its effect reduces gradually. The effect of the inner baffle-container radius ratio on non-dimensional frequency is monotonic for higher values of the inner baffle-container radius ratio parameter. It is observed that when the inner-outer radius ratio increases, non-dimensional frequency increases monotonically. It is clear that when an annular baffle is introduced at the container wall in the free liquid surface plane, it shows a great influence on natural frequencies. As the natural frequency increases, the sloshing mass decreases thereby bringing stability to the overall structure including the vehicle in which the liquid container is being transported. From figures it is clear that the mode corresponding to $m = 1$ is the mode with the lowest frequency. In other words, the annular baffle plays a very important role on the sloshing frequency of liquid. Control on sloshing frequencies not only reduces the splashing of fluid but also increases the stability of the system. All the conclusions are made on the basis of numerical experiments.

Chapter 4

Linear sloshing in a vertical circular cylinder with a curved bottom in the presence of a rigid baffle

4.1 Introduction

A vertical circular cylinder is considered with an uneven bottom which is filled with a liquid whose height is h on an otherwise flat bottom. Sloshing frequencies are obtained for the liquid without and with an annular baffle mounted on the wall of the cylinder at the free surface. It is observed that by increasing the width of the baffle, the natural frequencies can be significantly increased. Investigations are also carried out for different values of Bond number which depicts different states of surface tension, and also for varying values of the part of the radius in the fluid region. It is also observed that by increasing the fluid height inside the container, the natural frequencies can be increased which results in reduction of sloshing. Results show the dependence of sloshing frequencies on baffle-width, liquid height ratio as well as on maximum elevation of the bottom. It is observed that frequency increases in presence of surface tension. It is shown that fundamental sloshing frequency increases when baffle-width increases. The results here are shown for a particular curved bottom. All observations are supported by appropriate graphs.

4.2 Statement and formulation of the problem

An incompressible and inviscid fluid is assumed to perform irrotational motion in a circular cylinder of radius R_1 with an uneven bottom. The cylinder is filled with a liquid whose height is h on an otherwise flat bottom. We choose cylindrical coordinates (r, θ, z) in which z is measured vertically upwards from the undisturbed free surface $z = 0$ with

the origin O chosen on it and $z = -h + \epsilon f(r)$ as the rigid uneven bottom where $\epsilon(\ll 1)$ is a non-dimensional parameter and $f(r)$ is a smooth function with the property that $f(r) \to 0$ as $r \to R_1$, h denotes the uniform finite depth of the fluid in the absence of the unevenness at the bottom. Figure 4.2 depicts the physical problem.

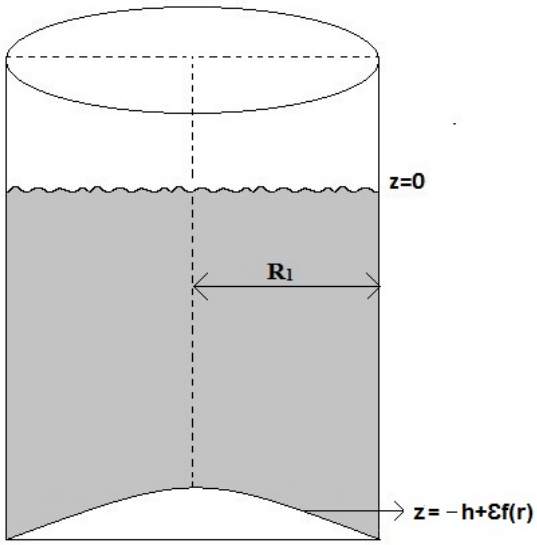

Figure 4.1: Schematic diagram of the problem

The considerations, as above, allow us to describe the fluid motion by a velocity potential $\Phi(r, \theta, z, t)$. The boundary value problem (BVP) for the corresponding sloshing problem is given by

$$\nabla^2\Phi = 0, \qquad r < R_1, \quad 0 \le \theta \le 2\pi, \quad -h + \epsilon f(r) < z < 0,$$

i.e.,

$$\frac{\partial^2\Phi}{\partial r^2} + \frac{1}{r}\frac{\partial\Phi}{\partial r} + \frac{1}{r^2}\frac{\partial^2\Phi}{\partial\theta^2} + \frac{\partial^2\Phi}{\partial z^2} = 0, r < R_1, 0 \le \theta \le 2\pi, -h + \epsilon f(r) < z < 0, \tag{4.1}$$

with the boundary wall condition

$$\frac{\partial\Phi}{\partial r} = 0 \qquad \text{at} \quad r = R_1, \tag{4.2}$$

and the impermeable bottom boundary condition

$$\frac{\partial\Phi}{\partial n} = 0 \qquad \text{at} \quad z = -h + \epsilon f(r), \tag{4.3}$$

which can be transformed to a condition satisfied at $z = -h$ by a Taylor series expansion. Since ϵ is very small, so neglecting $O(\epsilon^2)$ terms, the bottom boundary condition (4.3) can be expressed in an appropriate form as

$$\frac{\partial \Phi}{\partial z} = \epsilon \left(f'(r) \frac{\partial \Phi}{\partial r} - f(r) \frac{\partial^2 \Phi}{\partial z^2} \right) \quad \text{at} \quad z = -h. \tag{4.4}$$

The condition at the free surface $z = 0$ is obtained from the kinematic condition

$$\frac{\partial \Phi}{\partial z} = \frac{\partial \eta}{\partial t} \tag{4.5}$$

and the dynamic boundary condition (with surface tension included)

$$\frac{\partial \Phi}{\partial t} + g\eta - \frac{\sigma}{\rho} \left[\frac{\partial^2 \eta}{\partial r} + \frac{1}{r} \frac{\partial \eta}{\partial r} + \frac{1}{r^2} \frac{\partial^2 \eta}{\partial \theta^2} \right] = \text{constant}, \tag{4.6}$$

where $\eta(r, \theta, t)$ is the free surface elevation, σ the surface tension, ρ the density of the fluid and g the gravitational constant. Combining Eqs. (4.5) and (4.6), the free surface condition is obtained as

$$\frac{\partial^2 \Phi}{\partial t^2} + g \frac{\partial \Phi}{\partial z} + \frac{\sigma}{\rho} \frac{\partial^3 \Phi}{\partial z^3} = 0. \tag{4.7}$$

4.2.1 Solution procedure

For determining the natural frequencies of the liquid, we require the solution of the above BVP. We seek a solution which is harmonic in time, so that the velocity potential $\Phi(r, \theta, z, t)$ can be expressed as

$$\Phi(r, \theta, z, t) = \phi(r, z) \exp\{\iota(m\theta + \omega t)\}, \tag{4.8}$$

where ω is the angular wave frequency.
Then $\phi(r, z)$ satisfies the following equations (corresponding to Eqs. (4.1), (4.2) and (4.4))

$$\frac{\partial^2 \phi}{\partial r^2} + \frac{1}{r} \frac{\partial \phi}{\partial r} - \frac{m^2}{r^2} \phi + \frac{\partial^2 \phi}{\partial z^2} = 0, \quad r < R_1, \quad -h + \epsilon f(r) < z < 0, \tag{4.9}$$

$$\frac{\partial \phi}{\partial r} = 0 \quad \text{at} \quad r = R_1, \tag{4.10}$$

$$\frac{\partial \phi}{\partial z} = \epsilon \left(f'(r) \frac{\partial \phi}{\partial r} - f(r) \frac{\partial^2 \phi}{\partial z^2} \right) \quad \text{at} \quad z = -h. \tag{4.11}$$

In order to solve the above boundary value problem, we employ a perturbation technique involving a small parameter ϵ by introducing a perturbed velocity potential $\phi_1(r, z)$ so as to assume $\phi(r, z)$ to be of the form

$$\phi(r, z) = \phi_0(r, z) + \epsilon \phi_1(r, z) + O(\epsilon^2). \tag{4.12}$$

Now the BVP is converted to the following two boundary value problems by applying (4.12) to Eqs. (4.9) – (4.11)

BVP I:

$$\frac{\partial^2\phi_0}{\partial r^2}+\frac{1}{r}\frac{\partial\phi_0}{\partial r}-\frac{m^2}{r^2}\phi_0+\frac{\partial^2\phi_0}{\partial z^2}=0, r<R_1, -h+\epsilon f(r)<z<0, \tag{4.13}$$

$$\frac{\partial\phi_0}{\partial r}=0 \qquad \text{at} \quad r=R_1, \tag{4.14}$$

$$\frac{\partial\phi_0}{\partial z}=0 \qquad \text{at} \quad z=-h, \tag{4.15}$$

and

BVP II:

$$\frac{\partial^2\phi_1}{\partial r^2}+\frac{1}{r}\frac{\partial\phi_1}{\partial r}-\frac{m^2}{r^2}\phi_1+\frac{\partial^2\phi_1}{\partial z^2}=0, r<R_1, -h+\epsilon f(r)<z<0, \tag{4.16}$$

$$\frac{\partial\phi_1}{\partial r}=0 \qquad \text{at} \quad r=R_1, \tag{4.17}$$

$$\frac{\partial\phi_1}{\partial z}=\left(f'(r)\frac{\partial\phi_0}{\partial r}-f(r)\frac{\partial^2\phi_0}{\partial z^2}\right)\equiv p(r) \quad \text{at} \quad z=-h. \tag{4.18}$$

Solution for BVP I

The boundary value problem for ϕ_0, given by Eqs. (4.13) – (4.15), permits the exact solution which can be obtained by the separation of variables method and is given by

$$\phi_0(r,z)=\sum_{n=1}^{\infty}A_{mn}J_m\left(\frac{k_{mn}}{R_1}r\right)\frac{\cosh\left\{\frac{k_{mn}}{R_1}(z+h)\right\}}{\cosh\left\{\frac{k_{mn}}{R_1}(h)\right\}}, \tag{4.19}$$

where k_{mn} are the zeros of the first derivative of Bessel's function:

$$J'_m(kr)=0 \qquad \text{at} \quad r=R_1.$$

Solution for BVP II

Now the reduced boundary value problem for ϕ_1, given by Eqs. (4.16) – (4.18), can be solved by introducing finite Hankel transform with respect to r. Since the problem is set up in cylindrical coordinates and contains a non-zero Neumann boundary condition (4.18) at the bottom, employing finite Hankel transform seems to be appropriate. The m-th order finite Hankel transform of $\phi_1(r,z)$ with respect to r is defined as

$$\mathcal{H}_m\{\phi_1(r,z)\}=\int_0^{R_1}r\phi_1(r,z)J_m\left(\frac{k_{mn}}{R_1}r\right)dr=\bar{\phi}_1(k_{mn},z), \qquad 0\le r\le R_1. \tag{4.20}$$

The inversion formula is given by [11]

$$\phi_1(r,z) = \frac{2}{R_1^2}\sum_{n=1}^{\infty}\bar{\phi}_1(k_{mn},z)\frac{J_m(\frac{k_{mn}}{R_1}r)}{J_{m+1}^2(k_{mn})}, \tag{4.21}$$

where the summation is taken over all the positive roots of $J'_m(kR_1)=0$. Now applying finite Hankel transform to Eqs. (4.16) and (4.18), we get the following transformed BVP:

$$\frac{d^2}{dz^2}\bar{\phi}_1(k_{mn},z) - \frac{k_{mn}^2}{R_1^2}\bar{\phi}_1(k_{mn},z) = 0, \tag{4.22}$$

$$\frac{d}{dz}\bar{\phi}_1(k_{mn},z) = \bar{p}(k_{mn}) \quad \text{at} \quad z=-h, \tag{4.23}$$

where $\bar{p}(k_{mn})$ is the finite Hankel transform of $p(r)$ given by

$$\bar{p}(k_{mn}) = \frac{A_{mn}}{\cosh(\frac{k_{mn}}{R_1}h)}\bar{p}_1(k_{mn}),$$

with

$$\bar{p}_1(k_{mn}) = \int_0^{R_1} r\left[\frac{k_{mn}}{R_1}f'(r)J'_m\left(\frac{k_{mn}}{R_1}r\right) - \left(\frac{k_{mn}}{R_1}\right)^2 f(r)J_m\left(\frac{k_{mn}}{R_1}r\right)\right]\times J_m\left(\frac{k_{mn}}{R_1}r\right)dr.$$

Solving Eq. (4.22), we obtain

$$\bar{\phi}_1(k_{mn},z) = B\cosh\left(\frac{k_{mn}}{R_1}z\right) + C\sinh\left(\frac{k_{mn}}{R_1}z\right),$$

where B and C are to be determined. Applying the boundary condition (4.23), we evaluate $\bar{\phi}_1(k_{mn},z)$ as

$$\bar{\phi}_1(k_{mn},z) = \left[B_{mn}\frac{\cosh\left\{\frac{k_{mn}}{R_1}(z+h)\right\}}{\cosh(\frac{k_{mn}}{R_1}h)} + A_{mn}\frac{R_1}{k_{nm}}\bar{p}_1(k_{nm})\frac{\sinh(\frac{k_{nm}}{R_1}z)}{\cosh^2(\frac{k_{mn}}{R_1}h)}\right]. \tag{4.24}$$

Inversion gives us

$$\phi_1(r,z) = \frac{2}{R_1^2}\sum_{n=1}^{\infty}\left[B_{mn}\frac{\cosh\left\{\frac{k_{mn}}{R_1}(z+h)\right\}}{\cosh\left(\frac{k_{mn}}{R_1}h\right)} + A_{mn}\frac{R_1\sinh\left(\frac{k_{mn}}{R_1}z\right)}{k_{mn}\cosh^2\left(\frac{k_{mn}}{R_1}h\right)}\bar{p}_1(k_{mn})\right] \times\frac{J_m\left(\frac{k_{mn}}{R_1}r\right)}{J_{m+1}^2(k_{mn})}. \tag{4.25}$$

4.2.2 Determination of frequency equation

For a fixed mode m, we use $N-1$ points satisfying the free surface condition for $\Phi_1(r,\theta,z,t)=\phi_1(r,z)e^{\iota(m\theta+\omega t)}$ to obtain

$$\sum_{n=1}^{N-1}\left[B_{mn}\left\{-\omega^2+\left(g\frac{k_{mn}}{R_1}+\frac{\sigma}{\rho}\left(\frac{k_{mn}}{R_1}\right)^3\right)\tanh\frac{k_{mn}}{R_1}h\right\}+ A_{mn}\left\{\frac{\bar{p}_1(k_{mn})}{\cosh^2(\frac{k_{mn}}{R_1}h)}\right\}\left\{g+\frac{\sigma}{\rho}\left(\frac{k_{mn}}{R_1}\right)^2\right\}\right]\times\frac{J_m\left(k_{mn}\frac{n_1}{N}\right)}{J^2_{m+1}(k_{mn})}=0 \tag{4.26}$$

for $n_1=1,2,\ldots,N-1$. This above system represents $N-1$ equations in $N-1$ unknowns. It is consistent if the determinant vanishes. The condition of vanishing determinant is nothing but the frequency equation itself, i.e.,

$$\omega^2_{mn}=\frac{k_{mn}}{R_1}\left\{g+\frac{\sigma}{\rho}\left(\frac{k_{mn}}{R_1}\right)^2\right\}\tanh\left(\frac{k_{mn}}{R_1}h\right). \tag{4.27}$$

After non-dimensionalizing, the frequency equation can be written as

$$\omega^{*2}_{mn}=\frac{\omega^2_{mn}}{g/R_1}=k_{mn}\left(1+\frac{k^2_{mn}}{Bo}\right)\tanh\left(k_{mn}\frac{h}{R_1}\right), \tag{4.28}$$

where ω^*_{mn} is the non-dimensional frequency and $Bo=(\rho g R_1^2)/\sigma$ is the Bond number. Note that the role of the function $f(r)$ is very significant for our problem since it is instrumental in evaluating $\bar{p}_1(k_{mn})$ and our frequency equation is valid only for those k_{mn} which are the zeros of $\bar{p}_1(k_{mn})$ and it arises from the condition of non-zero solution of (4.26).

4.2.3 Numerical discussion

Axisymmetric oscillations

For the first mode $m=0$, the fluid motion is symmetric about the origin. In this case k_{0n} are the roots of $J'_{0n}(k_{0n}\frac{r}{R_1})_{r=R_1}=0$. Here we restrict ourselves to the lowest sloshing mode $\omega^*_{01}(m=0,n=1)$ which is the mode that exhibits the largest sloshing mass participating in the sloshing process. Let us consider a special case of the uneven bottom as follows:

$$f(r)=A\cos\left(\frac{r\pi}{2R_1}\right),$$

where A is the maximum elevation of the bottom. Considering the function $f(r)$ with the described property makes the bottom smooth and curved. Assuming a bottom of this special kind imposes one extra condition for determining frequency. While dealing with Eq. (4.26) for determining the determinant, we find that our required results come out accurately for smaller values of A.

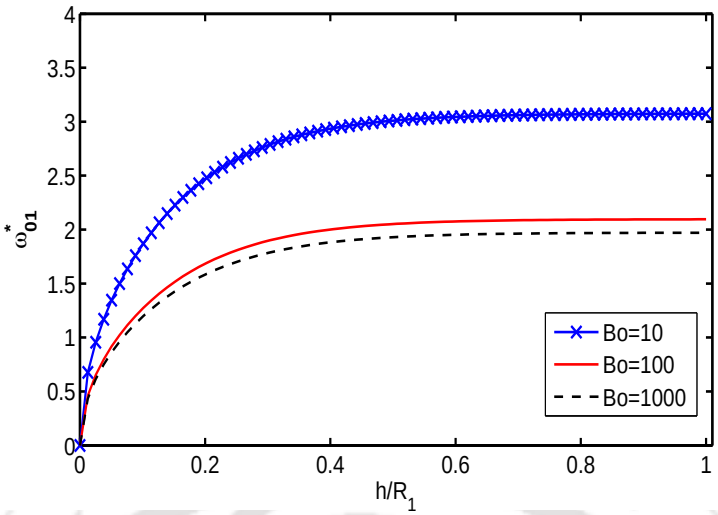

Figure 4.2: Sloshing frequency $\omega_{01}^*(m = 0, n = 1)$ vs height ratio h/R_1 for $Bo = 10, 100, 1000$;

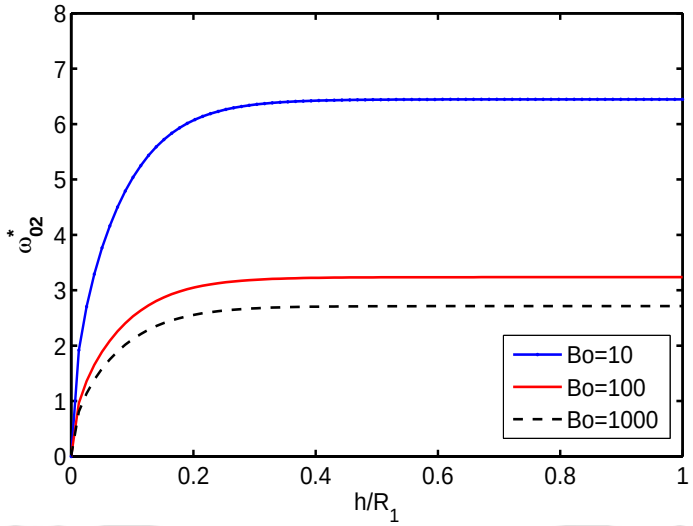

Figure 4.3: Sloshing frequency $\omega_{02}^*(m = 0, n = 2)$ vs height ratio h/R_1 for $Bo = 10, 100, 1000$;

Asymmetric oscillations

For the asymmetric sloshing modes, the very first mode, $m = 1$, is the lowest mode and k_{1n} are the roots of $J'_{1n}(k_{1n}\frac{r}{R_1})_{r=R_1} = 0$. Here we wish to examine the behaviour of the modes ω_{11}^* and ω_{12}^*. The bottom of the cylinder $f(r)$ is taken as same as before.

4.2.4 Results

Figures 4.2−4.5 show the effect of surface tension on sloshing frequencies. We investigate the natural frequencies as a function of liquid height ratio h/R_1 for different Bond

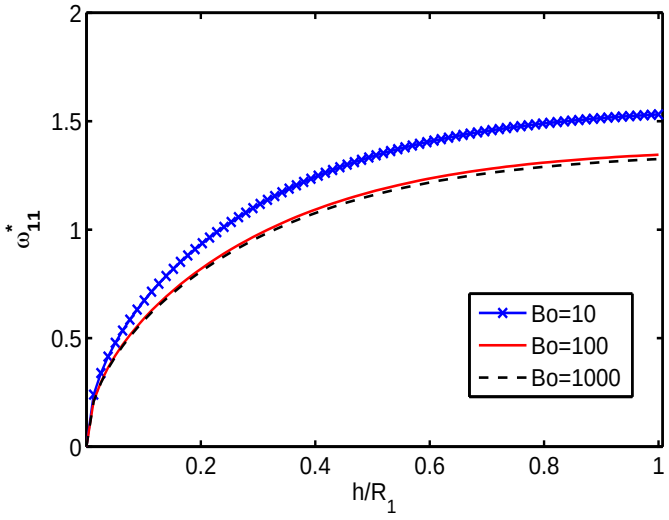

Figure 4.4: Sloshing frequency $\omega^*_{11}(m = 1, n = 1)$ vs height ratio h/R_1 for $Bo = 10, 100, 1000$;

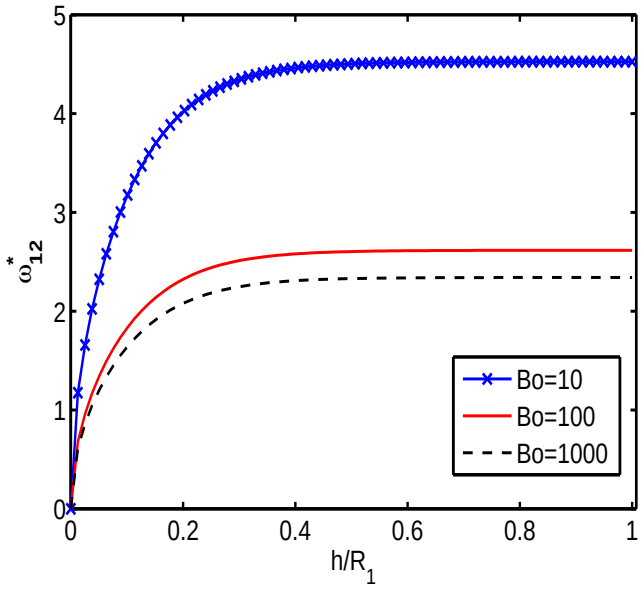

Figure 4.5: Sloshing frequency $\omega^*_{12}(m = 1, n = 2)$ vs height ratio h/R_1 for $Bo = 10, 100, 1000$;

numbers. For three different values of Bond number taken as $Bo = 10, 100, 1000$, we plot the frequency versus liquid height ratio.

Figures 4.2 and 4.3 show the graphs corresponding to ω^*_{01} and ω^*_{02}, respectively, versus h/R_1. Frequency for Bond number $Bo = 10$ is much higher than the ones corresponding to Bond numbers $Bo = 100, 1000$. Frequency increases very rapidly for an increase in liquid height ratio but only for smaller values. But for large values of h/R_1, the increase is not very substantial although the increasing tendency persists. Frequency

corresponding to ω_{02}^* is much higher than that for ω_{01}^* corresponding to different Bond numbers. More sloshing is observed corresponding to the smallest root.

In Figs. 4.4 and 4.5, frequency curves are drawn against h/R_1. Curves corresponding to ω_{11}^* show rapid change in frequency with increasing h/R_1 in a continuous manner whereas curves corresponding to ω_{12}^* show the initial increment in frequency with increasing h/R_1 for small values and after that frequency converges to a fixed value. Frequencies in the first mode corresponding to ω_{11}^* are dominant compared to all other higher modes. Frequency corresponding to ω_{11}^* produces more sloshing compared to ω_{12}^*.

It is observed that frequency is higher corresponding to smaller Bond number. It is also observed that the lower modes are the modes which exhibit the larger sloshing mass in the process.

4.3 Sloshing frequencies in the presence of a baffle at the free surface

The same cylinder is now considered with the introduction of an annular baffle mounted on the cylinder wall at the free surface. Our objective is to investigate the effect of the baffle on the sloshing frequencies. An annular baffle of width $w = (1-\alpha)R_1$, where $0 < \alpha \leq 1$, is introduced to cover some part of the free surface. Figure 4.6 depicts the physical problem. In this case the BVP is almost same as in the previous case except for

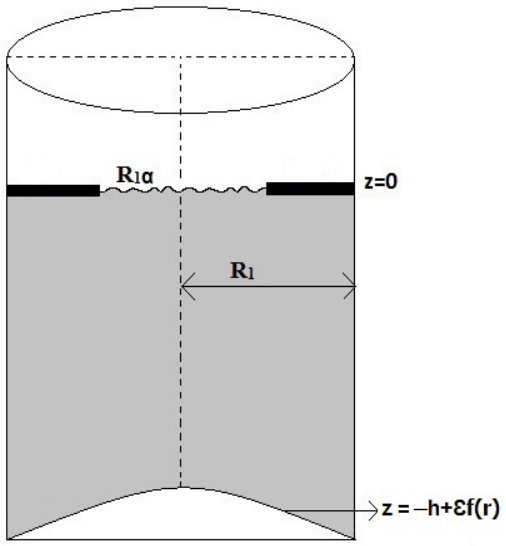

Figure 4.6: Schematic diagram of the problem with baffle at free surface

the free surface condition. Since the free surface condition is valid only for the uncovered part at $z = 0$, so now the condition at $z = 0$ can be split into two conditions as follows:

$$\frac{\partial \Phi}{\partial z} = 0 \quad \text{at} \quad z = 0 \quad \text{in the range} \quad \alpha \leq \frac{r}{R_1} \leq 1, \tag{4.29}$$

$$\frac{\partial^2 \Phi}{\partial t^2} + g\frac{\partial \Phi}{\partial z} + \frac{\sigma}{\rho}\frac{\partial^3 \Phi}{\partial z^3} = 0 \quad \text{at} \quad z = 0 \quad \text{in the range} \quad 0 \leq \frac{r}{R_1} < \alpha. \tag{4.30}$$

For a fixed mode m, we use N_1+1 points including $\frac{r}{R_1} = \alpha$ and $\frac{r}{R_1} = 1$ satisfying the impermeability condition (4.29) for $\Phi_1(r, \theta, z, t) = \phi_1(r, z)e^{\iota(m\theta+\omega t)}$ giving rise to the condition

$$\sum_{n=1}^{N_1+N_2} \left[B_{mn}\frac{k_{mn}}{R_1}\tanh\left(\frac{k_{mn}}{R_1}h\right) + A_{mn}\frac{\bar{p}_1(k_{mn})}{\cosh^2(\frac{k_{mn}}{R_1}h)} \right] \times \frac{J_m\left\{k_{mn}\left(\alpha + \frac{(1-\alpha)n_1}{N_1}\right)\right\}}{J^2_{m+1}(k_{mn})} = 0 \tag{4.31}$$

for $n_1 = 0, 1, 2, \ldots, N_1$.

The rest $N_2 - 1$ points satisfy the reduced free surface condition (4.30) giving

$$\sum_{n=1}^{N_1+N_2} \left[B_{mn}\left(-\omega^2 + \left\{ g\frac{k_{mn}}{R_1} + \frac{\sigma}{\rho}\left(\frac{k_{mn}}{R_1}\right)^3 \right\}\tanh\left(\frac{k_{mn}}{R_1}h\right)\right) + A_{mn}\left\{\frac{\bar{p}_1(k_{mn})}{\cosh^2(\frac{k_{mn}}{R_1}h)}\right\}\left\{ g + \frac{\sigma}{\rho}\left(\frac{k_{mn}}{R_1}\right)^2 \right\} \right] \times \frac{J_m\left(k_{mn}\frac{\alpha n_2}{N_2}\right)}{J^2_{m+1}(k_{mn})} = 0 \tag{4.32}$$

for $n_2 = 1, 2, \ldots, N_2 - 1$.

This system consisting of Eqs. (4.31) and (4.32) represents N_1+N_2 homogeneous algebraic equations in the coefficients $A_{m1}, A_{m2}, \ldots, A_{m(N_1+N_2)}$, $B_{m1}, B_{m2}, \ldots, B_{m(N_1+N_2)}$. The condition of a non-trivial solution gives rise to the frequency equation for determining the approximate sloshing frequencies of the liquid in the container.

4.3.1 Numerical description and results

The effect of baffle on the free surface is evaluated numerically. For a baffle of width $w = R_1(1-\alpha)$, the behaviour of sloshing frequencies is investigated for various α values. We investigate the dependence of the natural sloshing frequency ω^*_{mn} on the liquid height ratio h/R_1 for fixed Bond number $Bo = 100$ for various baffle-widths. The case $\alpha = 1$ represents the situation with no baffle on the free surface. We investigate the effect of the baffle corresponding to the lowest sloshing mode $m = 0$ and then for $m = 1$.

We determine the free oscillations in a circular cylinder with an uneven bottom for two different modes, since corresponding modes are independent of each other. Dimensionless sloshing frequency ω^*_{mn} is plotted as a function of the ratio of fluid depth to radius for various α values in Figs. $4.7 - 4.10$. We observe that the frequency increases

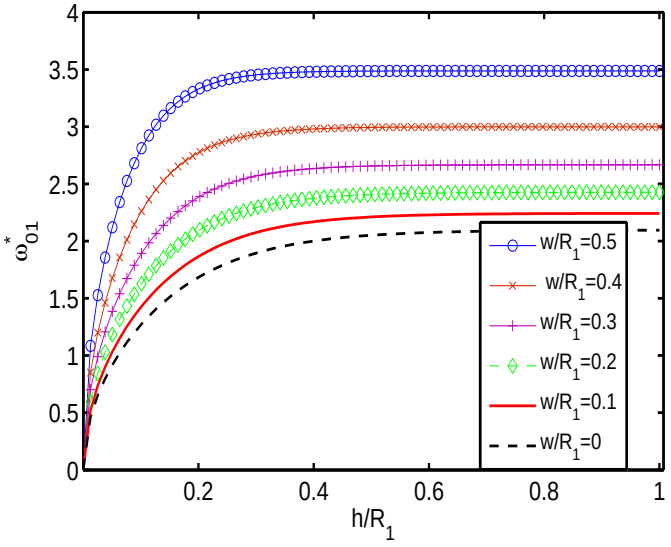

Figure 4.7: Sloshing frequency $\omega^*_{01}(m = 0, n = 1)$ for different annular baffles of width $w/R_1 = (1 - \alpha)$ vs height ratio h/R_1 for $Bo = 100$;

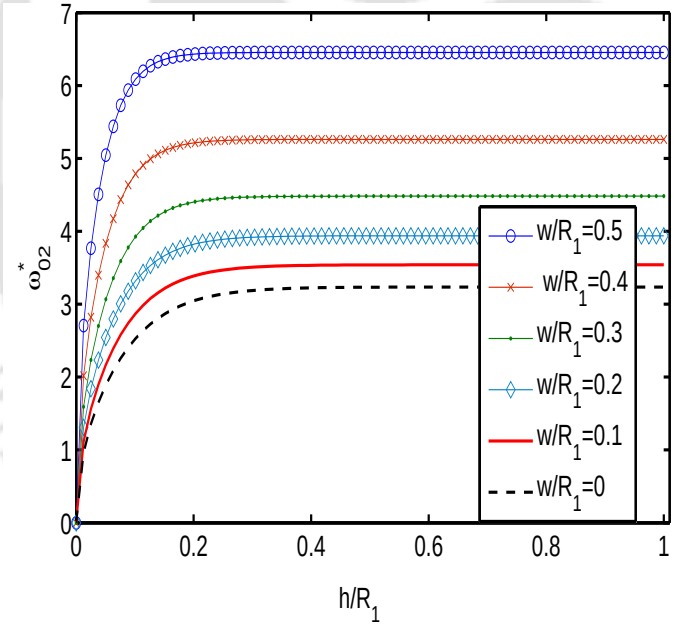

Figure 4.8: Sloshing frequency $\omega^*_{02}(m = 0, n = 2)$ for different annular baffles of width $w/R_1 = (1 - \alpha)$ vs height ratio h/R_1 for $Bo = 100$;

with an increasing baffle-width. $w/R_1 = 0$ is the case when there is no baffle on the free surface.

Figures 4.7 and 4.8 show the frequency curves against h/R_1 for a fixed Bond number $Bo = 100$ for various baffle-widths. Fundamental frequency for ω^*_{01} corresponding to a baffle-width $w/R_1 = 0.5$ is approximately twice compared to the frequency correspond-

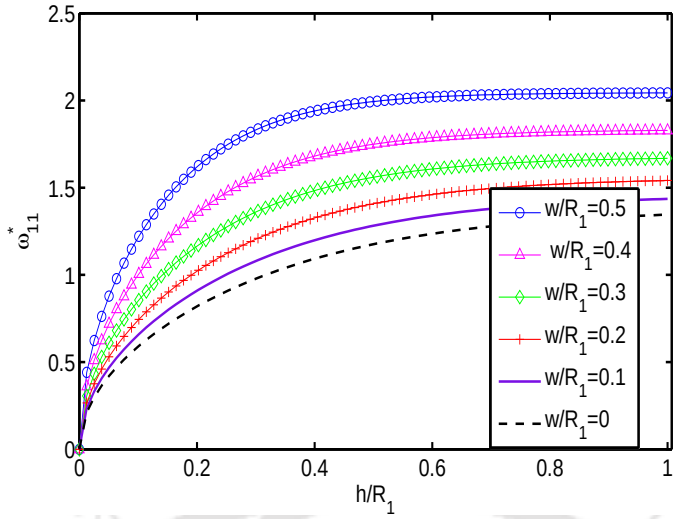

Figure 4.9: Sloshing frequency $\omega^*_{11}(m = 1, n = 1)$ for different annular baffles of width $w/R_1 = (1 - \alpha)$ vs height ratio h/R_2 for $Bo = 100$;

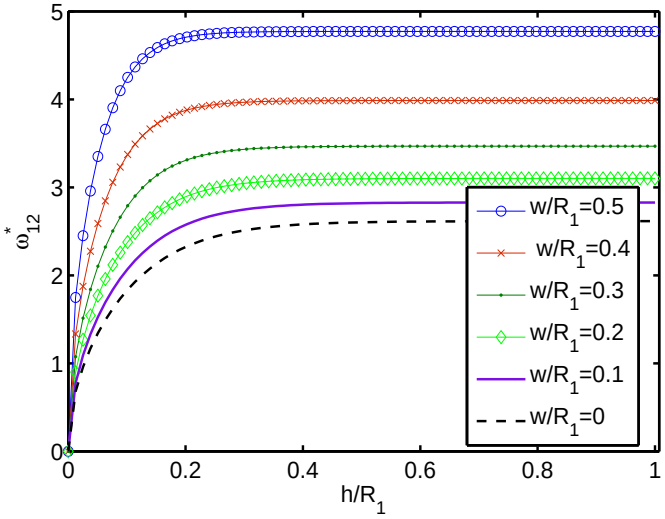

Figure 4.10: Sloshing frequency $\omega^*_{12}(m = 1, n = 2)$ for different annular baffles of width $w/R_1 = (1 - \alpha)$ vs height ratio h/R_1 for $Bo = 100$;

ing to $w/R_1 = 0$, i.e., when there is no baffle at the free surface. Frequency increases rapidly with increasing h/R_1 for less height of the cylinder but there is no appreciable change when the height increases further. It increases with an increasing baffle-width. It is observed that the behaviour of frequency corresponding to ω^*_{02} is much more stable compared to that corresponding to ω^*_{01}. Frequency for ω^*_{02} increases for small values of h/R_1 and then converges to a fixed value. Fundamental frequency for ω^*_{02} corresponding to a baffle-width $w/R_1 = 0.5$ is more than twice compared to the frequency corresponding to $w/R_1 = 0$, i.e., when there is no baffle at the free surface.

In Figs. 4.9 and 4.10, frequency curves are drawn against liquid height ratio h/R_1 for

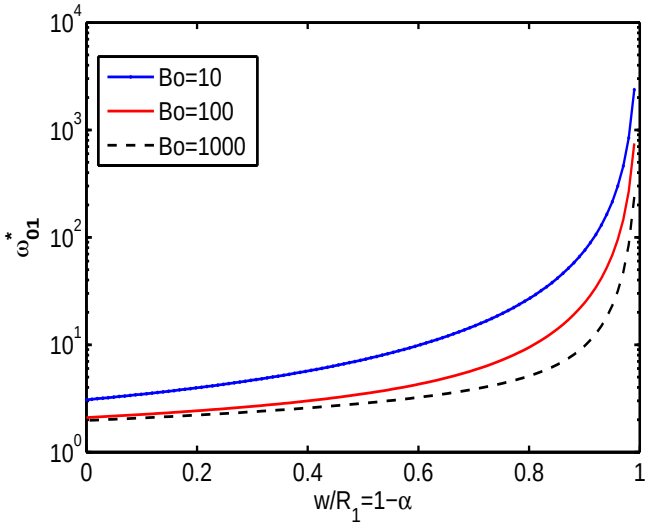

Figure 4.11: Effect of baffle-width $w/R_1 = (1-\alpha)$ at height ratio $h/R_1 = 1$ for different Bond numbers

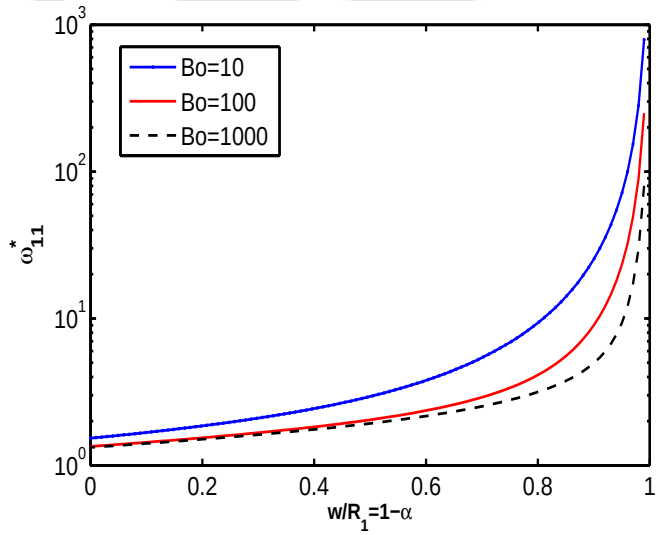

Figure 4.12: Effect of baffle-width $w/R_1 = (1-\alpha)$ at height ratio $h/R_1 = 1$ for different Bond numbers

a fixed Bond number $Bo = 100$ for various baffle-widths. Curves corresponding to ω^*_{11} show a continuous increment in frequency with increasing h/R_1 as well as with increasing baffle-width whereas curves corresponding to ω^*_{12} show a stable behaviour with increasing h/R_1. Frequency corresponding to ω^*_{11} increases continuously with increasing h/R_1 for less height of the cylinder but there is no appreciable change when the height increases further. It increases with an increasing baffle-width. Frequency corresponding to ω^*_{12} increases for small values of h/R_1 and for higher values it converges to a fixed value. ω^*_{12},

corresponding to a baffle-width $w/R_1 = 0.5$, is approximately twice as compared to the frequency for baffle-width $w/R_1 = 0$. The dominant mode of oscillations corresponds to the smallest root. Here $\omega^*_{11}(n = 1, m = 1)$ is the lowest sloshing mode which exhibits the largest fluid mass in the process of sloshing.

Figures 4.11 and 4.12 show the dimensionless fundamental sloshing frequency as a function of the magnitude of the baffle-width $w/R_1 = 1 - \alpha$ for a fixed liquid height ratio $h/R_1 = 1$ for different Bond numbers $Bo = 10, 100, 1000$. For smaller values of the baffle-width, the values of the frequencies corresponding to all the Bond numbers are very small. Any significant increase in frequencies is observed only for $w/R_1 \geq 0.059$. There is a sharp increase in frequencies when the value of w/R_1 is very high (w/R_1=0.95). The highest frequency corresponds to the smallest Bond number $Bo = 10$. In fact, it can be seen that the values of frequency corresponding to $Bo = 10$ is much higher than those corresponding to $Bo = 100, 1000$.

4.4 Conclusions

In this work, we consider a vertical circular cylinder with an uneven bottom which is filled with a liquid whose height is h on an otherwise flat bottom. A semi analytical approach based on linearized water wave theory is employed to investigate the sloshing frequencies in the configuration. A closed form solution is obtained by employing finite Hankel transform with the assumption that the geometry can be approximated by one that permits the exact solution. We investigate the sloshing frequencies for different baffle-widths, fluid heights and different Bond numbers. Results show the dependence of sloshing frequencies on baffle-width, liquid height ratio as well as on maximum elevation of the bottom. We consider a specific form of the curved bottom for which results are obtained for small values of A, the maximum elevation of the bottom. It is observed that frequency increases in the presence of surface tension. It is shown that fundamental sloshing frequency increases when baffle-width increases. In fact it is observed that the frequency has very high values corresponding to higher values of the baffle-width. It is clear that when an annular baffle is introduced at the container wall in the free liquid surface plane, it yields increased natural frequencies. Control on sloshing frequencies not only reduces the splashing of fluid but also increases the stability of the system. It is expected that our results will be valid for any arbitrary bottom with small elevation and the procedure adopted here may be applied to various arbitrary coverage of the free liquid surface.

Chapter 5

Liquid sloshing in a circular cylindrical container containing a two-layer fluid

5.1 Introduction

In this work, a semi-analytical approach is used to investigate sloshing in an immiscible, incompressible and inviscid two-layer fluid. We evaluate natural sloshing frequencies of a two-layer fluid of different layer-wise densities $\rho_1 < \rho_2$ with an interface and a surface in a vertical circular cylinder. On the basis of the velocity potential formulation of the fluid motion inside the container, an infinite system of homogeneous linear equation is obtained. We demonstrate the effects of the parameters such as fluid heights and density ratio on the natural sloshing frequencies. The results are supported by relevant graphs.

5.2 Statement and formulation of the problem

Two immiscible, incompressible and inviscid fluids are assumed to perform irrotational motion in a vertical circular cylinder partially filled with fluid. The radius of the cylinder is taken as R_1. We introduce cylindrical coordinate system (r, θ, z) in which z is measured vertically upwards from the mean interface. The origin O is considered at the interface and hence $z = 0$ is the mean position of the interface of the two fluids while $z = h_1$ represents the free surface and $z = -h_2$ the bottom of the cylinder. By $\rho = \rho_1/\rho_2 (< 1)$, we denote the ratio of the densities ρ_1 of upper fluid and ρ_2 of lower fluid. Linear water wave theory is utilized to describe the fluid motion inside the container. Figure 5.1 depicts the physical problem.

With the above assumptions, the fluid flow can now be described in terms of a

velocity potential Φ that satisfies Laplace's equation

$$\frac{\partial^2\Phi}{\partial r^2}+\frac{1}{r}\frac{\partial\Phi}{\partial r}+\frac{1}{r^2}\frac{\partial^2\Phi}{\partial\theta^2}+\frac{\partial^2\Phi}{\partial z^2}=0 \qquad \text{in} \quad \Omega, \tag{5.1}$$

where Ω is fluid domain of the container, along with rigid boundary conditions

$$\frac{\partial\Phi}{\partial\mathbf{n}}=0 \qquad \text{on} \quad \Gamma, \tag{5.2}$$

where Γ is solid wetted interface and $\mathbf{n}$ is the outward normal to Γ, and

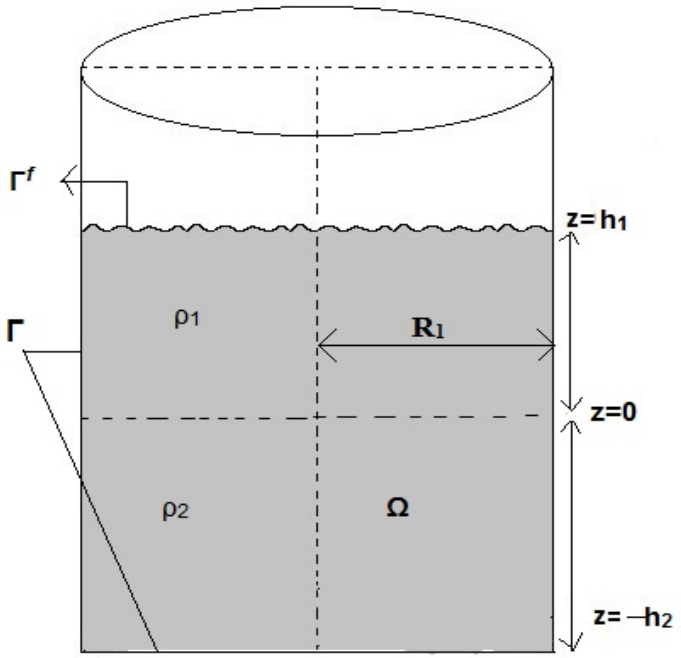

Figure 5.1: Schematic diagram of the problem

free surface condition

$$\frac{\partial\Phi}{\partial\mathbf{n}}+\frac{1}{g}\frac{\partial^2\Phi}{\partial t^2}=0 \qquad \text{on} \quad \Gamma^f, \tag{5.3}$$

where Γ^f is the free surface.

5.2.1 Boundary Value Problems (BVP) for upper and lower fluids

Due to the presence of two immiscible fluids, the boundary value problem described by Eqs. $(5.1)-(5.3)$ can be written as two boundary value problems corresponding to each fluid. The velocity potential in upper fluid is denoted by Φ_1 and that in lower fluid by Φ_2. According to Eq. (5.1), each velocity potential satisfies Laplace's equation.

The boundary value problem in upper fluid is given by

$$\frac{\partial^2\Phi_1}{\partial r^2}+\frac{1}{r}\frac{\partial\Phi_1}{\partial r}+\frac{1}{r^2}\frac{\partial^2\Phi_1}{\partial\theta^2}+\frac{\partial^2\Phi_1}{\partial z^2}=0, \tag{5.4}$$

with the boundary wall condition

$$\left(\frac{\partial\Phi_1}{\partial r}\right)_{r=R_1}=0. \tag{5.5}$$

The boundary value problem in lower fluid is given by

$$\frac{\partial^2\Phi_2}{\partial r^2}+\frac{1}{r}\frac{\partial\Phi_2}{\partial r}+\frac{1}{r^2}\frac{\partial^2\Phi_2}{\partial\theta^2}+\frac{\partial^2\Phi_2}{\partial z^2}=0, \tag{5.6}$$

with the boundary wall condition

$$\left(\frac{\partial\Phi_2}{\partial r}\right)_{r=R_1}=0, \tag{5.7}$$

and the bottom boundary condition

$$\left(\frac{\partial\Phi_2}{\partial z}\right)_{z=-h_2}=0. \tag{5.8}$$

Free surface condition will be satisfied by the velocity potential Φ_1:

$$\frac{\partial\Phi_1}{\partial z}+\frac{1}{g}\frac{\partial^2\Phi_1}{\partial t^2}=0 \qquad \text{at} \quad z=h_1. \tag{5.9}$$

5.2.2 Solutions of BVP for different fluids

We write the velocity potential as time harmonic in the following form

$$\Phi(r,\theta,z,t)=\phi(r,\theta,z)e^{\iota\omega t}, \tag{5.10}$$

where ω is natural angular wave frequency. Corresponding potentials for both fluids take the form as follows

$$\Phi_i(r,\theta,z,t)=\phi_i(r,\theta,z)e^{\iota\omega t}, \qquad i=1,2. \tag{5.11}$$

Introducing Eq. (5.11) into Eqs. (5.5), (5.7) and (5.8), the corresponding conditions get converted to

$$\left(\frac{\partial\phi_1}{\partial r}\right)_{r=R_1}=0, \tag{5.12}$$

$$\left(\frac{\partial\phi_2}{\partial r}\right)_{r=R_1}=0, \quad \left(\frac{\partial\phi_2}{\partial z}\right)_{z=-h_2}=0. \tag{5.13}$$

On the basis of linear water wave theory, the boundary-value problem (5.1) – (5.3) is a linear eigenvalue problem. We apply superposition principle to find the mode shape of the liquid domain. In order to set up and solve the BVPs in each sub-domain independently, we are required to impose one extra (otherwise non-existent) boundary condition at the interface due to lack of sufficient boundary conditions - one at a time for one component, depending on the number of interfaces available in each sub-domain. It is to be noted that these extra conditions are later suitably absorbed while using the overall matching conditions across the interfaces. By superposition principle, ϕ_i for $i = 1, 2$, can be written as

$$\phi_i = \sum_{j=1}^{k_i} \phi_i^j, \tag{5.14}$$

where ϕ_i^j is the j-th component of ϕ_i and k_i denotes the number of liquid interfaces in i-th fluid. With the help of (5.14), each ϕ_i takes the following forms:

$$\phi_1 = \phi_1^1 + \phi_1^2, \tag{5.15}$$

$$\phi_2 = \phi_2^2, \tag{5.16}$$

where ϕ_i^1 corresponds to the component of the velocity potential in the respective regions due to the non-rigid condition at the surface $z = h_1$; ϕ_i^2 to that component of the velocity potential due to the non-rigid condition at the mean surface $z = 0$. In order to maintain the periodicity of Φ_i, ϕ_i^j can be assumed to take the form

$$\phi_i^j = \sum_{m=0}^{\infty} \phi_{im}^j \cos m\theta, \tag{5.17}$$

where m is an integer identifying an azimuthal mode. The boundary conditions for ϕ_i^j in both fluids can be found out with the help of Eqs. (5.12) – (5.13). Rigid boundary conditions in both fluids are as follows:
For upper fluid:

$$\left(\frac{\partial \phi_1^1}{\partial r}\right)_{r=R_1} = 0, \qquad \left(\frac{\partial \phi_1^1}{\partial z}\right)_{z=0} = 0, \tag{5.18}$$

$$\left(\frac{\partial \phi_1^2}{\partial r}\right)_{r=R_1} = 0, \qquad \left(\phi_1^2\right)_{z=h_1} = 0. \tag{5.19}$$

For lower fluid:

$$\left(\frac{\partial \phi_2^2}{\partial r}\right)_{r=R_1} = 0, \qquad \left(\frac{\partial \phi_2^2}{\partial z}\right)_{z=-h_2} = 0. \tag{5.20}$$

Now we introduce the following dimensionless quantities in order to non-dimensionalize the parameters as given below:

$$\xi = \frac{r}{R_1}, \quad \eta = \frac{z}{R_1}, \quad \beta_1 = \frac{h_1}{R_1}, \quad \beta_2 = \frac{h_2}{R_1}, \quad \omega^* = \omega\sqrt{\frac{R_1}{g}}. \tag{5.21}$$

The boundary value problems in different sub-domains allow separation of variables in (r, θ, z)-coordinate system for ϕ_i^j and permit the exact solutions which can be obtained in terms of eigenfunctions. The corresponding solutions for both fluids can be written as follows:

For upper fluid:

$$\phi_1^1 = \sum_{n=1}^{\infty} A_{1mn}^1 \cosh(\lambda_{mn}\eta) J_m(\lambda_{mn}\xi) + A_{100}^1 \delta_m^1, \tag{5.22}$$

$$\phi_1^2 = \sum_{n=1}^{\infty} A_{1mn}^2 \frac{\sinh(\lambda_{mn}(\eta - \beta_1))}{\cosh(\lambda_{mn}\beta_1)} J_m(\lambda_{mn}\xi) + A_{100}^2 (\eta - \beta_1)\delta_m^1, \tag{5.23}$$

where λ_{mn} are zeros of

$$J_m'(\lambda_{mn}) = 0, \tag{5.24}$$

and

$$\delta_m^1 = \begin{cases} 1, & \text{if } m = 0, \\ 0, & \text{otherwise.} \end{cases}$$

For lower fluid:

$$\phi_2^2 = \sum_{n=1}^{\infty} A_{2mn}^2 \frac{\cosh(\lambda_{mn}(\eta + \beta_2))}{\cosh(\lambda_{mn}\beta_2)} J_m(\lambda_{mn}\xi) + A_{200}^2 \delta_m^1. \tag{5.25}$$

5.2.3 Matching conditions

In order to utilize the matching conditions on mean interface and free surface, we truncate the series solutions after N terms. These conditions imply the continuity of pressure and velocity across the interfaces. The following are the matching conditions used across different interfaces:

(A) $\frac{\partial \phi_1}{\partial \eta} = \frac{\partial \phi_2}{\partial \eta}$ at $\eta = 0$:

$$\sum_{n=1}^{N} A_{1mn}^2 \lambda_{mn} J_m(\lambda_{mn}\xi) + A_{100}^2 = \sum_{n=1}^{N} A_{2mn}^2 \lambda_{mn} \tanh(\lambda_{mn}\beta_2) J_m(\lambda_{mn}\xi). \tag{5.26}$$

(B) $\rho\left(\frac{\partial \phi_1}{\partial \eta} - \omega^{*2}\phi_1\right) = \frac{\partial \phi_2}{\partial \eta} - \omega^{*2}\phi_2$ at $\eta = 0$:

$$\rho\left[\sum_{n=1}^{N} A^2_{1mn}\lambda_{mn}J_m(\lambda_{mn}\xi) + A^2_{100} - \omega^{*2}\left\{\sum_{n=1}^{N} A^1_{1mn}J_m(\lambda_{mn}\xi) + A^1_{100} - \sum_{n=1}^{N} A^2_{1mn}J_m(\lambda_{mn}\xi)\tanh\lambda_{mn}\beta_1 - A^2_{100}\beta_1\right\}\right]$$
$$= A^2_{2mn}J_m(\lambda_{mn}\xi)\lambda_{mn}\tanh\lambda_{mn}\beta_2 - \omega^{*2}\left\{\sum_{n=1}^{N} A^2_{2mn}J_m(\lambda_{mn}\xi) + A^2_{200}\right\}. \quad (5.27)$$

(C) $\frac{\partial\phi_1}{\partial\eta} - \omega^{*2}\phi_1 = 0 \quad$ at $\quad \eta = \beta_1$:

$$\sum_{n=1}^{N} A^1_{1mn}J_m(\lambda_{mn}\xi)\lambda_{mn}\sinh\lambda_{mn}\beta_1 + \sum_{n=1}^{N} A^2_{1mn}J_m(\lambda_{mn}\xi)\frac{\lambda_{mn}}{\cosh\lambda_{mn}\beta_1} + A^2_{100}$$
$$-\omega^{*2}\left\{\sum_{n=1}^{N} A^1_{1mn}J_m(\lambda_{mn}\xi)\cosh\lambda_{mn}\beta_1 + A^1_{100}\right\} = 0. \quad (5.28)$$

Equations (5.26) – (5.28) give rise to a homogenous linear system. Now to determine the unknowns and the non-dimensional frequency, we truncate the system at a fixed number N, apply orthogonality of Bessel functions and form a square matrix whose elements are coefficients of a Bessel series. Consequently, we get a square matrix of order $3N$ in A^j_{imn} unknowns which has the form

$$[M - \omega^{*2}\bar{M}]X = 0, \quad (5.29)$$

where

$$X = [A^1_{1mn}, A^2_{1mn}, A^2_{2mn}]^T, \quad (5.30)$$

$$M = \begin{bmatrix} [a^{11}_{mn\bar{n}}] & [a^{12}_{mn\bar{n}}] & [0] \\ [0] & [a^{22}_{mn\bar{n}}] & [a^{23}_{mn\bar{n}}] \\ [0] & [a^{32}_{mn\bar{n}}] & [a^{33}_{mn\bar{n}}] \end{bmatrix}, \quad (5.31)$$

and

$$\bar{M} = \begin{bmatrix} [\bar{a}^{11}_{mn\bar{n}}] & [0] & [0] \\ [0] & [0] & [0] \\ [\bar{a}^{31}_{mn\bar{n}}] & [\bar{a}^{32}_{mn\bar{n}}] & [\bar{a}^{33}_{mn\bar{n}}] \end{bmatrix}. \quad (5.32)$$

The expressions of the non-zero elements $a^{ij}_{mn\bar{n}}$ of the matrix are given by the coefficients of the Bessel series. The system given by (5.29) must have a non-trivial solution for the vanishing determinant condition. The condition for non-trivial solution of (5.29) gives us the values of ω^*. The detailed expressions for the non-zero coefficients of the matrix are provided in Appendix B.

5.3 Numerical results and discussion

In this section, we carry out some numerical experiments to study the effects of various parameters on the sloshing frequency. In order to do that, we present a method the convergence of which is discussed next in brief.

5.3.1 Convergence

In order to demonstrate the high accuracy of the proposed method, a convergence study on the non-dimensional frequency parameters is carried out. All numerical calculations are carried out by using MATHEMATICA and MATLAB. 'NIntigrate' command is used to evaluate the integrals. Table 5.1 displays a convincing convergence of $\omega^*_{mn}, m = 0, 1; n = 1, 2, 3$, where ω^*_{mn} is a non-dimensional parameter which represents the n-th frequency of the m-th mode. The values of ω^*_{mn} are obtained correct up to five decimal places. Table 5.1 shows fast convergence of the frequency parameters even for small number of truncated terms.

Table 5.1: Convergence of $\omega^*_{mn}(m = 0, 1; n = 1, 2, 3)$ versus number of truncated terms for $\rho = 0.63$, $\beta_1 = 1$ and for two different values of β_2

m	β_2	$N = 3$	$N = 6$	$N = 9$	$N = 12$	$N = 15$
0	0.5	0.9199387299	0.9199387299	0.9199387299	0.9199387299	0.9199387299
		1.2612464956	1.2612464956	1.2612464956	1.2612464956	1.2612464956
		1.5196097957	1.5196097957	1.5196097957	1.5196097962	1.5196097967
	1	0.9320786799	0.9320786799	0.9320786799	0.9320786799	0.9320786799
		1.2619409692	1.2619409692	1.2619409692	1.2619409692	1.2619409691
		1.5196453789	1.5196453789	1.5196453788	1.5196453785	1.5196453792
1	0.5	0.5758471883	0.5758471883	0.5758471883	0.5758471883	0.5758471883
		1.0968071056	1.0968071056	1.0968071056	1.0968071056	1.0968071056
		1.3491350977	1.3491350977	1.3491350977	1.3491350979	1.3491350982
	1	0.6270637202	0.6270637202	0.6270637202	0.6270637202	0.6270637202
		1.1000570908	1.1000570908	1.1000570908	1.1000570908	1.1000570908
		1.3555831669	1.3555831669	1.3555831667	1.3555831671	1.3555831675

5.3.2 Natural frequencies versus different parameter ratio

We carry out a number of numerical experiments here to strengthen the analytical results obtained. Curves are drawn for non-dimensional frequency versus different values of β_1, β_2 and for different values of density ratio ρ for $m = 0, 1, 2$. Dimensionless sloshing

frequency $\omega_{mn}^{*2}(m = 0, 1, 2; n = 1)$ is plotted as a function of the fluid depth to radius for the fixed value of density ratio $\rho = 0.63$. This value of ρ is chosen since we have come across a number of related works carried out in which this value of ρ is being considered.

Figures $5.2 - 5.4$ show the plots for the non-dimensional sloshing frequencies versus upper fluid height to the radius of the container. In all the figures, curves are drawn for different values of lower fluid depth to the radius for $\beta_2 = 0.25, 0.5, 0.75, 1$.

In Fig. 5.2, curves are drawn for four different depths of lower fluid: taken as $\beta_2 =$

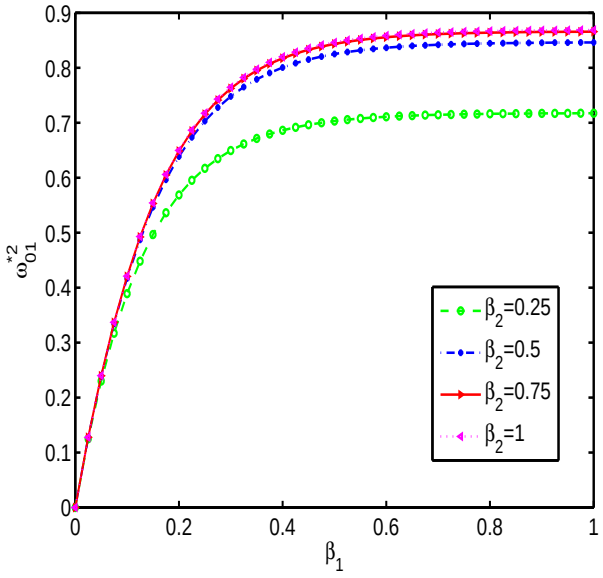

Figure 5.2: Non-dimensional sloshing frequency ω_{01}^{*2} versus β_1 for different values of β_2 for $\rho = 0.63$

$0.25, 0.5, 0.75, 1$. Each curve shows that non-dimensional sloshing frequency increases as the height of the upper fluid increases. A sudden increment is observed in the frequency for small values of β_1. It is clearly observed that ω_{01}^{*2} increases with an increasing value of lower fluid depth but difference in increment decreases gradually with an increasing value of lower fluid depth. It is also observed that when lower fluid depth is equal to upper fluid height, frequency is maximum and after that no change takes place.

In Fig. 5.3, curves are drawn for four different depths of lower fluid. Each curve shows non-dimensional sloshing frequency as a function of the upper fluid height to the radius of the container. It is clearly observed that non-dimensional frequency increases gradually with an increasing value of lower fluid depth but the difference in increment decreases gradually with increasing values of lower fluid depth.

In Fig. 5.4, the curves show the dependence of non-dimensional sloshing frequency on upper fluid height. In this mode also, non-dimensional frequency increases with an

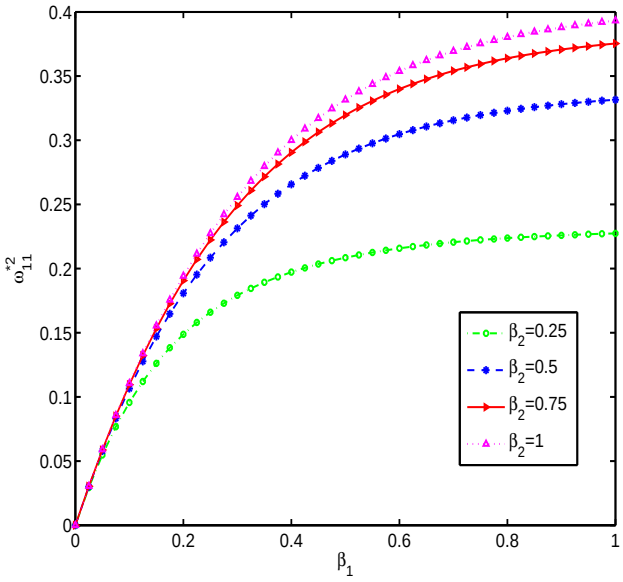

Figure 5.3: Non-dimensional sloshing frequency ω_{11}^{*2} versus β_1 for different values of β_2 for $\rho = 0.63$

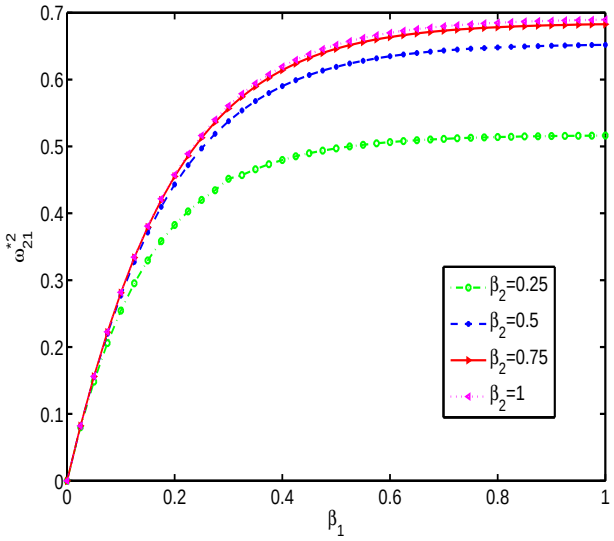

Figure 5.4: Non-dimensional sloshing frequency ω_{21}^{*2} versus β_1 for different values of β_2 for $\rho = 0.63$

increasing value of upper fluid. It is also observed that when lower fluid depth is equal to upper fluid height, frequency is maximum and after that no change takes place.

In Fig. 5.5, non-dimensional frequency is shown as a function of upper fluid height for the fixed value of lower fluid depth taken as $\beta_2 = 0.5$. It is observed that non-dimensional sloshing frequency for the mode corresponding to $m = 1$ is much lower compared to the other two curves corresponding to $m = 0, 2$. It is clearly noticeable

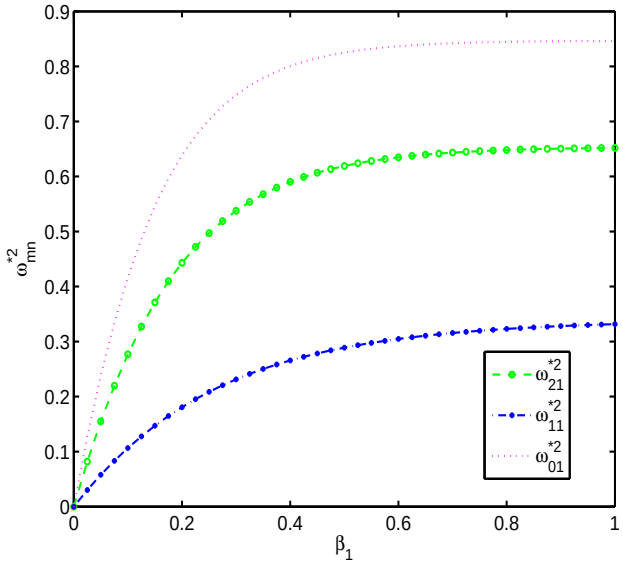

Figure 5.5: Non-dimensional sloshing frequency ω_{mn}^{*2} versus β_1 for different mode for $\beta_2 = 0.5$, $\rho = 0.63$

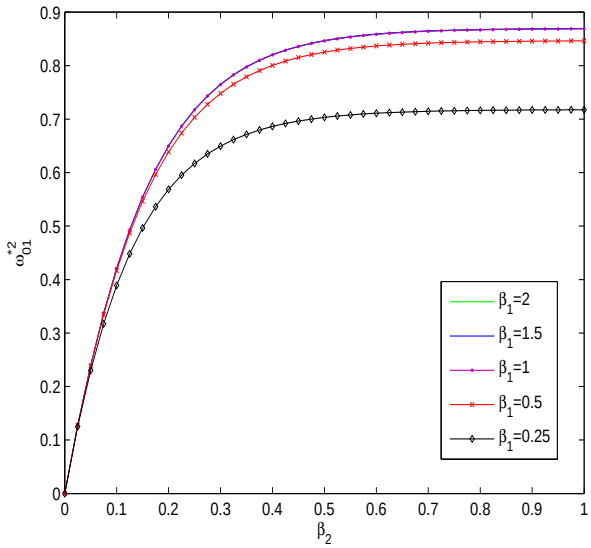

Figure 5.6: Non-dimensional sloshing frequency ω_{01}^{*2} versus β_2 for different values of β_1 for $\rho = 0.63$

that $m = 1$ is the sloshing mode which has the lowest sloshing frequency.

Figures $5.6 - 5.8$ show the plots for the non-dimensional sloshing frequencies versus lower fluid depth to the radius of the container. In all the figures, curves are drawn for different values of upper fluid height to radius for $\beta_1 = 0.25, 0.5, 1, 1.5, 2$.

In Figs. 5.6 and 5.8, curves are drawn for different heights of upper fluid taken as $\beta_1 = 0.25, 0.5, 1, 1.5, 2$. Each curve shows that non-dimensional sloshing frequency increases

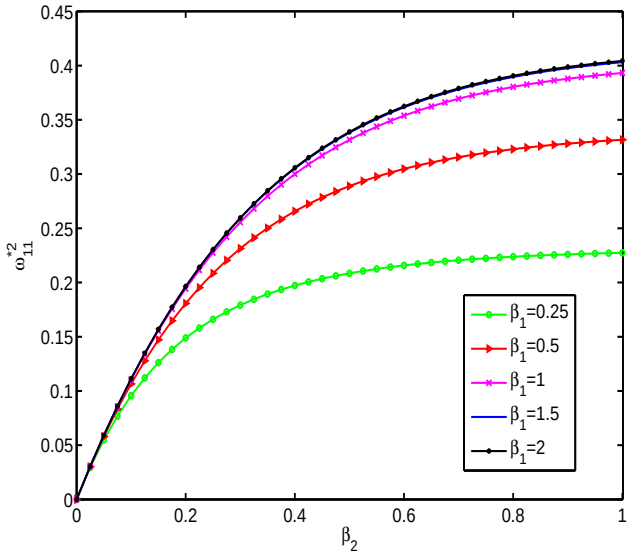

Figure 5.7: Non-dimensional sloshing frequency ω_{11}^{*2} versus β_2 for different values of β_1 for $\rho = 0.63$

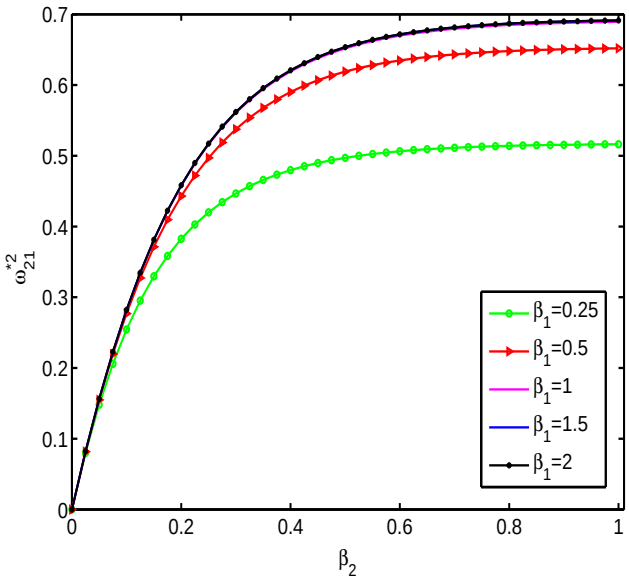

Figure 5.8: Non-dimensional sloshing frequency ω_{21}^{*2} versus β_2 for different values of β_1 for $\rho = 0.63$

as depth of the lower fluid increases. A sudden increment is observed in frequency for small values of β_2. It is clearly observed that non-dimensional frequency increases with an increasing value of β_1 but the difference in increment decreases gradually with an increasing value of β_1. It is also observed that when higher values of β_1 are considered than those of β_2, no change is observed in the value of ω_{01}^{*2}.

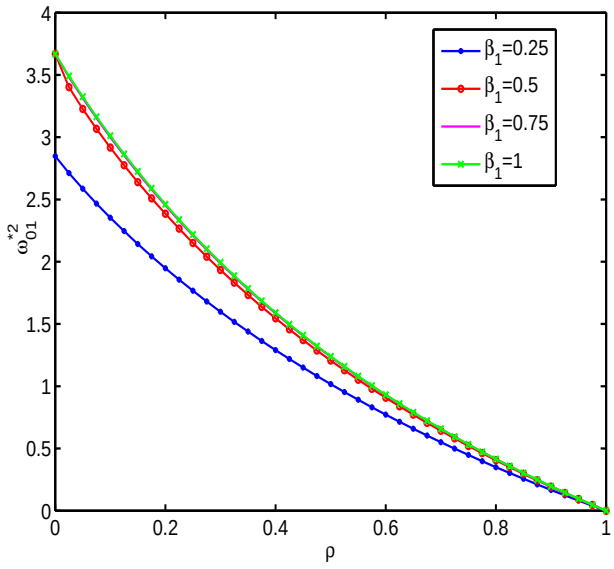

Figure 5.9: Non-dimensional sloshing frequency ω_{01}^{*2} versus ρ for different values of β_1 for $\beta_2 = 0.5$

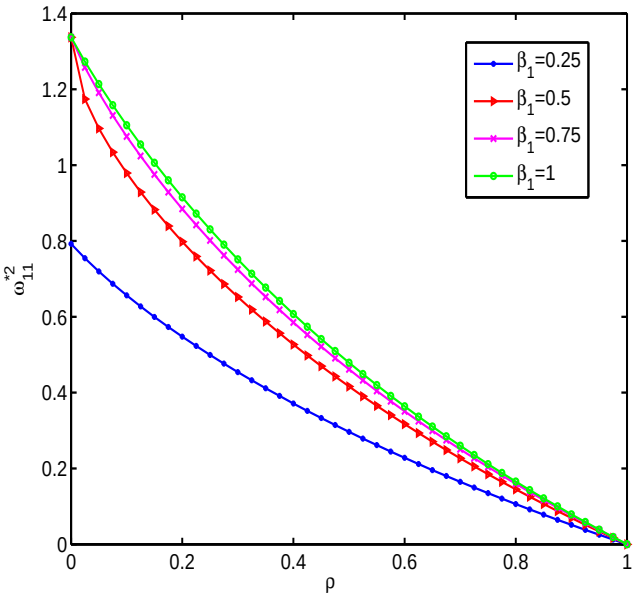

Figure 5.10: Non-dimensional sloshing frequency ω_{11}^{*2} versus ρ for different values of β_1 for $\beta_2 = 0.5$

In Fig. 5.7 also, the same set of fixed parameters is chosen. It is observed that non-dimensional frequency ω_{11}^{*2} increases gradually as β_2 increases. For small values of upper fluid height, ω_{11}^{*2} is much lower as compared to the case when higher values of upper fluid height are considered.

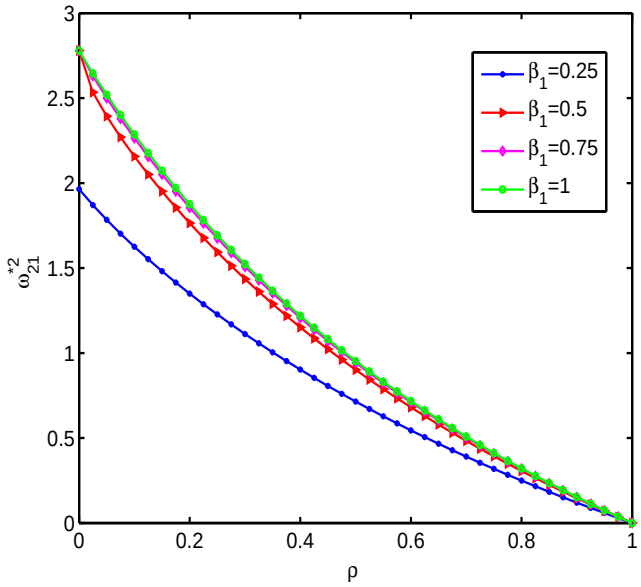

Figure 5.11: Non-dimensional sloshing frequency ω_{21}^{*2} versus ρ for different values of β_1 for $\beta_2 = 0.5$

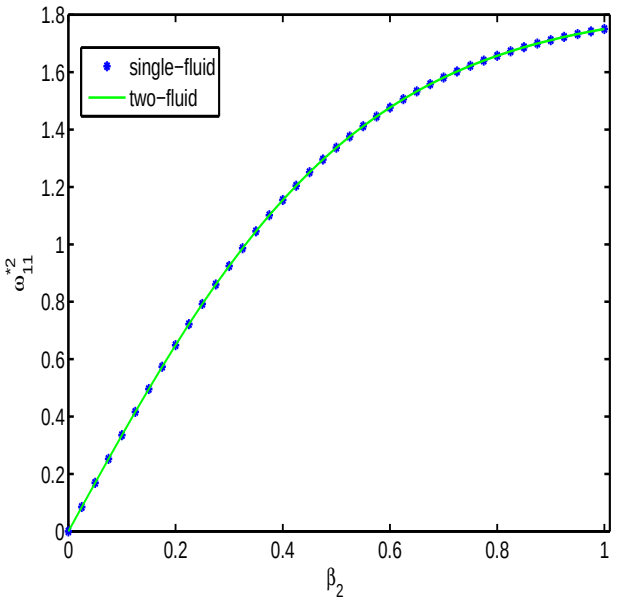

Figure 5.12: Non-dimensional sloshing frequency ω_{11}^{*2} versus β_2 for $\beta_1 = 0$; $\rho = 0.63$

Figures $5.9 - 5.11$ show the plots for the non-dimensional sloshing frequencies versus density ratio for different modes. In all the cases, lower fluid depth β_2 is kept fixed at $\beta_2 = 0.5$. In all the figures, curves are drawn for different values of upper fluid height to radius for $\beta_1 = 0.25, 0.5, 0.75, 1$. It is observed that an increasing density ratio lowers the non-dimensional frequency. It is also observed that when density of upper fluid is

same as that of lower fluid, no sloshing takes place. It is shown that non-dimensional frequency is much lower for lower values of upper fluid height compared to other values of upper fluid height. In all the cases, non-dimensional frequency decreases gradually.

In Fig. 5.12, plots show the non-dimensional frequency for $m = 1$. We consider the case of single-layer fluid and plot the frequency. The case of a two-layer fluid, by choosing $\beta_1 = 0$, can be converted into that for a single-layer fluid. In both the cases, we get the same result as shown in Fig. 5.12. Hence by choosing $\beta_1 = 0$, results can be obtained for a single layer fluid.

5.4 Conclusions

In this work, the sloshing of a two-layer incompressible fluid inside a vertical circular cylinder is investigated. The natural sloshing frequencies are calculated by employing linear water wave theory. We investigate the effects of fluid heights and density ratio on natural sloshing frequencies. It is found that non-dimensional sloshing frequency increases with an increasing fluid height. A rapid increment is observed in the value of non-dimensional frequency for small values of upper fluid height as well as for lower liquid depth. It is shown that non-dimensional frequency lowers its value with an increasing density ratio. The non-dimensional frequency decreases rapidly with increasing density ratio. When $\rho \to 1$, non-dimensional frequency vanishes, i.e., no sloshing takes place. A comparison case is also discussed to verify the particular two-layer fluid results. If we take $\beta_1 = 0$, the result matches with a single-layer fluid problem. Strong numerical evidence supports our results.

Chapter 6

Liquid sloshing in a circular cylindrical container containing a two-layer fluid in presence of baffle

6.1 Introduction

In this work, we extend the work done in the previous chapter. We evaluate natural sloshing frequencies of a two-layer fluid of different layer-wise densities $\rho_1 < \rho_2$ with an interface and a surface in a vertical circular cylinder in presence of a rigid annular baffle placed at the free surface. The fluid domain is divided into sub-domains to obtain the solutions. Boundary value problem is set up for each sub-domain. On the basis of the velocity potential formulation of the fluid motion inside the container, an infinite system of homogeneous linear equation is obtained. We study the effects of the parameters such as fluid heights, baffle-width and density ratio on the natural sloshing frequencies. The results are supported by relevant graphs.

6.2 Statement and formulation of the problem

Two immiscible, incompressible and inviscid fluids are assumed to perform irrotational motion in a vertical circular cylinder partially filled with fluid. The radius of the cylinder is taken as R_1. We introduce cylindrical coordinate system (r, θ, z) in which z is measured vertically upwards from the mean interface. The origin O is considered at the interface and hence $z = 0$ is the mean position of the interface of the two fluids. $z = h_1$ represents the free surface and $z = -h_2$ the bottom of the cylinder. By $\rho = \rho_1/\rho_2 (< 1)$, we denote the ratio of the densities ρ_1 of upper fluid and ρ_2 of lower fluid. Linear water wave theory is utilized to describe the fluid motion inside the container. Figure 6.1 depicts the physical problem.

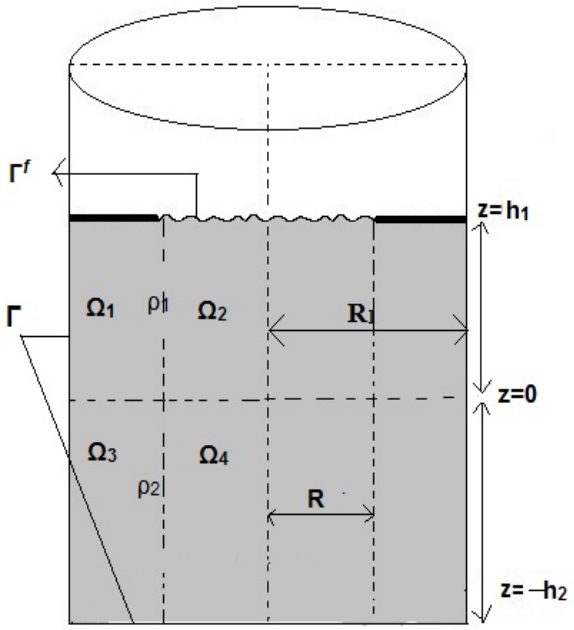

Figure 6.1: Schematic diagram for the problem

With the above assumptions, the fluid flow can now be described in terms of a velocity potential Φ that satisfies Laplace's equation

$$\frac{\partial^2\Phi}{\partial r^2}+\frac{1}{r}\frac{\partial\Phi}{\partial r}+\frac{1}{r^2}\frac{\partial^2\Phi}{\partial\theta^2}+\frac{\partial^2\Phi}{\partial z^2}=0 \qquad \text{in} \quad \Omega, \tag{6.1}$$

where Ω is fluid domain of the container, along with rigid boundary conditions

$$\frac{\partial\Phi}{\partial\mathbf{n}}=0 \qquad \text{on} \quad \Gamma, \tag{6.2}$$

where Γ is solid wetted interface and $\mathbf{n}$ is the outward normal to Γ, and free surface condition

$$\frac{\partial\Phi}{\partial\mathbf{n}}+\frac{1}{g}\frac{\partial^2\Phi}{\partial t^2}=0 \qquad \text{on} \quad \Gamma^f, \tag{6.3}$$

where Γ^f is the free surface.

6.2.1 Boundary Value Problems (BVP) for upper and lower fluids

Due to the presence of two immiscible fluids, and the presence of a rigid baffle inside the fluid domain, solution to the boundary-value problem (6.1) – (6.3) cannot be obtained directly. In order to find an analytical solution for the BVP, a semi-analytical approach is used for which the liquid domain is divided into four sub-domains. For each sub-domain,

velocity potential $\Phi(r,\theta,z,t)$ can be written as $\Phi_i(r,\theta,z,t),\ (r,\theta,z)\in\Omega_i,\ i=1,2,3,4$. According to Eq. (6.1), each velocity potential satisfies Laplace's equation

$$\frac{\partial^2\Phi_i}{\partial r^2}+\frac{1}{r}\frac{\partial\Phi_i}{\partial r}+\frac{1}{r^2}\frac{\partial^2\Phi_i}{\partial\theta^2}+\frac{\partial^2\Phi_i}{\partial z^2}=0 \qquad \text{in} \quad \Omega_i. \tag{6.4}$$

The corresponding impermeability conditions at rigid boundaries are given by

$$\left(\frac{\partial\Phi_1}{\partial r}\right)_{r=R_1}=0, \quad \left(\frac{\partial\Phi_1}{\partial z}\right)_{z=h_1}=0, \tag{6.5a}$$

$$\left(\frac{\partial\Phi_3}{\partial r}\right)_{r=R_1}=0, \quad \left(\frac{\partial\Phi_3}{\partial z}\right)_{z=-h_2}=0, \tag{6.5b}$$

$$\left(\frac{\partial\Phi_4}{\partial r}\right)_{z=-h_2}=0. \tag{6.5c}$$

Free surface condition is satisfied by the velocity potential Φ_2 only since only Ω_2 contains free surface. Now the corresponding free surface condition is as follows:

$$\frac{\partial\Phi_2}{\partial z}+\frac{1}{g}\frac{\partial^2\Phi_2}{\partial t^2}=0 \qquad \text{at} \quad z=h_1, \tag{6.6}$$

6.2.2 Solutions of BVP for upper and lower fluids in each sub-domains

We write the velocity potential as time harmonic in the following form:

$$\Phi(r,\theta,z,t)=\phi(r,\theta,z)e^{\iota\omega t}, \tag{6.7}$$

which defines natural wave frequency ω and Φ is 2π-periodic. Corresponding potentials in different domains take the form as follows:

$$\Phi_i(r,\theta,z,t)=\phi_i(r,\theta,z)e^{\iota\omega t}. \tag{6.8}$$

Inserting Eq. (6.8) into Eqs. $(6.5a)-(6.5c)$, the corresponding conditions get converted to

$$\left(\frac{\partial\phi_1}{\partial r}\right)_{r=R_1}=0, \quad \left(\frac{\partial\phi_1}{\partial z}\right)_{z=h_1}=0, \tag{6.9a}$$

$$\left(\frac{\partial\phi_3}{\partial r}\right)_{r=R_1}=0, \quad \left(\frac{\partial\phi_3}{\partial z}\right)_{z=-h_2}=0, \tag{6.9b}$$

$$\left(\frac{\partial\phi_4}{\partial r}\right)_{z=-h_2}=0. \tag{6.9c}$$

On the basis of assumption of linear water wave theory, the boundary value problem $(6.1)-(6.3)$ is a linear eigenvalue problem. We employ superposition principle to find the

mode shape of the liquid domain. In every sub-domain, there are rigid boundaries as well as non-rigid boundaries. Non-rigid boundaries are the liquid interfaces of two successive sub-domains. In order to set up and solve BVPs in each sub-domain independently, we are required to impose extra (otherwise non-existent) boundary conditions at the interface due to lack of sufficient boundary conditions - one or two at a time for one component, depending on the number of interfaces available in each sub-domain. It is to be noted that these extra conditions are later suitably absorbed while using the overall matching conditions across the interfaces. By superposition principle, ϕ_i in Ω_i can be written as

$$\phi_i = \sum_{j=1}^{k_i} \phi_i^j, \tag{6.10}$$

where ϕ_i^j is the j-th component of ϕ_i and k_i denotes the number of liquid interfaces in Ω_i. With the help of (6.11), each ϕ_i in corresponding Ω_i takes the following form:

$$\phi_1 = \phi_1^2 + \phi_1^3, \tag{6.11}$$

$$\phi_2 = \phi_2^1 + \phi_2^2 + \phi_2^3, \tag{6.12}$$

$$\phi_3 = \phi_3^2 + \phi_3^3, \tag{6.13}$$

$$\phi_4 = \phi_4^2 + \phi_4^3, \tag{6.14}$$

where ϕ_i^1 corresponds to the component of the velocity potential in the respective region due to the non-rigid condition at the free surface $z = h_1$ only; ϕ_i^2 to that component of the velocity potential due to the non-rigid condition at the vertical interface $r = R$ and ϕ_i^3 to that component of the velocity potential due to the non-rigid condition at the surface of separation of two-fluids at $z = 0$. In order to maintain the periodicity of Φ, ϕ_i^j is written in the form

$$\phi_i^j = \sum_{m=0}^{\infty} \phi_{im}^j \cos m\theta. \tag{6.15}$$

The boundary conditions for ϕ_i^j in the sub-domains can be found out with the help of Eqs. $(6.9a) - (6.9c)$. Rigid boundary conditions in different sub-domains are obtained as follows:

For Ω_1:

$$\left(\frac{\partial \phi_1^2}{\partial r}\right)_{r=R_1} = 0, \qquad \left(\frac{\partial \phi_1^2}{\partial z}\right)_{z=h_1} = 0, \qquad \left(\frac{\partial \phi_1^2}{\partial z}\right)_{z=0} = 0. \tag{6.16}$$

$$\left(\frac{\partial \phi_1^3}{\partial r}\right)_{r=R_1} = 0, \qquad \left(\frac{\partial \phi_1^3}{\partial z}\right)_{z=h_1} = 0, \qquad \left(\frac{\partial \phi_1^3}{\partial r}\right)_{r=R} = 0. \tag{6.17}$$

For Ω_2:

$$\left(\frac{\partial \phi_2^1}{\partial r}\right)_{r=R} = 0, \qquad \left(\frac{\partial \phi_2^1}{\partial z}\right)_{z=0} = 0, \tag{6.18}$$

$$\left(\phi_2^2\right)_{z=h_1} = 0, \qquad \left(\frac{\partial \phi_2^2}{\partial z}\right)_{z=0} = 0, \tag{6.19}$$

$$\left(\frac{\partial \phi_2^3}{\partial r}\right)_{r=R} = 0, \qquad \left(\phi_2^3\right)_{z=h_1} = 0. \tag{6.20}$$

For Ω_3:

$$\left(\frac{\partial \phi_3^2}{\partial r}\right)_{r=R_1} = 0, \qquad \left(\frac{\partial \phi_3^2}{\partial z}\right)_{z=-h_2} = 0, \qquad \left(\frac{\partial \phi_3^2}{\partial z}\right)_{z=0} = 0, \tag{6.21}$$

$$\left(\frac{\partial \phi_3^3}{\partial r}\right)_{r=R_1} = 0, \qquad \left(\frac{\partial \phi_3^3}{\partial r}\right)_{r=R} = 0, \qquad \left(\frac{\partial \phi_3^3}{\partial z}\right)_{z=-h_2} = 0. \tag{6.22}$$

For Ω_4:

$$\left(\frac{\partial \phi_4^2}{\partial z}\right)_{z=-h_2} = 0, \qquad \left(\frac{\phi_4^2}{\partial z}\right)_{z=0} = 0, \tag{6.23}$$

$$\left(\frac{\partial \phi_4^3}{\partial r}\right)_{z=-h_2} = 0, \qquad \left(\frac{\partial \phi_4^3}{\partial r}\right)_{r=R} = 0. \tag{6.24}$$

Now we introduce the following dimensionless quantities in order to non-dimensionalize the parameters:

$$\xi = \frac{r}{R_1}, \quad \eta = \frac{z}{R_1}, \quad \gamma = \frac{R}{R_1}, \beta_1 = \frac{h_1}{R_1}, \quad \beta_2 = \frac{h_2}{R_1}, \quad \omega^* = \omega\sqrt{\frac{R_1}{g}}. \tag{6.25}$$

The boundary value problems in different sub-domains allow separation of variables in (r, θ, z)-coordinate system for ϕ_i^j and permit the exact solutions which can be obtained in terms of eigenfunctions. The corresponding solutions for different sub-domains can be written as follows:

For sub-domain Ω_1:

$$\begin{aligned}\phi_1^2 &= \sum_{n=1}^{\infty} A_{1mn}^2 \cos\left(\frac{n\pi}{\beta_1}\eta\right) \frac{\left[I_m\left(\frac{n\pi}{\beta_1}\xi\right) K_m'\left(\frac{n\pi}{\beta_1}\right) - I_m'\left(\frac{n\pi}{\beta_1}\right) K_m\left(\frac{n\pi}{\beta_1}\xi\right)\right]}{K_m'\left(\frac{n\pi}{\beta_1}\right)} \\ &\quad + A_{1m0}^2\left(\xi^m + \xi^{-m}\right)\delta_m^2 + A_{100}^2\delta_m^1, \end{aligned} \tag{6.26}$$

$$\begin{aligned}\phi_1^3 &= \sum_{n=1}^{\infty} A_{1mn}^3 \frac{\cosh k_{mn}(\eta - \beta_1)}{\cosh k_{mn}\beta_1} \times \\ &\quad \frac{\left[J_m\left(k_{mn}\xi\right) Y_m'\left(k_{mn}\right) - J_m'\left(k_{mn}\right) Y_m\left(k_{mn}\xi\right)\right]}{Y_m'\left(k_{mn}\right)} + A_{100}^3\delta_m^1, \end{aligned} \tag{6.27}$$

where k_{mn} are the zeros of

$$J'_m(k_{mn})Y'_m(k_{mn}\gamma) - J'_m(k_{mn}\gamma)Y'_m(k_{mn}) = 0. \tag{6.28}$$

For sub-domain Ω_2:

$$\phi_2^1 = \sum_{n=1}^{\infty} A_{2mn}^1 \cosh(\lambda_{mn}\eta) \times J_m(\lambda_{mn}\xi) + A_{200}^1\delta_m^1, \tag{6.29}$$

$$\phi_2^2 = \sum_{n=1}^{\infty} A_{2mn}^2 \cos\left(\frac{(2n-1)\pi}{2\beta_1}\eta\right) \times I_m\left(\frac{(2n-1)\pi}{2\beta_1}\xi\right) \tag{6.30}$$

$$\phi_2^3 = \sum_{n=1}^{\infty} A_{2mn}^3 \frac{\sinh\lambda_{mn}(\eta-\beta_1)}{\cosh\lambda_{mn}\beta_1} \times J_m(\lambda_{mn}\xi) + A_{200}^3\delta_m^1(\eta-\beta_1), \tag{6.31}$$

where λ_{mn} are the zeros of

$$J'_m(\lambda_{mn}\gamma) = 0. \tag{6.32}$$

For sub-domain Ω_3:

$$\phi_3^2 = \sum_{n=1}^{\infty} A_{3mn}^2 \cos\left(\frac{n\pi}{\beta_2}\eta\right) \frac{\left[I_m\left(\frac{n\pi}{\beta_2}\xi\right)K'_m\left(\frac{n\pi}{\beta_2}\right) - I'_m\left(\frac{n\pi}{\beta_2}\right)K_m\left(\frac{n\pi}{\beta_2}\xi\right)\right]}{K'_m\left(\frac{n\pi}{\beta_2}\right)}$$
$$+A_{3m0}^2\left(\xi^m + \xi^{-m}\right)\delta_m^2 + A_{300}^2\delta_m^1, \tag{6.33}$$

$$\phi_3^3 = \sum_{n=1}^{\infty} A_{3mn}^3 \frac{\cosh k_{mn}(\eta+\beta_2)}{\cosh k_{mn}\beta_2} \times$$
$$\frac{\left[J_m\left(k_{mn}\xi\right)Y'_m\left(k_{mn}\right) - J'_m\left(k_{mn}\right)Y_m\left(k_{mn}\xi\right)\right]}{Y'_m\left(k_{mn}\right)} + A_{300}^3\delta_m^1. \tag{6.34}$$

For sub-domain Ω_4:

$$\phi_4^2 = \sum_{n=1}^{\infty} A_{4mn}^2 \cos\left(\frac{n\pi}{\beta_2}\eta\right) \times I_m\left(\frac{n\pi}{\beta_2}\xi\right) + A_{4m0}^2\xi^m\delta_m^2 + A_{400}^2 \tag{6.35}$$

$$\phi_4^3 = \sum_{n=1}^{\infty} A_{4mn}^3 \frac{\cosh\lambda_{mn}(\eta+\beta_2)}{\cosh\lambda_{mn}\beta_2} \times J_m(\lambda_{mn}\xi) + A_{400}^3\delta_m^1. \tag{6.36}$$

The coefficients A_{imn}^j are still unknown. To find A_{imn}^j and the non-dimensional frequency ω^*, we apply the matching conditions on the interfaces between two successive sub-domains and the surface of separation of two fluids along with the free surface condition.

6.2.3 Matching conditions

In order to utilize the matching conditions on mean interface and free surface, we truncate the series solutions after N terms. These conditions imply the continuity of pressure and velocity across the interfaces. The following are the matching conditions used across different interfaces:

(A) $\phi_3 = \phi_4$ at $\xi = \gamma$:

$$\sum_{n=1}^{N} A^2_{3mn} \cos\left(\frac{n\pi}{\beta_2}\eta\right) \frac{\left[I_m\left(\frac{n\pi}{\beta_2}\gamma\right) K'_m\left(\frac{n\pi}{\beta_2}\right) - I'_m\left(\frac{n\pi}{\beta_2}\right) K_m\left(\frac{n\pi}{\beta_2}\gamma\right)\right]}{K'_m\left(\frac{n\pi}{\beta_2}\right)}$$

$$+A^2_{3m0}\left(\gamma^m + \gamma^{-m}\right)\delta^2_m + A^2_{300}\delta^1_m + \sum_{n=1}^{N} A^3_{3mn} \frac{\cosh k_{mn}(\eta+\beta_2)}{\cosh k_{mn}\beta_2} \times$$

$$\frac{\left[J_m\left(k_{mn}\gamma\right) Y'_m\left(k_{mn}\right) - J'_m\left(k_{mn}\right) Y_m\left(k_{mn}\gamma\right)\right]}{Y'_m\left(k_{mn}\right)} + A^3_{300}\delta^1_m$$

$$= \sum_{n=1}^{N} A^2_{4mn} \cos\left(\frac{n\pi}{\beta_2}\eta\right) \times I_m\left(\frac{n\pi}{\beta_2}\gamma\right) + A^2_{4m0}\gamma^m\delta^2_m + A^2_{400}\delta^1_m +$$

$$\sum_{n=1}^{N} A^3_{4mn} \frac{\cosh \lambda_{mn}(\eta+\beta_2)}{\cosh \lambda_{mn}\beta_2} \times J_m(\lambda_{mn}\gamma) + A^3_{400}\delta^1_m. \tag{6.37}$$

(B) $\frac{\partial\phi_3}{\partial\xi} = \frac{\partial\phi_4}{\partial\xi}$ at $\xi = \gamma$:

$$\sum_{n=1}^{N} A^2_{3mn} \left(\frac{n\pi}{\beta_2}\right) \cos\left(\frac{n\pi}{\beta_2}\eta\right) \frac{\left[I'_m\left(\frac{n\pi}{\beta_2}\gamma\right) K'_m\left(\frac{n\pi}{\beta_2}\right) - I'_m\left(\frac{n\pi}{\beta_2}\right) K'_m\left(\frac{n\pi}{\beta_2}\gamma\right)\right]}{K'_m\left(\frac{n\pi}{\beta_2}\right)}$$

$$+A^2_{3m0} m\left(\gamma^{m-1} - \gamma^{-m-1}\right)\delta^2_m$$

$$= \sum_{n=1}^{N} A^2_{4mn} \left(\frac{n\pi}{\beta_2}\right) \cos\left(\frac{n\pi}{\beta_2}\eta\right) \times I'_m\left(\frac{n\pi}{\beta_2}\gamma\right) + A^2_{4m0} m\gamma^{m-1}\delta^2_m. \tag{6.38}$$

(C) $\phi_1 = \phi_2$ at $\xi = \gamma$:

$$\sum_{n=1}^{N} A^2_{1mn} \cos\left(\frac{n\pi}{\beta_1}\eta\right) \frac{\left[I_m\left(\frac{n\pi}{\beta_1}\gamma\right) K'_m\left(\frac{n\pi}{\beta_1}\right) - I'_m\left(\frac{n\pi}{\beta_1}\right) K_m\left(\frac{n\pi}{\beta_1}\gamma\right)\right]}{K'_m\left(\frac{n\pi}{\beta_1}\right)}$$

$$+A^2_{1m0}\left(\gamma^m + \gamma^{-m}\right)\delta^2_m + A^2_{100}\delta^1_m + \sum_{n=1}^{N} A^3_{1mn} \frac{\cosh k_{mn}(\eta-\beta_1)}{\cosh k_{mn}\beta_1}$$

$$\times \frac{\left[J_m\left(k_{mn}\gamma\right) Y'_m\left(k_{mn}\right) - J'_m\left(k_{mn}\right) Y_m\left(k_{mn}\gamma\right)\right]}{Y'_m\left(k_{mn}\right)} + A^3_{100}\delta^1_m +$$

$$\sum_{n=1}^{N} A^1_{2mn} \cosh(\lambda_{mn}\eta) \times J_m(\lambda_{mn}\gamma) + A^1_{200}\delta^1_m +$$

$$\sum_{n=1}^{N} A^2_{2mn} \cos\left(\frac{(2n-1)\pi}{2\beta_1}\eta\right) \times I_m\left(\frac{(2n-1)\pi}{2\beta_1}\gamma\right) +$$

$$\sum_{n=1}^{N} A^3_{2mn} \frac{\sinh \lambda_{mn}(\eta-\beta_1)}{\cosh \lambda_{mn}\beta_1} \times J_m(\lambda_{mn}\gamma) + A^3_{200}\delta^1_m(\eta-\beta_1). \tag{6.39}$$

(D) $\frac{\partial\phi_1}{\partial\xi} = \frac{\partial\phi_2}{\partial\xi}$ at $\xi = \gamma$:

$$\sum_{n=1}^{N} A_{1mn}^2 \left(\frac{n\pi}{\beta_1}\right) \cos\left(\frac{n\pi}{\beta_1}\eta\right) \frac{\left[I_m'\left(\frac{n\pi}{\beta_1}\gamma\right) K_m'\left(\frac{n\pi}{\beta_1}\right) - I_m'\left(\frac{n\pi}{\beta_1}\right) K_m'\left(\frac{n\pi}{\beta_1}\gamma\right)\right]}{K_m'\left(\frac{n\pi}{\beta_1}\right)}$$
$$+A_{1m0}^2 m\left(\gamma^{m+1} + \gamma^{-m-1}\right)\delta_m^2 =$$
$$\sum_{n=1}^{N} A_{2mn}^2 \left(\frac{(2n-1)\pi}{2\beta_1}\right) \cos\left(\frac{(2n-1)\pi}{2\beta_1}\eta\right) \times I_m'\left(\frac{(2n-1)\pi}{2\beta_1}\gamma\right). \tag{6.40}$$

(E) $\frac{\partial\phi_2}{\partial\eta} = \frac{\partial\phi_4}{\partial\eta}$ at $\eta = 0$:

$$\sum_{n=1}^{N} A_{2mn}^3 \lambda_{mn} \times J_m(\lambda_{mn}\xi) + A_{200}^3\delta_m^1 = \sum_{n=1}^{N} A_{4mn}^3 \lambda_{mn} \times \tanh\lambda_{mn}\beta_2 \times J_m(\lambda_{mn}\xi). \tag{6.41}$$

(F) $\rho\left(\frac{\partial\phi_2}{\partial\eta} - \omega^{*2}\phi_2\right) = \frac{\partial\phi_4}{\partial\eta} - \omega^{*2}\phi_4$ at $\eta = 0$:

$$\rho\left[\sum_{n=1}^{N} A_{2mn}^3 \lambda_{mn} \times J_m(\lambda_{mn}\xi) + A_{200}^3\delta_m^1 - \omega^{*2}\left\{\sum_{n=1}^{N} A_{2mn}^1 \times J_m(\lambda_{mn}\xi) + A_{200}^1\delta_m^1 + \right.\right.$$
$$\sum_{n=1}^{N} A_{2mn}^2 \times I_m\left(\frac{(2n-1)\pi}{2\beta_1}\xi\right) + \sum_{n=1}^{N} A_{2mn}^3 \times -\tanh\lambda_{mn}\beta_1 \times J_m(\lambda_{mn}\xi) +$$
$$\left.\left. A_{200}^3\delta_m^1(-\beta_1)\right\}\right] = \sum_{n=1}^{N} A_{4mn}^3 \lambda_{mn} \times \tanh\lambda_{mn}\beta_2 \times J_m(\lambda_{mn}\xi) - \omega^{*2}\left\{\sum_{n=1}^{N} A_{4mn}^2 \times \right.$$
$$\left. I_m\left(\frac{n\pi}{\beta_2}\xi\right) + A_{4m0}^2\xi^m\delta_m^2 + A_{400}^2\delta_m^1 + \sum_{n=1}^{N} A_{4mn}^3 \times J_m(\lambda_{mn}\xi) + A_{400}^3\delta_m^1\right\}. \tag{6.42}$$

(G) $\frac{\partial\phi_1}{\partial\eta} = \frac{\partial\phi_3}{\partial\eta}$ at $\eta = 0$:

$$\sum_{n=1}^{N} A_{1mn}^3 \times k_{mn} \times -\tanh k_{mn}\beta_1 \times \frac{\left[J_m(k_{mn}\xi)\, Y_m'(k_{mn}) - J_m'(k_{mn})\, Y_m(k_{mn}\xi)\right]}{Y_m'(k_{mn})}$$
$$= \sum_{n=1}^{N} A_{3mn}^3 \times k_{mn} \times \tanh k_{mn}\beta_2 \times \frac{\left[J_m(k_{mn}\xi)\, Y_m'(k_{mn}) - J_m'(k_{mn})\, Y_m(k_{mn}\xi)\right]}{Y_m'(k_{mn})} \tag{6.43}$$

(H) $\rho\left(\frac{\partial\phi_1}{\partial\eta} - \omega^{*2}\phi_1\right) = \frac{\partial\phi_3}{\partial\eta} - \omega^{*2}\phi_3$ at $\eta = 0$:

$$\rho\left[\sum_{n=1}^{N}A^3_{1mn}\times k_{mn}\times -\tanh k_{mn}\beta_1\times\frac{\left[J_m\left(k_{mn}\xi\right)Y'_m\left(k_{mn}\right)-J'_m\left(k_{mn}\right)Y_m\left(k_{mn}\xi\right)\right]}{Y'_m\left(k_{mn}\right)}\right.$$
$$-\omega^{*2}\left\{\sum_{n=1}^{N}A^2_{1mn}\frac{\left[I_m\left(\frac{n\pi}{\beta_1}\xi\right)K'_m\left(\frac{n\pi}{\beta_1}\right)-I'_m\left(\frac{n\pi}{\beta_1}\right)K_m\left(\frac{n\pi}{\beta_1}\xi\right)\right]}{K'_m\left(\frac{n\pi}{\beta_1}\right)}+A^2_{1m0}\left(\xi^m+\xi^{-m}\right)\delta^2_m+\right.$$
$$\left.\left.+A^2_{100}\delta^1_m+\sum_{n=1}^{N}A^3_{1mn}\times\frac{\left[J_m\left(k_{mn}\xi\right)Y'_m\left(k_{mn}\right)-J'_m\left(k_{mn}\right)Y_m\left(k_{mn}\xi\right)\right]}{Y'_m\left(k_{mn}\right)}+A^3_{100}\delta^1_m\right\}\right]$$
$$=\sum_{n=1}^{N}A^3_{3mn}\times k_{mn}\tanh k_{mn}\beta_2\times\frac{\left[J_m\left(k_{mn}\xi\right)Y'_m\left(k_{mn}\right)-J'_m\left(k_{mn}\right)Y_m\left(k_{mn}\xi\right)\right]}{Y'_m\left(k_{mn}\right)}$$
$$-\omega^{*2}\left\{\sum_{n=1}^{N}A^2_{3mn}\times\frac{\left[I_m\left(\frac{n\pi}{\beta_2}\xi\right)K'_m\left(\frac{n\pi}{\beta_2}\right)-I'_m\left(\frac{n\pi}{\beta_2}\right)K_m\left(\frac{n\pi}{\beta_2}\xi\right)\right]}{K'_m\left(\frac{n\pi}{\beta_2}\right)}+A^2_{3m0}\left(\xi^m+\xi^{-m}\right)\delta^2_m\right.$$
$$\left.+A^2_{300}\delta^1_m+\sum_{n=1}^{N}A^3_{3mn}\times\frac{\left[J_m\left(k_{mn}\xi\right)Y'_m\left(k_{mn}\right)-J'_m\left(k_{mn}\right)Y_m\left(k_{mn}\xi\right)\right]}{Y'_m\left(k_{mn}\right)}+A^3_{300}\delta^1_m\right\}. \quad (6.44)$$

(I) $\frac{\partial\phi_2}{\partial\eta}-\omega^{*2}\phi_2=0$ at $\eta=\beta_1$:

$$\sum_{n=1}^{N}A^1_{2mn}\times\lambda_{mn}\sinh(\lambda_{mn}\beta_1)\times J_m(\lambda_{mn}\xi)+\sum_{n=1}^{N}A^2_{2mn}\left(-\frac{(2n-1)\pi}{2\beta_1}\right)\sin\left(\frac{(2n-1)\pi}{2\beta_1}\beta_1\right)$$
$$\times I_m\left(\frac{(2n-1)\pi}{2\beta_1}\xi\right)\sum_{n=1}^{N}A^3_{2mn}\frac{\lambda_{mn}}{\cosh\lambda_{mn}\beta_1}\times J_m(\lambda_{mn}\xi)+A^3_{200}\delta^1_m-\omega^{*2}\left\{\sum_{1}^{N}+A^1_{2mn}\right.$$
$$\left.\cosh(\lambda_{mn}\beta_1)\times J_m(\lambda_{mn}\xi)+A^1_{200}\right\}=0. \quad (6.45)$$

Equations (6.37) – (6.45) give rise to a homogenous linear system in unknowns A^j_{imn}. Now to determine the unknowns and non-dimensional frequency, we truncate the system at a fixed number N, use Fourier-Bessel series expansion and then form a square matrix whose elements are coefficients of a Fourier-Bessel series. Here we get a square matrix of order $9N$ in A^j_{imn} unknowns which has the form

$$MX=0, \quad (6.46)$$

where

$$X=[A^2_{1mn},A^3_{1mn},A^1_{2mn},A^2_{2mn},A^3_{2mn},A^2_{3mn},A^3_{3mn},A^2_{4mn},A^3_{4mn}]^T, \quad (6.47)$$

and

$$M = \begin{bmatrix} [0] & [0] & [0] & [0] & [0] & [a^{16}_{mn\bar{n}}] & [a^{17}_{mn\bar{n}}] & [a^{18}_{mn\bar{n}}] & [a^{19}_{mn\bar{n}}] \\ [0] & [0] & [0] & [0] & [0] & [a^{26}_{mn\bar{n}}] & [0] & [a^{28}_{mn\bar{n}}] & [0] \\ [a^{31}_{mn\bar{n}}] & [a^{32}_{mn\bar{n}}] & [a^{33}_{mn\bar{n}}] & [a^{34}_{mn\bar{n}}] & [a^{35}_{mn\bar{n}}] & [0] & [0] & [0] & [0] \\ [a^{41}_{mn\bar{n}}] & [0] & [0] & [a^{44}_{mn\bar{n}}] & [0] & [0] & [0] & [0] & [0] \\ [0] & [0] & [0] & [0] & [a^{55}_{mn\bar{n}}] & [0] & [0] & [0] & [a^{59}_{mn\bar{n}}] \\ [0] & [0] & [a^{63}_{mn\bar{n}}] & [a^{64}_{mn\bar{n}}] & [a^{65}_{mn\bar{n}}] & [0] & [0] & [a^{68}_{mn\bar{n}}] & [a^{69}_{mn\bar{n}}] \\ [0] & [a^{72}_{mn\bar{n}}] & [0] & [0] & [0] & [0] & [a^{77}_{mn\bar{n}}] & [0] & [0] \\ [a^{81}_{mn\bar{n}}] & [a^{82}_{mn\bar{n}}] & [0] & [0] & [0] & [a^{86}_{mn\bar{n}}] & [a^{87}_{mn\bar{n}}] & [0] & [0] \\ [0] & [0] & [a^{93}_{mn\bar{n}}] & [a^{94}_{mn\bar{n}}] & [a^{95}_{mn\bar{n}}] & [0] & [0] & [0] & [0] \end{bmatrix}. \tag{6.48}$$

The expressions of the non-zero elements $a^{ij}_{mn\bar{n}}$ of the matrix are given by the coefficients of a Fourier-Bessel series. The system given by (6.46) must have a non-trivial solution for the vanishing determinant condition. The condition of the non-trivial solution of (6.46) gives us values of ω^*. The detailed expressions for the non-zero coefficients of the matrix M are provided in Appendix C.

6.3 Numerical results and discussion

We carry out a number of numerical experiments to strengthen the analytical results obtained here. All numerical calculations are carried out by using MATHEMATICA. 'NIntegrate' command is used to calculate the integrals numerically to compute the frequencies. The zeros of the determinant of the truncated system are plotted versus different parameters. The curves are drawn for non-dimensional frequency versus different values of γ, α and for different baffle positions in the liquid domain for $m = 1, 2$. Dimensionless sloshing frequency $\omega^{*2}_{mn}(m = 1, 2; n = 1, 2)$ is plotted for various γ values of a two-layer fluid inside a circular cylinder when a rigid annular baffle is placed on the free surface.

Figures $6.2 - 6.5$ show the plots of the first two non-dimensional sloshing frequencies against the density ratio. In all the cases, the height h_1/R_1 of the upper fluid is taken as $\beta_1 = 1$, the depth h_2/R_1 of the lower fluid is taken as $\beta_2 = 0.5$ which means the lower fluid has less height compared to the upper fluid. For each set of parameters, first two frequencies are plotted. In all the figures, the curves show the non-dimensional frequency curves for different values of $\gamma = 0.2, 0.4, 0.6$. It is observed that an increasing density ratio lowers the non-dimensional frequency. It is also observed that when density of upper fluid is same as that of lower fluid, non-dimensional frequency is zero. It is shown that non-dimensional frequency is much lower for higher values of γ compared to lower values of γ. In all the cases, non-dimensional frequency decreases gradually.

Figures $6.6 - 6.9$ show the plots of the first two non-dimensional sloshing frequencies

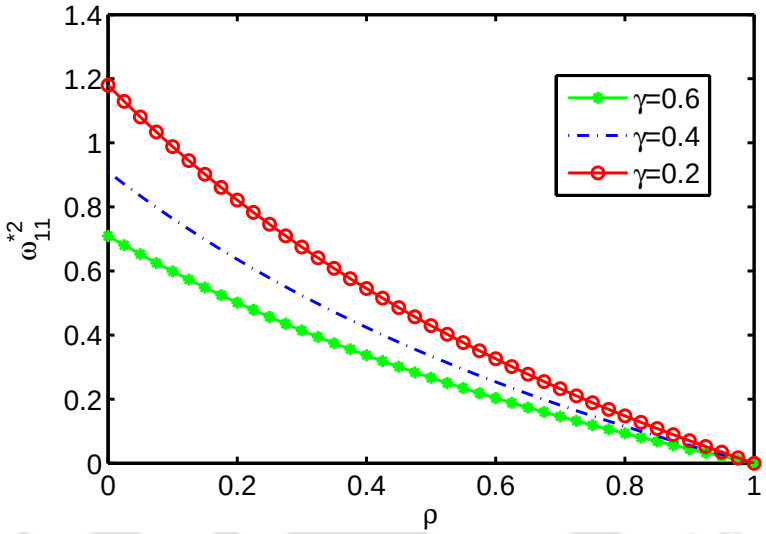

Figure 6.2: Non-dimensional sloshing frequency ω_{11}^{*2} versus ρ for different values of γ for $\beta_1 = 1$, $\beta_2 = 0.5$

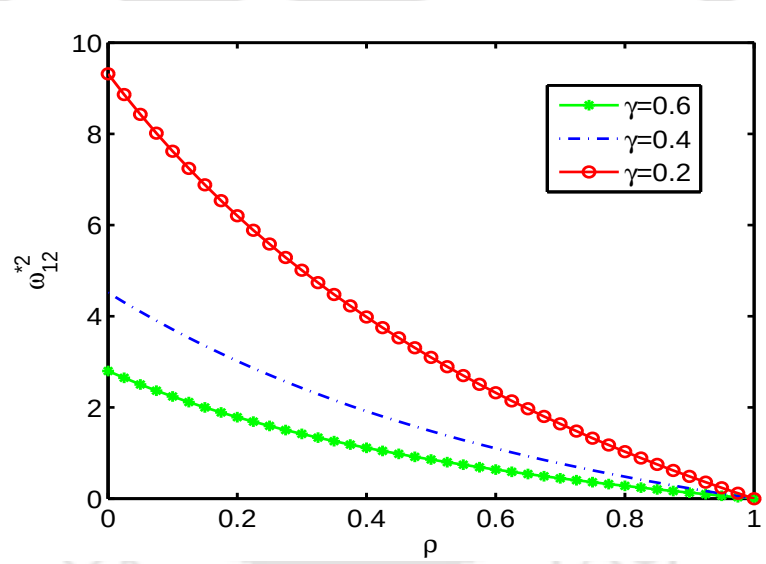

Figure 6.3: Non-dimensional sloshing frequency ω_{12}^{*2} versus ρ for different values of γ for $\beta_1 = 1$, $\beta_2 = 0.5$

against the upper fluid height ratio to the container radius denoted as β_1. In all the cases, the height h_2/R_1 of the upper fluid is taken as $\beta_2 = 0.5$ and the density ratio ρ has been kept fixed at 0.63. For each chosen set of parameters, first two frequencies are plotted versus density ratio. In all the figures, the curves show the non-dimensional frequency curves for different values of $\gamma = 0.2, 0.4, 0.6$.

Figures 6.6 and 6.8 show the first non-dimensional frequency curves for ω_{11}^{*2} and ω_{21}^{*2} against the upper fluid height ratio to the container. It is clearly observed that non-

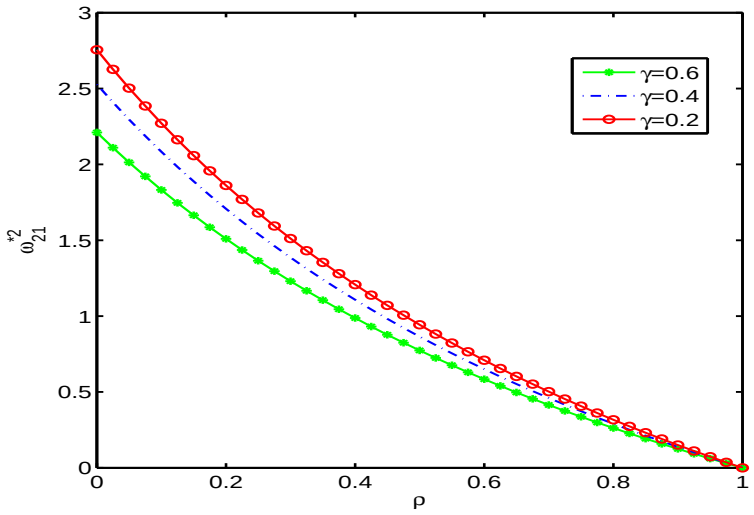

Figure 6.4: Non-dimensional sloshing frequency ω^{*2}_{21} versus ρ for different values of γ for $\beta_1 = 1$, $\beta_2 = 0.5$

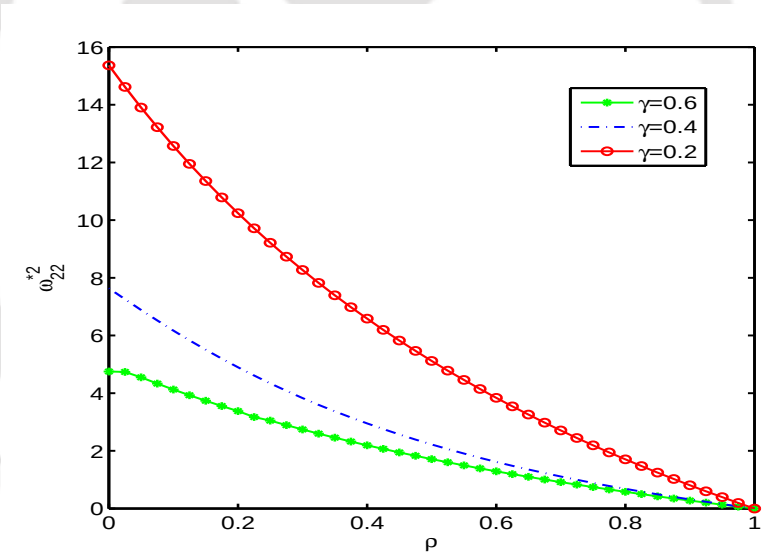

Figure 6.5: Non-dimensional sloshing frequency ω^{*2}_{22} versus ρ for different values of γ for $\beta_1 = 1$, $\beta_2 = 0.5$

dimensional frequency increases gradually with an increasing value of β_1, i.e., as the filled level of upper fluid increases, frequency increases. It is also observed that there is a significant increment in the value of non-dimensional frequency with a decreasing value of γ.

Figures 6.7 and 6.9 show the second non-dimensional frequency curves for ω^{*2}_{12} and ω^{*2}_{22} against the upper fluid height ratio to the container. In Figs. $6.7-6.9$, no significant change is observed in frequency with respect to β_1. It is observed that non-dimensional

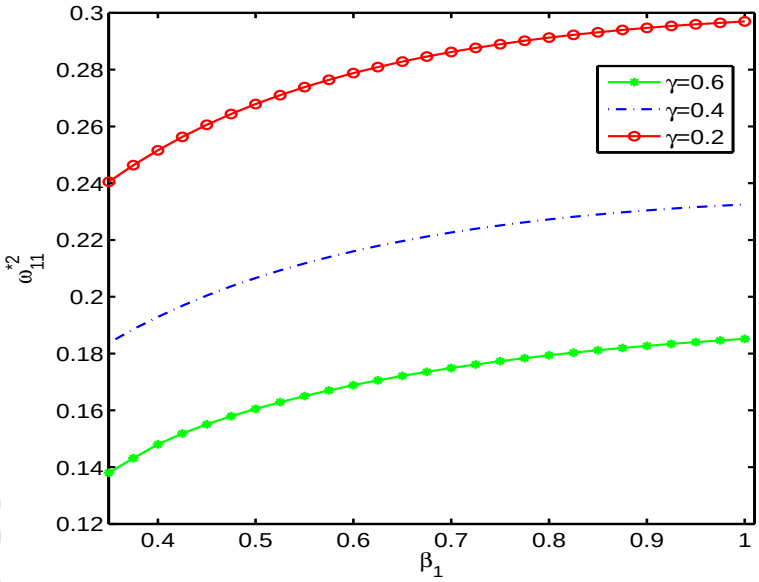

Figure 6.6: Non-dimensional sloshing frequency ω_{11}^{*2} versus β_1 for different values of γ for $\beta_2 = 0.5$, $\rho = 0.63$

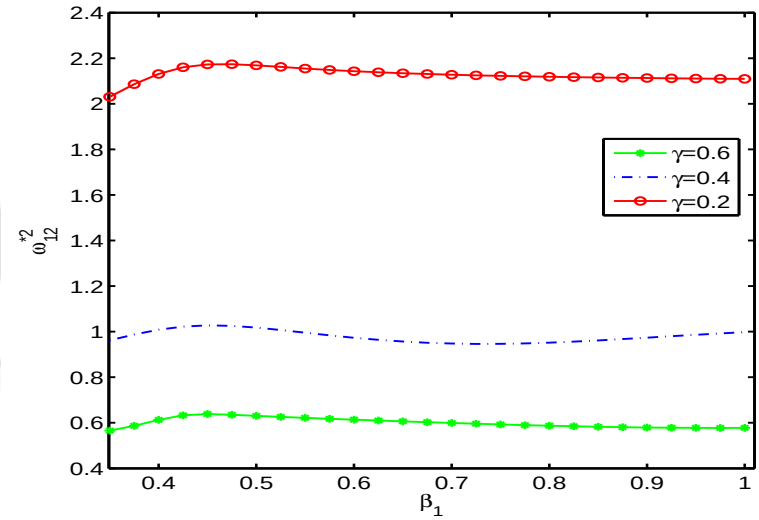

Figure 6.7: Non-dimensional sloshing frequency ω_{12}^{*2} versus β_1 for different values of γ for $\beta_2 = 0.5$, $\rho = 0.63$

frequency initially increases for small values of β_1 and then decreases very slowly showing insignificant change in frequency. It is also observed that there is a significant increment in the value of non-dimensional frequency with a decreasing value of γ.

Figures 6.10−6.13 show the plots of the first two non-dimensional sloshing frequencies against the lower fluid depth ratio to the container radius denoted as β_2. In all the cases, the height h_1/R_1 of the upper fluid is taken as $\beta_1 = 0.5$ and the density ratio ρ is kept

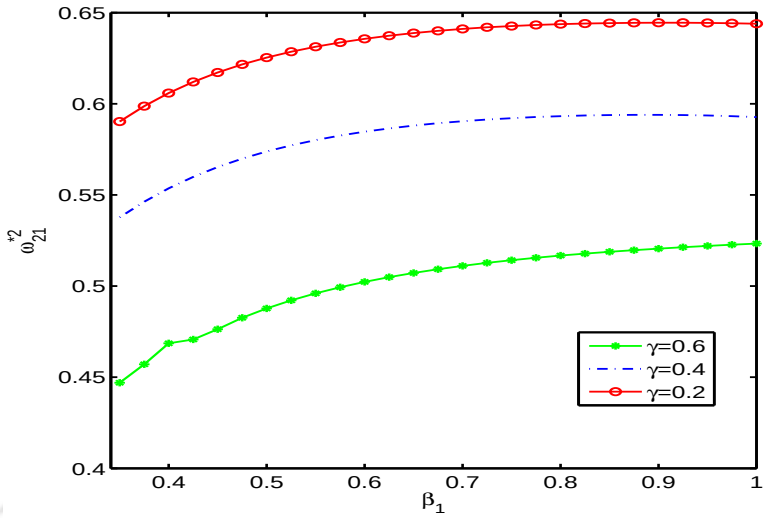

Figure 6.8: Non-dimensional sloshing frequency ω^{*2}_{21} versus β_1 for different values of γ for $\beta_2 = 0.5$, $\rho = 0.63$

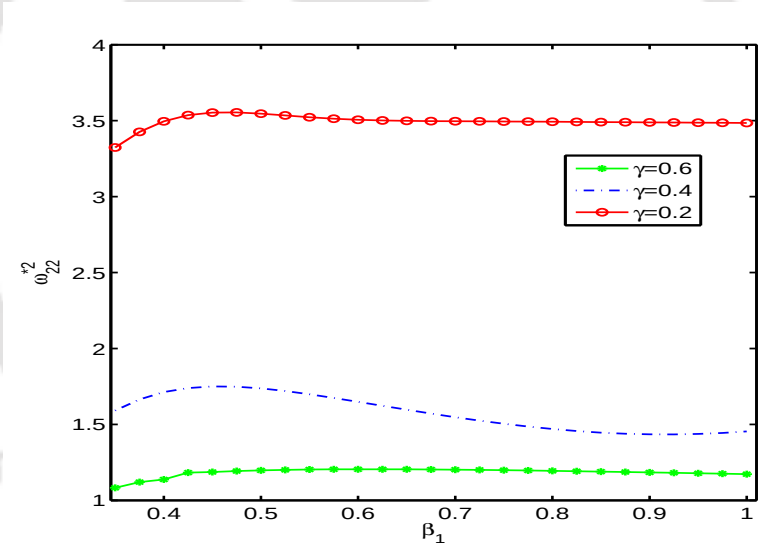

Figure 6.9: Non-dimensional sloshing frequency ω^{*2}_{22} versus β_1 for different values of γ for $\beta_2 = 0.5$, $\rho = 0.63$

fixed at 0.63. For each chosen set of parameters, first two frequencies are plotted versus density ratio. In all the figures, the curves show the non-dimensional frequency curves for different values of $\gamma = 0.2, 0.4, 0.6$.

Figures 6.10 and 6.12 show the first non-dimensional frequency curves for ω^{*2}_{11} and ω^{*2}_{21} against the lower fluid depth ratio to the container radius. It is clearly observed that non-dimensional frequency increases gradually with an increasing value of β_2, i.e., as the filled level of upper fluid increases, frequency increases. It is observed that non-

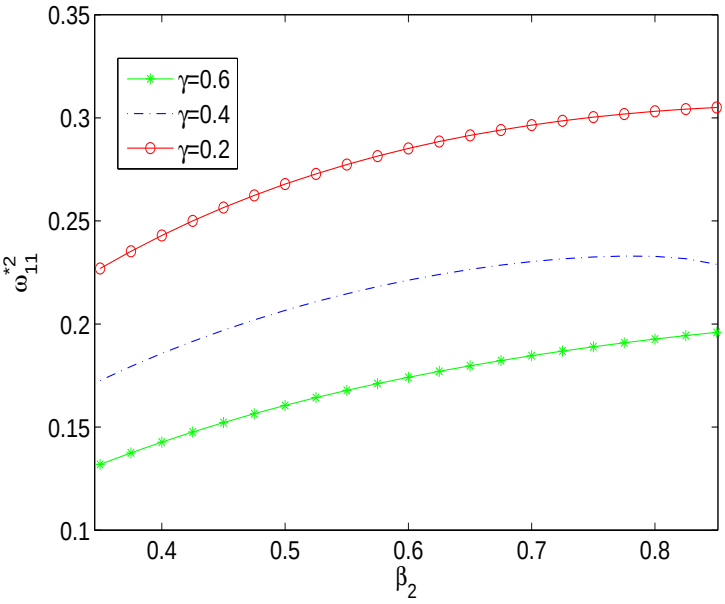

Figure 6.10: Non-dimensional sloshing frequency ω_{11}^{*2} versus β_2 for different values of γ for $\beta_1 = 0.5$, $\rho = 0.63$

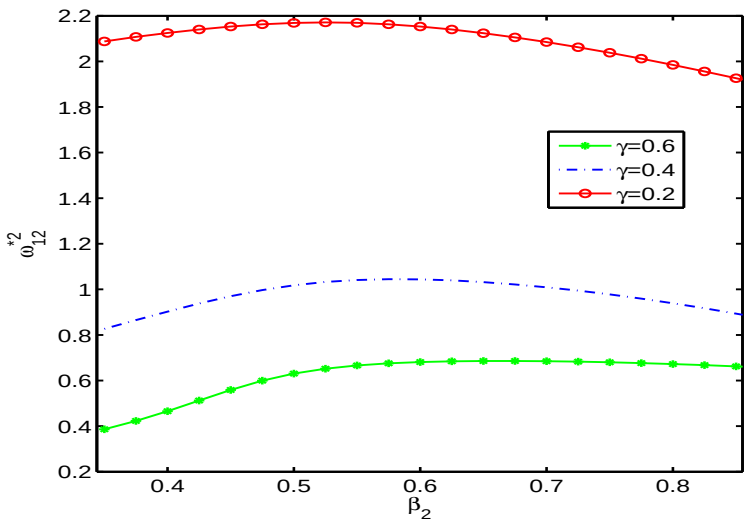

Figure 6.11: Non-dimensional sloshing frequency ω_{12}^{*2} versus β_2 for different values of γ for $\beta_1 = 0.5$, $\rho = 0.63$

dimensional frequency for ω_{11}^{*2} increases more rapidly with an increasing value of β_2 compared to that for ω_{21}^{*2}. It is shown that non-dimensional frequency increases with a decreasing value of γ.

Figures 6.11 and 6.13 show the second non-dimensional frequency curves for ω_{12}^{*2} and

ω_{22}^{*2} against the lower fluid depth ratio to the container radius. In Figs. 6.11 – 6.13, non-monotonic behaviour of non-dimensional frequency is observed frequency as β_2 increases. It is observed that non-dimensional frequency initially increases for small values of β_2 and the decreases with higher values of β_2. It is also observed that there is a significant change in the beviour of non-dimensional frequency with a decreasing value of γ.

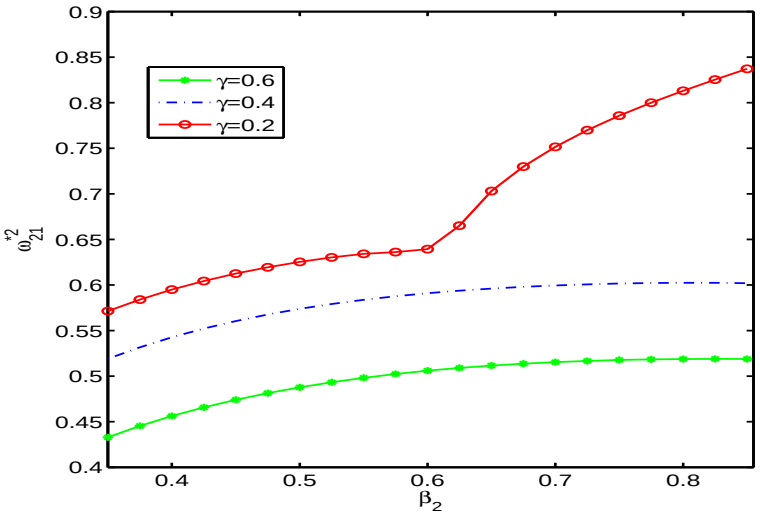

Figure 6.12: Non-dimensional sloshing frequency ω_{21}^{*2} versus β_2 for different values of γ for $\beta_1 = 0.5$, $\rho = 0.63$

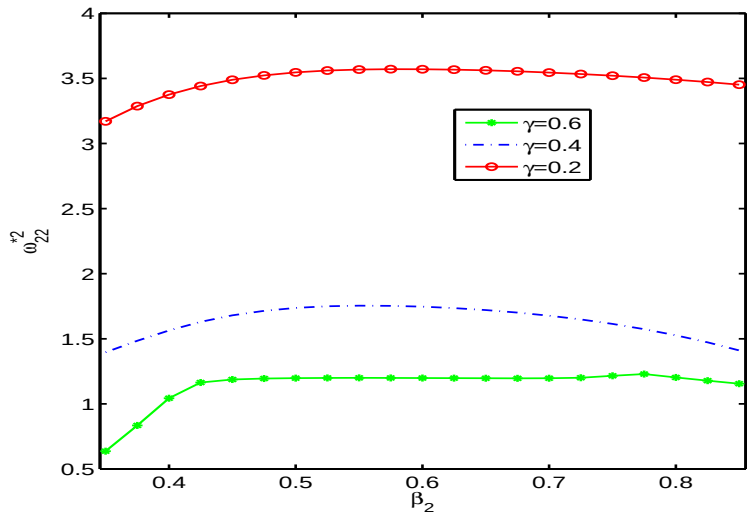

Figure 6.13: Non-dimensional sloshing frequency ω_{22}^{*2} versus β_2 for different values of γ for $\beta_1 = 0.5$, $\rho = 0.63$

6.4 Conclusions

In the work presented here, the sloshing frequencies of a two-layer incompressible fluid inside a vertical circular cylinder with a rigid annular baffle placed at the free surface are evaluated. We investigate the effects of fluid heights and density ratio on natural sloshing frequencies for different baffle-widths. It is found that the first non-dimensional sloshing frequency increases with an increasing fluid height while the second frequency shows non-monotonic behaviour. It is shown that non-dimensional frequency lowers its value with an increasing density ratio and vanishes when both fluids have same density. It is shown that frequency increases with an increasing value of baffle-width. It is observed that second frequency is significantly affected when baffle-width is more.

Chapter 7

Summary and future work

7.1 Summary of the thesis

This chapter is a brief overview of the important results obtained in the thesis describing their significance. Some highlights are also made on the scope of extension of considered problems and future investigations.

In this thesis, sloshing frequencies of a liquid in a cylindrical container with different configurations are investigated. Most part of the thesis is devoted to the evaluation of the sloshing frequencies when a rigid annular baffle is placed on the free surface of the liquid. The main objective of this thesis is to analyze the effect of various parameters on sloshing frequencies by using linear water wave theory.

In Chapter 2, a study on sloshing in an annular vertical circular cylindrical with a rigid annular baffle placed on the free surface is carried out. The boundary value problem within the fluid domain is set up in terms of velocity potential. The velocity potentials are found by using separation of variables method by using prescribed rigid boundary conditions on the solid-wetted wall. The baffle condition and the free surface condition is used for the velocity potential. An infinite linear homogenous system is obtained with the introduction of potential into baffle condition and free surface condition by using point allocation method. The zeros of the truncated determinant gives the value of sloshing frequencies. The effect of surface tension is also taken into account. The sloshing frequencies are computed by fixing the any two of the parameters considered as fluid height, baffle width and Bond number, then varying the remaining one. It is observed that natural frequencies can be shifted to a higher value by the introduction of a rigid annular baffle at the free surface. With an increasing value of the fluid height and the baffle-width, sloshing frequencies increases. The sloshing frequencies increases with an decreasing value of Bond number, i.e., the presence of surface tension on the free surface increases sloshing frequencies significantly.

In Chapter 3, the problem considered may be seen as an extension of Chapter 2. Here, a rigid annular baffle is placed inside the fluid domain instead of the free surface. The baffle width is considered negligible. The presence of baffle inside the fluid domain makes the fluid domain complex for solving the boundary value problem directly. In order to formulate the problem, fluid domain is divided into four sub-domains and then the boundary value problem is set up in each sub-domain in terms of velocity potential. The velocity potentials are obtained in each sub-domain with the help of superposition principle and separation of variables method. The matching conditions are used to maintain the continuity of pressure and velocity within the fluid domain. A truncated linear homogenous system of equations is obtained by using Fourier-Bessel series expansion for the matching conditions and free surface condition. The condition of vanishing determinant of a homogenous system for a non-zero solution gives the value of the sloshing frequencies. The baffle has a greater influence on sloshing frequencies when it is placed nearer to the free surface compared to the baffle placed towards the bottom. The sloshing frequency increases monotonically for an increasing value of the inner baffle radius ratio to the outer radius of the container. The introduction of baffle at the free surface is more beneficial compared to the introduction of baffle somewhere in the fluid domain.

In Chapter 4, sloshing is investigated for a vertical circular cylindrical container with an uneven bottom. The sloshing frequencies are evaluated for two cases: a complete free surface and when a baffle is placed at the free surface. In the second case, a rigid annular baffle is placed at the free surface mounted to the wall of the cylinder. The boundary value problem formulated within the fluid domain is solved by using separation of variables method and finite Hankel transform with the help of a perturbation technique. The effect of surface tension at the free surface is also considered. Results are obtained showing the dependence of sloshing frequencies on baffle-width, liquid height ratio as well as on maximum elevation of the bottom. Sloshing frequencies are obtained for a particular case of bottom. Sloshing frequency increases rapidly for lower values of fluid height and gradually becomes stable for higher values. The parameters such as increasing baffle-width and surface tension also shift the sloshing frequencies to a higher value.

Chapter 5 is concerned with the two-layer sloshing problem in a vertical circular cylindrical tank. The effect of surface tension is excluded at the free surface and the surface of separation of the two-fluid. The conditions of continuity of pressure and velocity are used at the surface of separation of the two fluids as matching conditions, which along with free surface condition, leads to a homogenous linear system of equations whose coefficients are determined by Fourier-Bessel series expansion. The zeros

of the truncated determinant are evaluated to obtain sloshing frequencies. The effects of lower-fluid depth, upper fluid height and density ratio are investigated on sloshing frequencies. The frequency is computed by fixing lower fluid depth and density ratio and then varying the upper fluid depth. The effect of upper fluid height on sloshing frequency is monotonic. For lower values of upper fluid height, frequency increases rapidly compared to the higher values of upper fluid height. In a similar manner, the effect of lower fluid height on sloshing frequency has been shown. The sloshing frequency increases monotonically with an increasing value of lower fluid depth. Sloshing frequencies are computed by fixing lower and upper fluid height, and the varying the density ratio. Sloshing frequency decreases monotonically with an increasing value of density and when both fluids have same density frequency vanishes.

Chapter 6 is an extension of the work done in Chapter 5. A rigid annular baffle is introduced at the free surface of the upper fluid mounted to the wall of the container. The liquid domain is divided into sub-domains to formulate the problem. The solutions in each sub-domain are found in terms of velocity potentials. Matching conditions are used at the interfaces of two successive sub-domains. The free surface condition and matching conditions give rise to a system of linear homogenous equations whose coefficients are obtained by using Fourier-Bessel series expansion method. The condition of vanishing determinant for a non-trivial solution of a homogenous system is used to obtain sloshing frequencies. The effects of upper fluid height, lower fluid depth and density ratio have been investigated for various baffle-widths. The sloshing frequency increases with an increasing value of upper fluid height and lower fluid height for all considered baffle width. With an increasing value of density ratio, sloshing frequency gradually gets reduced and it even vanishes when both the fluids have same density. Sloshing frequencies can be shifted to a higher value with the introduction of a rigid baffle at the free surface.

7.2 Future work

In this section, a brief outline of some problems which we plan to work in future is presented. We may consider some problems pertaining to an extension of the works presented in this thesis.

It is to be noted that in this thesis we have used analytical methods to find solutions within fluid domain and the baffle considered is always annular and rigid. Analytical methods do not work for complex geometry of containers and irregular shaped baffles. It is very difficult to solve nonlinear sloshing problems analytically. Nonlinearity in sloshing problems occurs in dynamic boundary condition on the free surface. Numerical investigations (FEM, FVM, BEM) and semi-analytical methods can be used to evaluate

sloshing frequencies. In most of the studies, results are obtained for vertical circular cylinders. We aim to consider different geometry. Thus we propose to investigate sloshing when the baffle is flexible and placed vertically in the fluid domain and also for nonlinear problems.

- We plan to consider elastic baffle as a damping device.
- Further, we wish to investigate non-linear sloshing for the problems already discussed.
- In sloshing problems, nonlinearity occurs at the free surface only. Reformulation of the problems will differ only in the free surface condition.
- We would like to attempt sloshing problem in a container under different kinds of motion like surge and pitch.

Bibliography

[1] Albright, N., and Concus, P., Small amplitude periodic sloshing modes of a liquid in a vertical right circular cylinder with a concave spheroidal bottom, *Report, U. S. Department of Energy*, 1977, 84 pages.

[2] Ambrosi, D., Hamiltonain formulation for surface waves in a layered fluid, *Wave Motion*, **31**, 2000, 71-76.

[3] Ansari, M. R., Abadi, R. D. F. and Ghasemi, M., Two phase modal analysis of nonlinear sloshing in a rectangular container, *Ocean Eng.*, *38*, 2011, 1277–1282.

[4] Bauer, H. F., Oscillations of immiscible liquid in a rectangular container: A new damper for excited structures, *J. Sound Vib.*, **93(1)**, 1984, 117–133.

[5] Bauer, H. F. and Eidel, W., Frictionless liquid sloshing in circular cylindrical container configurations, *Aerosp. Sci. Technol.*, **3**, 1999, 301–311.

[6] Bian, X., Perlin, M., Schultz, W. W. and Agarwal, M., Axisymmetric slosh frequencies of a liquid mass in a circular cylinder, *Phys. Fluids*, **15**, 2003, 3659–3664.

[7] Biswal, K., C., Bhattacharyya, S., K. and Sinha, P., K., Free-vibration analysis of liquid-filled tank with baffles, *J. Sound Vib.*, **259(1)**, 2003, 177–192.

[8] Buldakov, E., Lagrangian modelling of fluid sloshing in moving tanks, *J. Fluid Struct.*, **45**, 2014, 1–14.

[9] Chen, Z., Zong, Z., Li, H. T. and Li, J., An investigation into the pressure on solid walls in 2D sloshing using SPH method, *Ocean Eng.*, **59**, 2013, 129–141.

[10] Cox, E. A., Mortell, M. P., Pokrovskii, A. V. and Rasskazov, O., On chaotic wave patterns in periodically forced steady-state KdVB and extended KdVB equations, *Proc. R. Soc. Lond. A*, **461**, 2005, 2857–2885.

[11] Debnath, L., and Bhatta, D., Integral Transforms and Their Applications, Second Edition, *CRC Press*, Boca Raton, 2007.

[12] Evans, D. V., The wide-spacing approximation applied to multiple scattering and sloshing problems, *J. Fluid Mech.*, **210**, 1990, 647–658.

[13] Faltinsen, O. M., Rognebakke, O. F., Lukovsky, I. A. and Timokha, A. N., Multidimensional modal analysis of nonlinear sloshing in a rectangular tank with finite water depth, *J. Fluid Mech.*, **407**, 2000, 201–234.

[14] Faltinsen, O. M. and Timokha, A. N., An adaptive multimodal approach to nonlinear sloshing in a rectangular tank, *J. Fluid Mech.*, **432**, 2001, 167–200.

[15] Faltinsen, O. M. and Timokha, A. N., Asymptotic modal approximation of nonlinear resonant sloshing in a rectangular tank with small fluid depth, *J. Fluid Mech.*, **470**, 2002, 319–357.

[16] Faltinsen, O. M., Rognebakke, O. F. and Timokha, A. N., Resonant three-dimensional nonlinear sloshing in a square-base basin, *J. Fluid Mech.*, **487**, 2003, 1–42.

[17] Faltinsen, O. M., Rognebakke, O. F. and Timokha, A. N., Resonant three-dimensional nonlinear sloshing in a square-base basin. Part 2. Effect of higher modes, *J. Fluid Mech.*, **523**, 2005, 199–218.

[18] Gavrilyuk, I. P., Lukovskyb, I. A. and Timokha, A. N., Linear and nonlinear sloshing in a circular conical tank, *Fluid Dyn. Res.*, **37**, 2005, 399–429.

[19] Gavrilyuk, I., Lukovsky, I., Trotsenko, Yu. and Timokha, A., Sloshing in a vertical circular cylindrical tank with an annular baffle. Part 2. Nonlinear resonant waves, *J. Eng. Math.*, **57**, 2007, 57–78.

[20] Ibrahim, A. R., Liquid Sloshing Dynamics: Theory and Applications, *Cambridge University Press, Cambridge*, 2005.

[21] Jaiswal, O. R., Kulkarni, S. and Pathak, P., A study on sloshing frequencies of fluid-tank system, *14th World Conference on Earthquake Engineering, Beijing, China*, October 17-18, 2008.

[22] Jacobsen, L. S., Impulsive hydrodynamics of fluid inside a cylindrical tank and of fluid surrounding a cylindrical pier, *Bulletin of the Seismological Society of America*, **39**, 1949, 189–203.

[23] Kuttler, J. R. and Sigillito, V. G., Sloshing of liquids in cylindrical tanks, *AIAA J.*, **22**, 1984, 309-311.

[24] Mackey, D. and Cox, E. A., Dynamics of two-layer fluid sloshing problem, *IMA J. Appl. Math.*, **68**, 2003, 665–686.

[25] McIver, P. and McIver, M., Sloshing frequencies of longitudinal modes for a liquid contained in a trough, *J. Fluid Mech.*, **252**, 1993, 525–541.

[26] Miles, J. W., Nonlinear surface waves in closed basins, *J. Fluid Mech.*, **75**, 1976, 419–448.

[27] Miles, J. W., Internally resonant surface waves in a circular cylinder, *J. Fluid Mech.*, **149**, 1984, 1–14.

[28] Molin, B., Remy, F., Audiffren, C., Marcer, R., Ledour, A., Helland, S. and Mottaghi, M., Experimental and numerical study of liquid sloshing in a rectangular tank with three fluids, *International Offshore and Polar Engineering Conference*, 2012, 331–240.

[29] Ockendon, J. R. and Ockendon, H., Resonant surface waves, *J. Fluid Mech.*, **59**, 1973, 397–413.

[30] Ockendon, H., Ockendon, J. R. and Johnson, A. D., Resonant sloshing in shallow water, *J. Fluid Mech.*, **167**, 1986, 465–479.

[31] Papaspyrou, S., Karamanos, S. A. and Valougeorgis, D., Response of half full horizontal cylinders under transverse excitations, *J. Fluid Struct.*, **19**, 2004, 985–1003.

[32] Rocca, M. La, Sciortino, G. and Boniforti, M. A., A fully nonlinear model for sloshing in a rotating container, *Fluid Dyn. Res.*, **27**, 2000, pages 23.

[33] Sakata, M., Kimura, K. and Utsumi, M., Non-stationary response of non-linear liquid motion in a cylindrical tank subjected to random base excitation, *J. Sound Vib.*, **94(3)**, 1984, 351–363.

[34] Sciortino, G., Rocca, M. La and Boniforti, M. A., Hamiltonian formulation for the motion of a two-fluid system with free surface, *Nonlinear Oscil.*, **6**, 2003, 108–115.

[35] Sciortino, G., Adduce, C. and Rocca, M. La, Sloshing of a layered fluid with a free surface as a Hamiltonian system, *Phys. Fluids*, **21**, 2009, 16 pages.

[36] Shankar, P. N. and Kidambi R., A modal method for finite amplitude, nonlinear sloshing, *Pramana*, **59**, 2002, 631–651.

[37] Shankar, P. N., A simple method for studying low-gravity sloshing frequencies, *Proc. R. Soc. Lond. A*, **459**, 2003, 3109–3130.

[38] Shankar, P. N., Frequencies of gravity-capillary waves on highly curved interfaces with edge constraints, *Fluid Dyn. Res.*, **39**, 2007, 457–474.

[39] Sinai, Y. L., Fundamental sloshing frequencies of stratified two fluid system in closed prismatic tanks, *Int. J. Heat Fluid Fl.*, **6**, 1985, 142–144.

[40] Sirwah, Magdy A., Sloshing waves in a heated viscoelastic fluid layer in an excited rectangular tank, *Phys. Lett. A*, **378**, 2014, 3289–3300.

[41] Sorolla, E., Mosig, J. R. and Mattes, M., Algorithm to calculate a large number of roots of the cross-product of Bessel functions, *IEEE Trans. Antennas. Propag.*, **61**, 2013, 2180–2187.

[42] Takahara, H. and Kimura, K., Frequency responce of sloshing in an annular cylindrical tank subjected to pitching excitation, *J. Sound Vib.*, **331**, 2012, 3199-3212.

[43] Thiagarajan, K. P., Rakshit, D. and Repalle, N., The air water sloshing problem: Fundamental analysis and parametric studies on excitation and fill levels, *Ocean Eng.*, **38**, 2011, 498–508.

[44] Vaziri, N., Chern, M. J. and Borthwick, A. G. L., PSME model of parametric excitation of two-layer liquid in a tank, *Appl. Ocean Res.*, **43**, 2013, 214–222.

[45] Veletsos, A. S. and Yang, J. Y., Dynamics of fixed base liquid storage tanks, *Proceedings of U.S.-Japan seminar on Earthquake Engineering Research with Emphasis on Lifeline System, Japan Society for Promotion of Earthquake Engineering, Tokyo, Japan*, 1976, 317–341.

[46] Wang, J. D., Zhou, D. and Liu, W. Q., Sloshing of liquid in rigid cylindrical container with a rigid annular baffle. Part I: Free vibration, *Shock Vib.*, **19**, 2012, 1185–1203.

[47] Wang, J. D., Lo, S. H. and Zhou, D., Liquid sloshing in rigid cylindrical container with multiple rigid annular baffles: Free vibration, *J. Fluid Struct.*, **34**, 2012, 138–156.

[48] Yin, L., Wang, B., Ma, X. and Zou, J., The nonlinear sloshing of liquid in tank with pitching, *J. Appl. Mech.*, **66(4)**, 1999, 1032–1034.

[49] Yuanjun, He, Xingrui, Ma, Pingping, Wang and Benli, Wang, Low-gravity liquid nonlinear sloshing analysis in a tank under pitching excitation, *J. Sound Vib.*, **299**, 2007, 164–177.

[50] Zhou, D. and Liu, W. Q., Hydro-elastic vibrations of flexible rectangular tanks partially filled with liquid, *Int. J. Numer. Meth. Eng.*, **71 (2)**, 2007, 149-174.

Appendix A

Coefficients of matrix given by Eq. (3.46)

The detailed expressions for the non-zero coefficients of the matrix given by Eq. (3.46) are obtained as follows:

$$a^{11}_{mn\bar{n}} = -\delta_{n\bar{n}} \times \frac{\left[I'_m\left(\frac{n\pi}{\beta_1}\gamma\right) K'_m\left(\frac{n\pi}{\beta_1}\right) - I'_m\left(\frac{n\pi}{\beta_1}\right) K'_m\left(\frac{n\pi}{\beta_1}\gamma\right)\right]}{K'_m\left(\frac{n\pi}{\beta_1}\right)} \times \int_0^{\beta_1} \cos^2\left(\frac{n\pi}{\beta_1}\eta\right) d\eta \tag{A.1}$$

$$a^{12}_{mn\bar{n}} = \delta_{n\bar{n}} \times \frac{\left[I'_m\left(\frac{n\pi}{\beta_1}\gamma\right) K'_m\left(\frac{n\pi}{\beta_1}\alpha\right) - I'_m\left(\frac{n\pi}{\beta_1}\alpha\right) K'_m\left(\frac{n\pi}{\beta_1}\gamma\right)\right]}{K'_m\left(\frac{n\pi}{\beta_1}\alpha\right)} \times \int_0^{\beta_1} \cos^2\left(\frac{n\pi}{\beta_1}\eta\right) d\eta \tag{A.2}$$

$$a^{21}_{mn\bar{n}} = -\delta_{n\bar{n}} \times \frac{\left[I_m\left(\frac{n\pi}{\beta_1}\gamma\right) K'_m\left(\frac{n\pi}{\beta_1}\right) - I'_m\left(\frac{n\pi}{\beta_1}\right) K_m\left(\frac{n\pi}{\beta_1}\gamma\right)\right]}{K'_m\left(\frac{n\pi}{\beta_1}\right)} \times \int_0^{\beta_1} \cos^2\left(\frac{n\pi}{\beta_1}\eta\right) d\eta \tag{A.3}$$

$$a^{22}_{mn\bar{n}} = \delta_{n\bar{n}} \times \frac{\left[I_m\left(\frac{n\pi}{\beta_1}\gamma\right) K'_m\left(\frac{n\pi}{\beta_1}\alpha\right) - I'_m\left(\frac{n\pi}{\beta_1}\alpha\right) K_m\left(\frac{n\pi}{\beta_1}\gamma\right)\right]}{K'_m\left(\frac{n\pi}{\beta_1}\alpha\right)} \times \int_0^{\beta_1} \cos^2\left(\frac{n\pi}{\beta_1}\eta\right) d\eta \tag{A.4}$$

$$a^{23}_{mn\bar{n}} = \left[J_m\left(k_{m\bar{n}}\gamma\right)Y'_m\left(k_{m\bar{n}}\alpha\right) - J_m\left(k_{m\bar{n}}\alpha\right)Y'_m\left(k_{m\bar{n}}\gamma\right)\right] \times \int_0^{\beta_1}\left(e^{k_{m\bar{n}}\eta} + e^{-k_{m\bar{n}}\eta}\right)\cos\left(\frac{n\pi}{\beta_1}\eta\right)d\eta \tag{A.5}$$

$$a^{33}_{mn\bar{n}} = -\delta_{n\bar{n}} \times \left(e^{k_{mn}\beta_1} - e^{-k_{mn}\beta_1}\right) \times \int_\alpha^\gamma \xi\left[J_m\left(k_{mn}\xi\right)Y'_m\left(k_{mn}\alpha\right) - J_m\left(k_{mn}\alpha\right)Y'_m\left(k_{mn}\xi\right)\right]^2 d\xi \tag{A.6}$$

$$a^{38}_{mn\bar{n}} = \delta_{n\bar{n}} \times \left(e^{k_{mn}\beta_1} + e^{k_{mn}(2\beta_2-\beta_1)}\right) \times \int_\alpha^\gamma \xi\left[J_m\left(k_{mn}\xi\right)Y'_m\left(k_{mn}\alpha\right) - J_m\left(k_{mn}\alpha\right)Y'_m\left(k_{mn}\xi\right)\right]^2 d\xi \tag{A.7}$$

$$a^{42}_{mn\bar{n}} = (-1)^{\bar{n}+1}\int_\alpha^\gamma \xi\left[\frac{\left[I_m\left(\frac{\bar{n}\pi}{\beta_1}\xi\right)K'_m\left(\frac{\bar{n}\pi}{\beta_1}\alpha\right) - I'_m\left(\frac{\bar{n}\pi}{\beta_1}\alpha\right)K_m\left(\frac{\bar{n}\pi}{\beta_1}\xi\right)\right]}{K'_m\left(\frac{\bar{n}\pi}{\beta_1}\alpha\right)}\right] \times \left[J_m\left(k_{mn}\xi\right)Y'_m\left(k_{mn}\alpha\right) - J'_m\left(k_{mn}\alpha\right)Y_m\left(k_{mn}\xi\right)\right]d\xi \tag{A.8}$$

$$a^{43}_{mn\bar{n}} = -\delta_{n\bar{n}} \times \left(e^{k_{mn}\beta_1} + e^{-k_{mn}\beta_1}\right) \times \int_\alpha^\gamma \xi\left[J_m\left(k_{mn}\xi\right)Y'_m\left(k_{mn}\alpha\right) - J_m\left(k_{mn}\alpha\right)Y'_m\left(k_{mn}\xi\right)\right]^2 d\xi - \delta^2_m\frac{\gamma^m - \gamma^{-m}}{2\beta_1(1-\alpha^{2m})}\left[J_m\left(k_{m\bar{n}}\gamma\right)Y'_m\left(k_{m\bar{n}}\alpha\right) - J_m\left(k_{m\bar{n}}\alpha\right)Y'_m\left(k_{m\bar{n}}\gamma\right)\right] \times \int_0^{\beta_1}\left(e^{k_{m\bar{n}}\eta} + e^{-k_{m\bar{n}}\eta}\right)d\eta \times \int_\alpha^\gamma\left(\xi^{m+1} + \alpha^{2m}\xi^{-m+1}\right) \times \left[J_m\left(k_{mn}\xi\right)Y'_m\left(k_{mn}\alpha\right) - J_m\left(k_{mn}\alpha\right)Y'_m\left(k_{mn}\xi\right)\right]d\xi \tag{A.9}$$

$$a^{46}_{mn\bar{n}} = \delta_{n\bar{n}} \times 2e^{k_{mn}\beta_1}\int_\alpha^\gamma \xi\left[J_m\left(k_{mn}\xi\right)Y'_m\left(k_{mn}\alpha\right) - J_m\left(k_{mn}\alpha\right)Y'_m\left(k_{mn}\xi\right)\right]^2 d\xi \tag{A.10}$$

$$a^{47}_{mn\bar{n}} = \int_\alpha^\gamma \xi\left[J_m\left(k_{mn}\xi\right)Y'_m\left(k_{mn}\alpha\right) - J_m\left(k_{mn}\alpha\right)Y'_m\left(k_{mn}\xi\right)\right] \times \frac{\left[I_m\left(\frac{(2\bar{n}-1)\pi}{2(\beta_2-\beta_1)}\xi\right)K'_m\left(\frac{(2\bar{n}-1)\pi}{2(\beta_2-\beta_1)}\alpha\right) - I'_m\left(\frac{(2\bar{n}-1)\pi}{2(\beta_2-\beta_1)}\alpha\right)K_m\left(\frac{(2\bar{n}-1)\pi}{2(\beta_2-\beta_1)}\xi\right)\right]}{K'_m\left(\frac{(2\bar{n}-1)\pi}{2(\beta_2-\beta_1)}\alpha\right)}d\xi \tag{A.11}$$

$$a^{48}_{mn\bar{n}} = \delta_{n\bar{n}} \times \left(e^{k_{mn}\beta_1} - e^{-k_{mn}(2\beta_2-\beta_1)}\right) \times \int_{\alpha}^{\gamma} \xi[J_m\left(k_{mn}\xi\right) Y'_m\left(k_{mn}\alpha\right) - J_m\left(k_{mn}\alpha\right) Y'_m\left(k_{mn}\xi\right)]^2 d\xi \tag{A.12}$$

$$a^{55}_{mn\bar{n}} = -\delta_{n\bar{n}} \times \frac{\left[I'_m\left(\frac{(2n-1)\pi}{2(\beta_2-\beta_1)}\gamma\right) K'_m\left(\frac{(2n-1)\pi}{2(\beta_2-\beta_1)}\right) - I'_m\left(\frac{(2n-1)\pi}{2(\beta_2-\beta_1)}\right) K'_m\left(\frac{(2n-1)\pi}{2(\beta_2-\beta_1)}\gamma\right)\right]}{K'_m\left(\frac{(2n-1)\pi}{2(\beta_2-\beta_1)}\right)} \times \int_{\beta_1}^{\beta_2} \cos^2\left(\frac{(2n-1)\pi}{2(\beta_2-\beta_1)\pi}(\eta-\beta_1)\right) d\eta \tag{A.13}$$

$$a^{57}_{mn\bar{n}} = \delta_{n\bar{n}} \frac{\left[I'_m\left(\frac{(2n-1)\pi}{2(\beta_2-\beta_1)}\gamma\right) K'_m\left(\frac{(2n-1)\pi}{2(\beta_2-\beta_1)}\alpha\right) - I'_m\left(\frac{(2n-1)\pi}{2(\beta_2-\beta_1)}\alpha\right) K'_m\left(\frac{(2n-1)\pi}{2(\beta_2-\beta_1)}\gamma\right)\right]}{K'_m\left(\frac{(2n-1)\pi}{2(\beta_2-\beta_1)}\alpha\right)} \times \int_{\beta_1}^{\beta_2} \cos^2\left(\frac{(2n-1)\pi}{2(\beta_2-\beta_1)}(\eta-\beta_1)\right) d\eta \tag{A.14}$$

$$a^{64}_{mn\bar{n}} = -\left[J_m\left(\lambda_{m\bar{n}}\gamma\right) Y'_m\left(\lambda_{m\bar{n}}\right) - J_m\left(\lambda_{m\bar{n}}\right) Y'_m\left(\lambda_{m\bar{n}}\gamma\right)\right] \times \int_{\beta_1}^{\beta_2} \left(e^{\lambda_{m\bar{n}}\eta} + e^{\lambda_{m\bar{n}}(2\beta_1-\eta)}\right) \cos\left(\frac{(2n-1)\pi}{2(\beta_2-\beta_1)}(\eta-\beta_1)\right) d\eta \tag{A.15}$$

$$a^{65}_{mn\bar{n}} = -\delta_{n\bar{n}} \times \int_{\beta_1}^{\beta_2} \cos^2\left(\frac{(2n-1)\pi}{2(\beta_2-\beta_1)}(\eta-\beta_1)\right) d\eta \frac{\left[I_m\left(\frac{(2n-1)\pi}{2(\beta_2-\beta_1)}\gamma\right) K'_m\left(\frac{(2n-1)\pi}{2(\beta_2-\beta_1)}\right) - I'_m\left(\frac{(2n-1)\pi}{2(\beta_2-\beta_1)}\right) K_m\left(\frac{(2n-1)\pi}{2(\beta_2-\beta_1)}\gamma\right)\right]}{K'_m\left(\frac{(2n-1)\pi}{2(\beta_2-\beta_1)}\right)} + \delta^1_m \frac{(2\bar{n}-1)(-1)^{\bar{n}+1}\pi}{\omega^{*2}(\beta_2-\beta_1)(1-\gamma^2)} \times \int_{\beta_1}^{\beta_2} \cos\left(\frac{(2n-1)\pi}{2(\beta_2-\beta_1)}(\eta-\beta_1)\right) d\eta \times \int_{\gamma}^{1} \xi \frac{\left[I_m\left(\frac{(2\bar{n}-1)\pi}{2(\beta_2-\beta_1)}\xi\right) K'_m\left(\frac{(2\bar{n}-1)\pi}{2(\beta_2-\beta_1)}\right) - I'_m\left(\frac{(2\bar{n}-1)\pi}{2(\beta_2-\beta_1)}\right) K_m\left(\frac{(2\bar{n}-1)\pi}{2(\beta_2-\beta_1)}\xi\right)\right]}{K'_m\left(\frac{(2\bar{n}-1)\pi}{2(\beta_2-\beta_1)}\right)} d\xi \tag{A.16}$$

$$a^{66}_{mn\bar{n}} = \left[J_m\left(k_{m\bar{n}}\gamma\right) Y'_m\left(k_{m\bar{n}}\alpha\right) - J_m\left(k_{m\bar{n}}\alpha\right) Y'_m\left(k_{m\bar{n}}\gamma\right)\right] \times \int_{\beta_1}^{\beta_2} \left(e^{k_{m\bar{n}}\eta} + e^{k_{m\bar{n}}(2\beta_1-\eta)}\right) \cos\left(\frac{(2n-1)\pi}{2(\beta_2-\beta_1)}(\eta-\beta_1)\right) d\eta \tag{A.17}$$

$$
\begin{aligned}
a_{mn\bar{n}}^{67} &= \delta_{n\bar{n}} \times \int_{\beta_1}^{\beta_2} \cos^2\left(\frac{(2n-1)\pi}{2(\beta_2-\beta_1)}(\eta-\beta_1)\right) d\eta \times \\
&\frac{\left[I_m\left(\frac{(2n-1)\pi}{2(\beta_2-\beta_1)}\gamma\right) K_m'\left(\frac{(2n-1)\pi}{2(\beta_2-\beta_1)}\alpha\right) - I_m'\left(\frac{(2n-1)\pi}{2(\beta_2-\beta_1)}\alpha\right) K_m\left(\frac{(2n-1)\pi}{2(\beta_2-\beta_1)}\gamma\right)\right]}{K_m'\left(\frac{(2n-1)\pi}{2(\beta_2-\beta_1)}\alpha\right)} \\
&+\delta_m^1 \frac{(2\bar{n}-1)(-1)^{\bar{n}+1}\pi}{\omega^{*2}(\beta_2-\beta_1)(\gamma^2-\alpha^2)} \times \int_{\beta_1}^{\beta_2} \cos\left(\frac{(2n-1)\pi}{2(\beta_2-\beta_1)}(\eta-\beta_1)\right) d\eta \times \\
&\int_\alpha^\gamma \xi \frac{\left[I_m\left(\frac{(2\bar{n}-1)\pi}{2(\beta_2-\beta_1)}\xi\right) K_m'\left(\frac{(2\bar{n}-1)\pi}{2(\beta_2-\beta_1)}\alpha\right) - I_m'\left(\frac{(2\bar{n}-1)\pi}{2(\beta_2-\beta_1)}\alpha\right) K_m\left(\frac{(2\bar{n}-1)\pi}{2(\beta_2-\beta_1)}\xi\right)\right]}{K_m'\left(\frac{(2\bar{n}-1)\pi}{2(\beta_2-\beta_1)}\alpha\right)} d\xi
\end{aligned} \tag{A.18}
$$

$$
\begin{aligned}
a_{mn\bar{n}}^{68} &= \left[J_m\left(k_{m\bar{n}}\gamma\right) Y_m'\left(k_{m\bar{n}}\alpha\right) - J_m\left(k_{m\bar{n}}\alpha\right) Y_m'\left(k_{m\bar{n}}\gamma\right)\right] \\
&\times \int_{\beta_1}^{\beta_2} \left(e^{k_{m\bar{n}}\eta} - e^{k_{m\bar{n}}(2\beta_2-\eta)}\right) \cos\left(\frac{(2n-1)\pi}{2(\beta_2-\beta_1)}(\eta-\beta_1)\right) d\eta
\end{aligned} \tag{A.19}
$$

$$
\begin{aligned}
a_{mn\bar{n}}^{76} &= \delta_{n\bar{n}} k_{mn}\left(e^{k_{mn}\beta_2} - e^{k_{mn}(2\beta_1-\beta_2)}\right) \times \\
&\int_\alpha^\gamma \xi \left[J_m\left(k_{mn}\xi\right) Y_m'\left(k_{mn}\alpha\right) - J_m\left(k_{mn}\alpha\right) Y_m'\left(k_{mn}\xi\right)\right]^2 d\xi \\
&-\omega^{*2}\delta_{n\bar{n}}\left(e^{k_{mn}\beta_2} + e^{k_{mn}(2\beta_1-\beta_2)}\right) \times \\
&\int_\alpha^\gamma \xi \left[J_m\left(k_{mn}\xi\right) Y_m'\left(k_{mn}\alpha\right) - J_m\left(k_{mn}\alpha\right) Y_m'\left(k_{mn}\xi\right)\right]^2 d\xi
\end{aligned} \tag{A.20}
$$

$$
\begin{aligned}
a_{mn\bar{n}}^{77} &= \frac{(2\bar{n}-1)(-1)^{\bar{n}}\pi}{2(\beta_2-\beta_1)} \int_\alpha^\gamma \xi \times \left[J_m\left(k_{mn}\xi\right) Y_m'\left(k_{mn}\alpha\right) - J_m\left(k_{mn}\alpha\right) Y_m'\left(k_{mn}\xi\right)\right] \\
&\frac{\left[I_m\left(\frac{(2\bar{n}-1)\pi}{2(\beta_2-\beta_1)}\xi\right) K_m'\left(\frac{(2\bar{n}-1)\pi}{2(\beta_2-\beta_1)}\alpha\right) - I_m'\left(\frac{(2\bar{n}-1)\pi}{2(\beta_2-\beta_1)}\alpha\right) K_m\left(\frac{(2\bar{n}-1)\pi}{2(\beta_2-\beta_1)}\xi\right)\right]}{K_m'\left(\frac{(2\bar{n}-1)\pi}{2(\beta_2-\beta_1)}\alpha\right)} d\xi
\end{aligned} \tag{A.21}
$$

$$
a_{mn\bar{n}}^{78} = \delta_{n\bar{n}} 2k_{mn} e^{k_{mn}\beta_2} \int_\alpha^\gamma \xi \left[J_m\left(k_{mn}\xi\right) Y_m'\left(k_{mn}\alpha\right) - J_m\left(k_{mn}\alpha\right) Y_m'\left(k_{mn}\xi\right)\right]^2 d\xi \tag{A.22}
$$

$$
\begin{aligned}
a^{84}_{mn\bar{n}} &= \delta_{n\bar{n}}\lambda_{mn}\left(e^{\lambda_{mn}\beta_2} - e^{\lambda_{mn}(2\beta_1-\beta_2)}\right)\times \\
&\int_{\gamma}^{1} \xi\left[J_m\left(\lambda_{mn}\xi\right)Y'_m\left(\lambda_{mn}\right) - J_m\left(\lambda_{mn}\right)Y'_m\left(\lambda_{mn}\xi\right)\right]^2 d\xi \\
&-\omega^{*2}\delta_{n\bar{n}}\left(e^{\lambda_{mn}\beta_2} + e^{\lambda_{mn}(2\beta_1-\beta_2)}\right)\times \\
&\int_{\gamma}^{1} \xi\left[J_m\left(\lambda_{mn}\xi\right)Y'_m\left(\lambda_{mn}\right) - J_m\left(\lambda_{mn}\right)Y'_m\left(\lambda_{mn}\xi\right)\right]^2 d\xi
\end{aligned} \tag{A.23}
$$

$$
\begin{aligned}
a^{85}_{mn\bar{n}} &= \frac{(2\bar{n}-1)(-1)^{\bar{n}}\pi}{2(\beta_2-\beta_1)}\int_{\gamma}^{1} \xi \times \left[J_m\left(\lambda_{mn}\xi\right)Y'_m\left(\lambda_{mn}\right) - J_m\left(\lambda_{mn}\right)Y'_m\left(\lambda_{mn}\xi\right)\right] \\
&\frac{\left[I_m\left(\frac{(2\bar{n}-1)\pi}{2(\beta_2-\beta_1)}\xi\right)K'_m\left(\frac{(2\bar{n}-1)\pi}{2(\beta_2-\beta_1)}\right) - I'_m\left(\frac{(2\bar{n}-1)\pi}{2(\beta_2-\beta_1)}\right)K_m\left(\frac{(2\bar{n}-1)\pi}{2(\beta_2-\beta_1)}\xi\right)\right]}{K'_m\left(\frac{(2\bar{n}-1)\pi}{2(\beta_2-\beta_1)}\right)} d\xi
\end{aligned} \tag{A.24}
$$

Appendix B

Coefficients of matrix given by Eqs. (5.31) and (5.32)

The detailed expressions for the non-zero coefficients of the matrices given by Eqs. (5.31) and (5.32) are obtained as follows:

$$a^{11}_{mn\bar{n}} = \delta_{n\bar{n}} \times \lambda_{mn} \sinh \lambda_{mn}\beta_1 \times \int_0^1 \xi J_m^2(\lambda_{mn}\xi)d\xi, \tag{B.1}$$

$$a^{12}_{mn\bar{n}} = \delta_{n\bar{n}}(1-\delta^1_m) \times \frac{\lambda_{mn}}{\cosh \lambda_{mn}\beta_1} \times \int_0^1 \xi J_m^2(\lambda_{mn}\xi)d\xi, \tag{B.2}$$

$$a^{22}_{mn\bar{n}} = \delta_{n\bar{n}} \times \int_0^1 \xi J_m^2(\lambda_{mn}\xi)d\xi, \tag{B.3}$$

$$a^{23}_{mn\bar{n}} = -\delta_{n\bar{n}} \times \tanh \lambda_{mn}\beta_2 \times \int_0^1 \xi J_m^2(\lambda_{mn}\xi)d\xi, \tag{B.4}$$

$$a^{32}_{mn\bar{n}} = \delta_{n\bar{n}} \times \rho \times \lambda_{mn} \times \int_0^1 \xi J_m^2(\lambda_{mn}\xi)d\xi, \tag{B.5}$$

$$a^{33}_{mn\bar{n}} = -\delta_{n\bar{n}} \times \lambda_{mn} \tanh \lambda_{mn}\beta_2 \times \int_0^1 \xi J_m^2(\lambda_{mn}\xi)d\xi, \tag{B.6}$$

$$\bar{a}^{11}_{mn\bar{n}} = \delta_{n\bar{n}} \times \cosh \lambda_{mn}\beta_1 \times \int_0^1 \xi J_m^2(\lambda_{mn}\xi)d\xi, \tag{B.7}$$

$$\bar{a}^{31}_{mn\bar{n}} = \delta_{n\bar{n}} \times \rho \times \int_0^1 \xi J_m^2(\lambda_{mn}\xi)d\xi, \tag{B.8}$$

$$\bar{a}^{32}_{mn\bar{n}} = -\delta_{n\bar{n}} \times \rho \times \tanh \lambda_{mn}\beta_1 \times \int_0^1 \xi J_m^2(\lambda_{mn}\xi)d\xi, \tag{B.9}$$

$$\bar{a}^{33}_{mn\bar{n}} = -\delta_{n\bar{n}} \times \int_0^1 \xi J_m^2(\lambda_{mn}\xi)d\xi. \tag{B.10}$$

Appendix C

Coefficients of matrix given by Eq. (6.47)

The detailed expressions for the non-zero coefficients of the matrix given by Eq. (6.47) are obtained as follows:

$$a^{16}_{mn\bar{n}} = \delta_{n\bar{n}} \times \frac{\left[I_m\left(\frac{n\pi}{\beta_2}\gamma\right) K'_m\left(\frac{n\pi}{\beta_2}\right) - I'_m\left(\frac{n\pi}{\beta_2}\right) K_m\left(\frac{n\pi}{\beta_2}\gamma\right)\right]}{K'_m\left(\frac{n\pi}{\beta_2}\right)} \times \int_{-\beta_2}^{0} \cos^2\left(\frac{n\pi}{\beta_2}\eta\right) d\eta \tag{C.1}$$

$$a^{17}_{mn\bar{n}} = \frac{\left[J_m\left(k_{mn}\gamma\right) Y'_m\left(k_{mn}\right) - J'_m\left(k_{mn}\right) Y'_m\left(k_{mn}\gamma\right)\right]}{Y'_m\left(k_{mn}\right)} \times \int_{-\beta_2}^{0} \frac{\cosh k_{mn}(\eta+\beta_2)}{\cosh k_{mn}\beta_2} \cos\left(\frac{\bar{n}\pi}{\beta_2}\eta\right) d\eta \tag{C.2}$$

$$a^{18}_{mn\bar{n}} = -\delta_{n\bar{n}} \times I_m\left(\frac{n\pi}{\beta_2}\gamma\right) \times \int_{-\beta_2}^{0} \cos^2\left(\frac{n\pi}{\beta_2}\eta\right) d\eta \tag{C.3}$$

$$a^{19}_{mn\bar{n}} = -J_m\left(\lambda_{mn}\gamma\right) \times \int_{-\beta_2}^{0} \frac{\cosh \lambda_{mn}(\eta+\beta_2)}{\cosh \lambda_{mn}\beta_2} \cos\left(\frac{\bar{n}\pi}{\beta_2}\eta\right) d\eta \tag{C.4}$$

$$a^{26}_{mn\bar{n}} = \delta_{n\bar{n}}\left(\frac{n\pi}{\beta_2}\right) \times \frac{\left[I'_m\left(\frac{n\pi}{\beta_2}\gamma\right) K'_m\left(\frac{n\pi}{\beta_2}\right) - I'_m\left(\frac{n\pi}{\beta_2}\right) K'_m\left(\frac{n\pi}{\beta_2}\gamma\right)\right]}{K'_m\left(\frac{n\pi}{\beta_2}\right)} \times \int_{-\beta_2}^{0} \cos^2\left(\frac{n\pi}{\beta_2}\eta\right) d\eta \tag{C.5}$$

$$a^{28}_{mn\bar{n}} = -\delta_{n\bar{n}} \times \left(\frac{n\pi}{\beta_2}\right) I'_m\left(\frac{n\pi}{\beta_2}\gamma\right) \times \int_{-\beta_2}^{0} \cos^2\left(\frac{n\pi}{\beta_2}\eta\right) d\eta \tag{C.6}$$

$$a^{31}_{mn\bar{n}} = \delta_{n\bar{n}} \times \frac{\left[I_m\left(\frac{n\pi}{\beta_1}\gamma\right)K'_m\left(\frac{n\pi}{\beta_1}\right) - I'_m\left(\frac{n\pi}{\beta_1}\right)K_m\left(\frac{n\pi}{\beta_1}\gamma\right)\right]}{K'_m\left(\frac{n\pi}{\beta_1}\right)} \times \int_0^{\beta_1} \cos^2\left(\frac{n\pi}{\beta_1}\eta\right) d\eta \tag{C.7}$$

$$a^{32}_{mn\bar{n}} = \frac{\left[J_m\left(k_{mn}\gamma\right)Y'_m\left(k_{mn}\right) - J'_m\left(k_{mn}\right)Y'_m\left(k_{mn}\gamma\right)\right]}{Y_m\left(k_{mn}\right)} \times \int_0^{\beta_1} \frac{\cosh k_{mn}(\eta-\beta_1)}{\cosh k_{mn}\beta_1} \cos\left(\frac{\bar{n}\pi}{\beta_1}\eta\right) d\eta \tag{C.8}$$

$$a^{33}_{mn\bar{n}} = -J_m\left(\lambda_{mn}\gamma\right) \times \int_0^{\beta_1} \cosh\lambda_{mn}\eta \cos\left(\frac{\bar{n}\pi}{\beta_1}\eta\right) d\eta \tag{C.9}$$

$$a^{34}_{mn\bar{n}} = -I_m\left(\frac{(2n-1)\pi}{2\beta_1}\gamma\right) \times \int_0^{\beta_1} \cosh\left(\frac{(2n-)\pi}{2\beta_1}\eta\right) \cos\left(\frac{\bar{n}\pi}{\beta_1}\eta\right) d\eta$$

$$a^{35}_{mn\bar{n}} = -J_m\left(\lambda_{mn}\gamma\right) \times \int_0^{\beta_1} \frac{\sinh\lambda_{mn}(\eta-\beta_1)}{\cosh\lambda_{mn}\beta_1} \cos\left(\frac{\bar{n}\pi}{\beta_1}\eta\right) d\eta \tag{C.10}$$

$$a^{41}_{mn\bar{n}} = \delta_{n\bar{n}} \times \left(\frac{n\pi}{\beta_1}\right) \frac{\left[I'_m\left(\frac{n\pi}{\beta_1}\gamma\right)K'_m\left(\frac{n\pi}{\beta_1}\right) - I'_m\left(\frac{n\pi}{\beta_1}\right)K'_m\left(\frac{n\pi}{\beta_1}\gamma\right)\right]}{K'_m\left(\frac{n\pi}{\beta_1}\right)} \times \int_0^{\beta_1} \cos^2\left(\frac{n\pi}{\beta_1}\eta\right) d\eta \tag{C.11}$$

$$a^{44}_{mn\bar{n}} = -\left(\frac{(2n-1)\pi}{2\beta_1}\right) I'_m\left(\frac{(2n-1)\pi}{2\beta_1}\gamma\right) \times \int_0^{\beta_1} \cosh\left(\frac{(2n-)\pi}{2\beta_1}\eta\right) \cos\left(\frac{\bar{n}\pi}{\beta_1}\eta\right) d\eta \tag{C.12}$$

$$a^{55}_{mn\bar{n}} = \delta_{n\bar{n}} \times \lambda_{mn} \times \int_0^{\gamma} \xi J^2_m(\lambda_{mn}\xi) d\xi \tag{C.13}$$

$$a^{59}_{mn\bar{n}} = -\delta_{n\bar{n}} \times \lambda_{mn} \times \tanh\lambda_{mn} \times \beta_2 \int_0^{\gamma} \xi J^2_m(\lambda_{mn}\xi) d\xi \tag{C.14}$$

$$a^{63}_{mn\bar{n}} = \delta_{n\bar{n}} \times \rho\omega^{*2} \times \int_0^{\gamma} \xi J_m^2(\lambda_{mn}\xi)d\xi \tag{C.15}$$

$$a^{64}_{mn\bar{n}} = \rho\omega^{*2} \times \int_0^{\gamma} \xi I_m\left(\frac{(2n-1)\pi}{2\beta_1}\xi\right) J_m(\lambda_{m\bar{n}}\xi)d\xi \tag{C.16}$$

$$a^{65}_{mn\bar{n}} = -\delta_{n\bar{n}} \times \rho(\lambda_{mn} + \omega^{*2}\tanh\lambda_{mn}\beta_1) \times \int_0^{\gamma} \xi J_m^2(\lambda_{mn}\xi)d\xi \tag{C.17}$$

$$a^{68}_{mn\bar{n}} = -\omega^{*2} \times \int_0^{\gamma} \xi I_m\left(\frac{n\pi}{\beta_1}\xi\right) J_m(\lambda_{m\bar{n}}\xi)d\xi \tag{C.18}$$

$$a^{69}_{mn\bar{n}} = \delta_{n\bar{n}} \times (\lambda_{mn}\tanh\lambda_{mn}\beta_2 - \omega^{*2}) \times \int_0^{\gamma} \xi J_m^2(\lambda_{mn}\xi)d\xi \tag{C.19}$$

$$a^{72}_{mn\bar{n}} = \delta_{n\bar{n}} \times \int_{\gamma}^{1} \xi \frac{\left[J_m(k_{mn}\xi)\,Y'_m(k_{mn}) - J'_m(k_{mn})\,Y'_m(k_{mn}\xi)\right]^2}{Y'_m(k_{mn})}d\xi \times k_{mn} \times \tanh k_{mn}\beta_1 \tag{C.20}$$

$$a^{77}_{mn\bar{n}} = \delta_{n\bar{n}} \times \int_{\gamma}^{1} \xi \frac{\left[J_m(k_{mn}\xi)\,Y'_m(k_{mn}) - J'_m(k_{mn})\,Y'_m(k_{mn}\xi)\right]^2}{Y'_m(k_{mn})}d\xi \times k_{mn} \times \tanh k_{mn}\beta_2 \tag{C.21}$$

$$a^{81}_{mn\bar{n}} = \rho\omega^{*2} \times \int_{\gamma}^{1} \xi \frac{\left[I_m\left(\frac{n\pi}{\beta_1}\xi\right)K'_m\left(\frac{n\pi}{\beta_1}\right) - I'_m\left(\frac{n\pi}{\beta_1}\right)K_m\left(\frac{n\pi}{\beta_1}\xi\right)\right]}{K'_m\left(\frac{n\pi}{\beta_1}\right)} \times \frac{\left[J_m(k_{m\bar{n}}\xi)\,Y'_m(k_{m\bar{n}}) - J_m(k_{m\bar{n}})\,Y'_m(k_{m\bar{n}}\xi)\right]}{Y'_m(k_{m\bar{n}})}d\xi \tag{C.22}$$

$$a^{82}_{mn\bar{n}} = \delta_{n\bar{n}} \times \int_{\gamma}^{1} \xi \frac{\left[J_m(k_{mn}\xi)\,Y'_m(k_{mn}) - J'_m(k_{mn})\,Y'_m(k_{mn}\xi)\right]^2}{Y'_m(k_{mn})}d\xi \rho \times (\omega^{*2} + k_{mn} \times \tanh k_{mn}\beta_1) \tag{C.23}$$

$$a^{86}_{mn\bar{n}} = -\omega^{*2} \times \int_{\gamma}^{1} \xi \frac{\left[I_m\left(\frac{n\pi}{\beta_2}\xi\right)K'_m\left(\frac{n\pi}{\beta_2}\right) - I'_m\left(\frac{n\pi}{\beta_2}\right)K_m\left(\frac{n\pi}{\beta_2}\xi\right)\right]}{K'_m\left(\frac{n\pi}{\beta_2}\right)} \times \frac{\left[J_m(k_{m\bar{n}}\xi)\,Y'_m(k_{m\bar{n}}) - J_m(k_{m\bar{n}})\,Y'_m(k_{m\bar{n}}\xi)\right]}{Y'_m(k_{m\bar{n}})}d\xi \tag{C.24}$$

$$a^{87}_{mn\bar{n}} = \delta_{n\bar{n}} \times \int_{\gamma}^{1} \xi \frac{\left[J_m\left(k_{mn}\xi\right) Y'_m\left(k_{mn}\right) - J'_m\left(k_{mn}\right) Y'_m\left(k_{mn}\xi\right)\right]^2}{Y'_m\left(k_{mn}\right)} d\xi \times (k_{mn} \times \tanh k_{mn}\beta_2 - \omega^{*2}) \quad \text{(C.25)}$$

$$a^{93}_{mn\bar{n}} = \delta_{n\bar{n}} \times (\lambda_{mn} \sinh \lambda_{mn}\beta_1 - \omega^{*2} \cosh \lambda_{mn}\beta_1) \times \int_0^{\gamma} \xi J_m^2(\lambda_{mn}\xi) d\xi \quad \text{(C.26)}$$

$$a^{94}_{mn\bar{n}} = \left(\frac{(2n-1)\pi}{2\beta_1}\right)\left(1 - \frac{\delta^1_m}{\gamma^2}\right) \sin\left(\frac{(2n-1)\pi}{2}\right) \times \int_0^{\gamma} \xi I_m\left(\frac{(2n-1)\pi}{2\beta_1}\xi\right) J_m(\lambda_{m\bar{n}}\xi) d\xi \quad \text{(C.27)}$$

$$a^{95}_{mn\bar{n}} = \delta_{n\bar{n}} \times \left(\frac{\lambda_{mn}}{\cosh \lambda_{mn}\beta_1}\right) \times \int_0^{\gamma} \xi J_m^2(\lambda_{mn}\xi) d\xi \quad \text{(C.28)}$$

List of published and communicated papers

Based on the work carried out in this thesis, the following published and communicated papers have resulted:

1. N. Choudhary and S.N. Bora, "Linear sloshing in a vertical circular cylinder with curved bottom in the presence of a rigid baffle", *Journal of Advanced Research in Applied Mathematics*, 6(4), (2014), 29–45, (DOI:10.5373/jaram.1982.022514).

2. N. Choudhary and S.N. Bora, "Linear sloshing frequencies in the annular region of a circular cylindrical container in presence of baffle", *Communicated*.

3. N. Choudhary and S.N. Bora, "Sloshing frequencies in an annular region of a rigid circular cylindrical container with baffle placed inside liquid", *Communicated*.

4. N. Choudhary and S.N. Bora, "Study of liquid sloshing in a circular cylindrical container containing a two-layer fluid", *under preparation*.

5. N. Choudhary and S.N. Bora, "Liquid sloshing in a circular cylindrical container containing a two-layer fluid in presence of a rigid baffle placed at free surface", *under preparation*.